SAPIENZA
UNIVERSITÀ DI ROMA

Sapienza University of Rome

Department of Astronautical, Electrical and Energy Engineering
PhD in Engineering and Applied Science for Energy and Industry

PhD Thesis

Thermal Energy Storage: design and operation optimization of electrical power supply

Thesis Sapienza Advisor
Maria Carmen Falvo

Thesis Magaldi Advisor
Matteo Mauro

Candidate
Matteo Scanzano
1698750

Academic Year 2022-2023 (XXXVI cycle)

"Optimization is the secret sauce of engineering.
It's like finding the perfect recipe for success, where the main ingredient is efficiency, and the cooking instructions are written in algorithms."

Contents

List of Figures

List of Tables

Nomenclature

p	Instant power
β	Dimensionless input power
l	Instant power losses
e	Stored energy
P	Power capacity
L	Total energy losses
E	Energy capacity
T	Simulation duration
T_{step}	Simulation time step
T_{life}	Component lifetime
T_{store}	Storage duration
τ	Storage auto-discharge
η	Component efficiency
s	Activation state (0/1)
C	CAPEX cost
c	OPEX cost
$\tilde{c}$	Unbalance cost
M	CAPEX money
m	OPEX money
$\tilde{m}$	Unbalance money
$\mathbb{M}$	Total money
Λ	Mass
K	Technology-specific constant
D	Decarbonization level
Γ	Saved emissions
γ	Decarbonization cost

Acronyms

CO_2 carbon dioxide

CAPEX CAPital EXpenditure

COP Coefficient of Performance

CSTS Contactors as Secondary Tap Selector

EMC Electro-Magnetic Compatibility

EMS Energy Management System

ESTESO Elastic Software for Thermal Energy Storage Optimization

GHG Green-House Gases

GME Gestore Mercati Energetici

HTF Heat Transfer Fluid

LP Linear Programming

MGTES Magaldi Green Thermal Energy Storage

MILP Mixed Integer Linear Programming

OLTC On-Load Tap Changers

OPEX OPerational EXpenditure

P2H Power-to-Heat

P2P Power-to-Power

PV PhotoVoltaic

STEM Solar ThermoElectric Magaldi

TES Thermal Energy Storage

TSO Transmission System Operator

UPS Uninterruptible Power Supply

ZVS Zero Voltage Switching

Introduction

Mitigating Green-House Gases (GHG) emissions is of paramount importance in the context of global efforts to cope with climate change and ensure environmental sustainability [1]. A substantial proportion of emissions comes from the combustion of fossil fuels such as coal, oil, and natural gas, which act as valuable resources across multiple sectors. Among these, the industrial sector plays a pivotal role in the world's economic development, providing essential goods and services, but it is also a significant contributor to GHG emissions, primarily carbon dioxide (CO_2).

The pressing need to mitigate climate change has led nations worldwide to establish ambitious decarbonization targets, that act as pivotal milestones in reducing emissions and transitioning to sustainable energy systems. The "Fit for 55" package [2], one of the most recent GHG emission policies, aims to reduce Eurpoean emissions by at least 55% by 2030. European countries are also in the process of developing new legislation to make Europe climate-neutral by 2050.

Recognizing the urgency of the climate crisis, governments, industries, and international organizations have committed substantial investments to advance decarbonization efforts. For example, the 2023 Italian Transmission Network Development Plan [3] involves over 21 B€ of investments expected over the next 10 years to accelerate the energy transition in Italy, promoting the decarbonization of the country and reduce dependence on foreign sources. This investment represents a 17% increase compared to the previous plan. Worldwide, the total investment in the low-carbon energy transition was over 1000 B€ in 2022, a new record and a substantial increase from the previous year (Figure 1) [4].

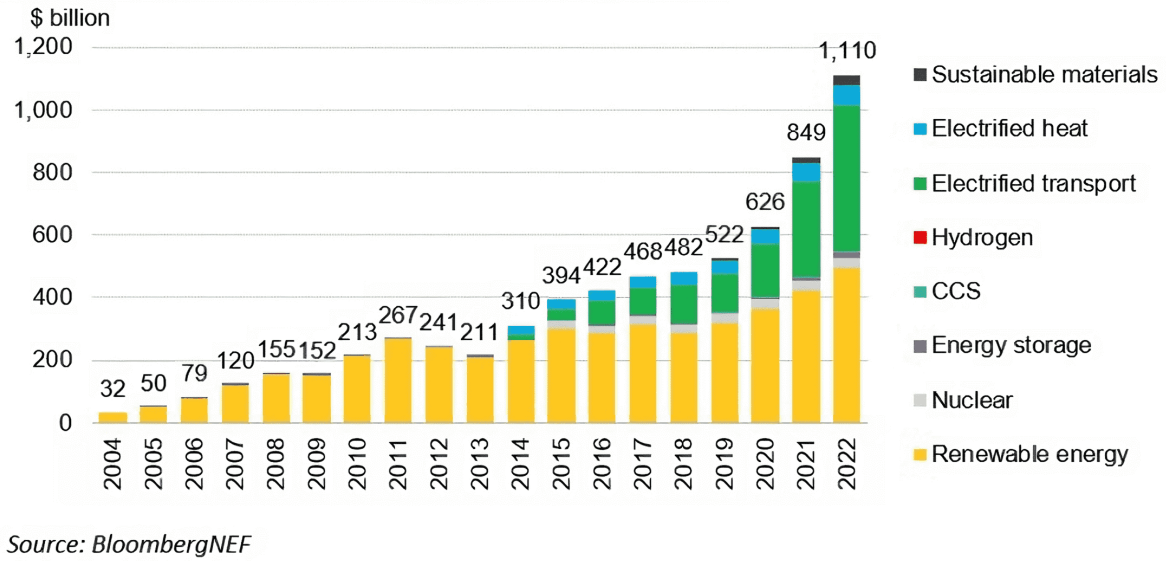

Figure 1: Global investment in energy transition by sector

The need to remove fossil fuels is constantly increasing the spread of renewable sources, able to produce clean energy, without emitting GHG. However, the integration of renewables into energy systems presents significant challenges [5, 6]. Among these, solar and wind sources are intermittent by nature, leading to critical fluctuations in energy supply. Therefore, to harness the full decarbonization potential of such sustainable sources, effective energy storage solutions are imperative [7].

Reducing the use of fossil fuels is not only a moral imperative to protect the planet, but also an economic and political need. In fact, the reliance on finite fossil fuels exposes industries to the volatility of global energy markets, and such a heavy dependence on these resources places nations at risk of energy supply disruptions from other countries, thereby compromising national energy security [8, 9]. The issue of energy autonomy has gained prominence in the last few years: the recent Ukraine conflict serves as a stark illustration of the link between global energy markets and international disputes. The great dependence of European countries on Russian natural gas highlighted the vulnerability of energy supply chains to political conflicts. Figure 2 shows the trend of gas [10] and electric energy [11] prices from 2019 to 2024.

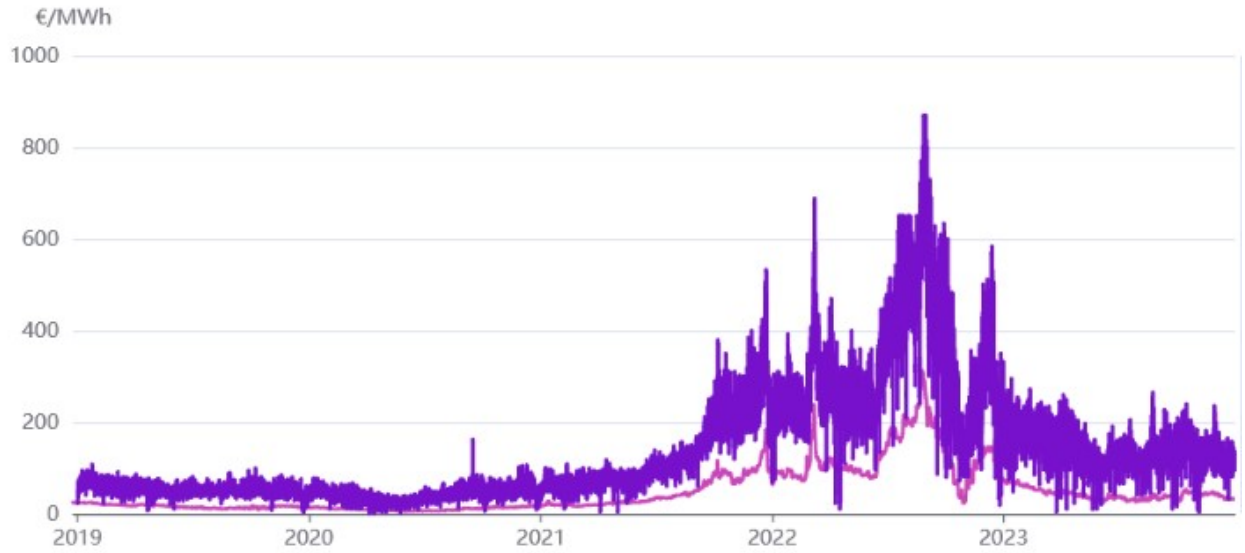

Figure 2: Italian day-ahead prices of gas and electricity between 2019 and 2024

To mitigate these vulnerabilities, European nations have actively striven for the diversification of their energy sources, increasing natural gas imports from other regions, and further promoting the use of renewable sources. The use of local renewable energy is an excellent strategy to increase energy autonomy. Fossil fuel deposits, like many other resources, tend to be concentrated in specific regions of the world, and such regions have always been the scene of conflicts for the supremacy over the deposits. Indeed, the energy transition presents a significant opportunity to "democratize" energy: solar and wind sources are broadly accessible worldwide.

It is essential to note that technological advancements can reduce emissions, but its widespread adoption relies on political will and, crucially, on the availability of raw materials. For this reason, it is important that research should focus on technologies that utilize readily available raw materials, steering clear of conflict-related dependencies. For example, the recent increase in electric vehicles has driven up the demand for lithium for battery production, arousing the interest of economic

powers for countries with large lithium reserves [12]. This highlights the importance of developing alternative storage technologies that do not rely on lithium. This concept can be referred to as "political sustainability": a broader and undoubtedly more complex objective to achieve compared to traditional environmental sustainability [13].

Founded over 90 years ago, Magaldi Group is a leader in the design and production of high-temperature conveyors, and its innovative solutions have been adopted in industries all around the world [14]. Magaldi Green Thermal Energy Storage (MGTES) is the result of Magaldi's expertise in high-temperature materials and its resolute commitment to the energy transition. This system utilizes sand to store thermal energy, providing a valid eco-friendly alternative to other traditional Thermal Energy Storage (TES) using molten salts.

Magaldi's success can be attributed, in no small part, to its enduring pursuit of excellence and innovation. In fact, the company has accumulated numerous patents over the years, highlighting their commitment to research and constant improvement [15]. To achieve this, the company undertakes different types of research and development initiatives, collaborating with top-ranked universities and research institutions, funding projects, studies and theses to integrate the latest technological advancements into Magaldi's products [16].

This PhD thesis represent the conclusion of one of these initiatives, whose primary objective was to design the power supply of a MGTES. A key aspect of this research has been the development of a multi-purpose software aimed at optimizing both the sizing and operation of the system, to ensure that the MGTES operates at peak efficiency, minimizing energy losses and operational costs while maximizing its contribution to reducing greenhouse gas emissions.

The thesis is composed by 6 chapters, focusing both on hardware and software. After this introduction, outlining the international context with its current global challenges about energy transition and renewable sources, Chapter 1 presents the state of the art on storage systems and algorithms involved in their optimization. Chapter 2 presents an overview of MGTES technology, along with its components and applications, then Chapter 3 focuses on the design of its power supply, comparing different options for its architecture and power control devices. Chapter 4 presents ESTESO, the unified multi-purpose software developed to simulate and optimize MGTES sizing and management, then Chapter 5 describes the models implemented in ESTESO, presenting the results of the sizing optimization of a typical Power-to-Heat system comprising MGTES. Finally, Chapter 6 summarizes the main key findings and takeaways, also outlining the ongoing and future developments of the research. Appendix A lists the publications related to the thesis, followed by open source libraries used by ESTESO, its interface pages and the equations generated for the modeled system. The thesis incorporates novelty in the following ways:

- **Technology**: this is the first PhD thesis extensively exploring MGTES, with a specific focus on its electrical charging system and power supply. This involved leveraging existing solutions in new ways, studying how to adapt them to MGTES particularities.
- **Hardware**: Chapter 3 presents a novel solution to control resistors power, employing custom transformers and contactors to achieve a reliable discrete power control without the use of power electronics, tackling the increasingly significant issues of recyclability and semiconductor supply chain security.

Chapter 1

State of the art on energy storage systems and their optimization

This Chapter provides an overview of energy storage systems, categorizing them according to different criteria and outlining their functions, then delving into major technologies in the field. Additionally, it examines commonly used algorithms for optimizing such technologies.

This information will serve as a foundation for subsequent Chapters, which will highlight the differences between MGTES and existing technologies, and underscore the necessary adjustments in the approach to design and operation compared to conventional practices.

1.1 Energy storage types and energy conversions

An energy storage system can be simply defined as a device capable of adsorbing power (charging) and delivering it at later time (discharging). This definition underscores the primary purpose of such systems: shifting energy in time. While all energy storage systems share this core objective, each technology features unique characteristics, making it suitable for specific applications. The environment interacting with the storage system can be modeled as a power source and a power demand, each one with its specific power profile.

An initial classification of energy storage systems can be based on the number of the connections with the environment ("ports"), used for energy exchange, i.e. charging and discharging.

- **1-port type**: the majority of energy storage system employ a single bidirectional connection with the external environment for both charging and discharging, so they adsorb and deliver energy in the same form ($f_{in} = f_{out} = f$). Typically, energy is stored in a different form than that used for charging and discharging ($f_{st} \neq f$), necessitating energy conversion. Therefore, such systems require to perform at least two conversions: one during charging ($f_{in} \rightarrow f$) and another during discharging ($f_{out} \rightarrow f$). Depending on the technology, the conversion may be performed using a single bidirectional device ($d_{in} = d_{out} = d$) or two distinct unidirectional devices ($d_{in} \neq d_{out}$). Trivially, if the energy is stored in the same form, no conversion is needed.

- **2-port type**: some energy storage systems use distinct unidirectional connections for charging and discharging, enabling them to manage different forms of input and output energy ($f_{in} \neq$

f_{out}). If the energy is stored in one of the forms used for charging or discharging, only one conversion is needed ($f_{in} \rightarrow f_{st} = f_{out}$ or $f_{in} = f_{st} \rightarrow f_{out}$). Otherwise, energy has to be converted two times ($f_{in} \rightarrow f_{st} \rightarrow f_{out}$), using different devices.

As depicted in the left diagram of Figure 1.1, systems comprising 1-port type storage devices have a direct connection between source and demand, and the storage system can modify the energy flow adding or subtracting power from a power node on this connection. For this reason, 1-port type systems can be defined as "power-adding". Conversely, as illustrated in the right diagram of Figure 1.1, 2-port type systems act as the connection between source and demand, without any direct connection between them. Therefore, 2-port type systems can be defined as "power-transfer".

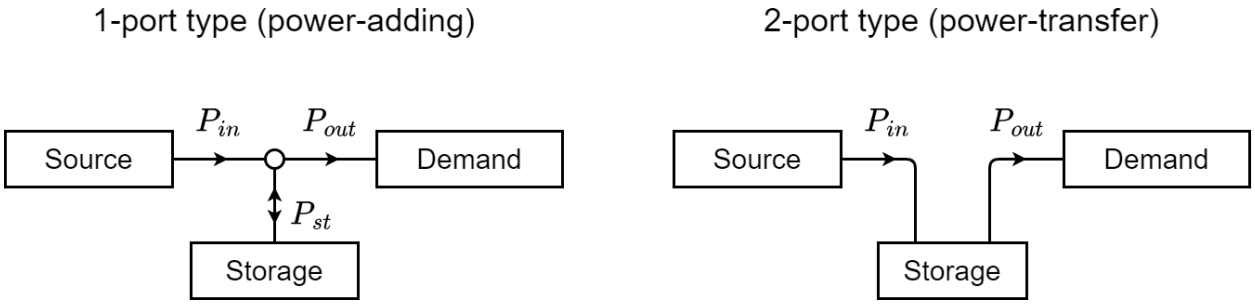

Figure 1.1: Two different storage types, based on the number of "ports", i.e. the connections used for energy exchange with the environment

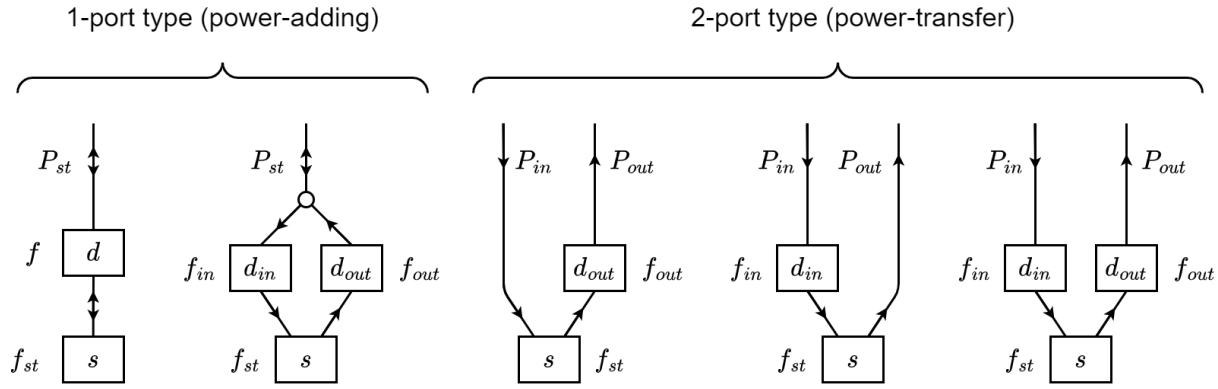

(a) $f \leftrightarrow f_{st}$ (b) $f_{in} \rightarrow f_{st} \rightarrow f_{out}$ (c) $f_{in} = f_{st} \rightarrow f_{out}$ (d) $f_{in} \rightarrow f_{st} = f_{out}$ (e) $f_{in} \rightarrow f_{st} \rightarrow f_{out}$

Figure 1.2: Possible options for the energy conversions performed by 1-port (power-adding) and 2-port (power-transfer) storage systems

The most relevant sizing parameters for energy storage systems are the storage capacity and the maximum charge or discharge power. It should be noted that in several cases, among both 1-port and 2-port type storage systems, the maximum charging and discharging powers are different. Such systems can be defined as "asymmetric", as opposed to "symmetric" ones, that have equal power limits for charging and discharging.

1.2 Energy storage functions

The simple yet powerful ability of storage systems to shift energy in time can be exploited in different ways, achieving different effects, depending on the needs of source and demand. In fact, in the absence of a storage system, the power profiles of the source shall be equal to the demand, to provide the required energy without interruptions or unbalance. On the contrary, energy storage allows the flexibility to adjust these profiles independently, fulfilling different "functions", described in this Section.

The functions performed by a storage system can be determined comparing the profile of a key quantity (e.g. source power) with a reference profile, then identifying the differences between them and classifying every discrepancy to a known function. Depending on the profile chosen as a reference, the analysis can be conducted in two perspectives, outlined below.

- **Before-after perspective**: this approach entails comparing the profile of a specific quantity (e.g. source or demand power) with and without the presence of storage. It can be adopted when upgrading existing systems to incorporate energy storage.
- **Source-demand perspective**: this approach involves comparing the power profiles of the energy source and the demand. It is particularly relevant for systems that cannot function effectively without energy storage devices.

Figure 1.3 summarizes different effects of a storage system, based on the impact on power profiles of source and demand, in the before-after perspective.

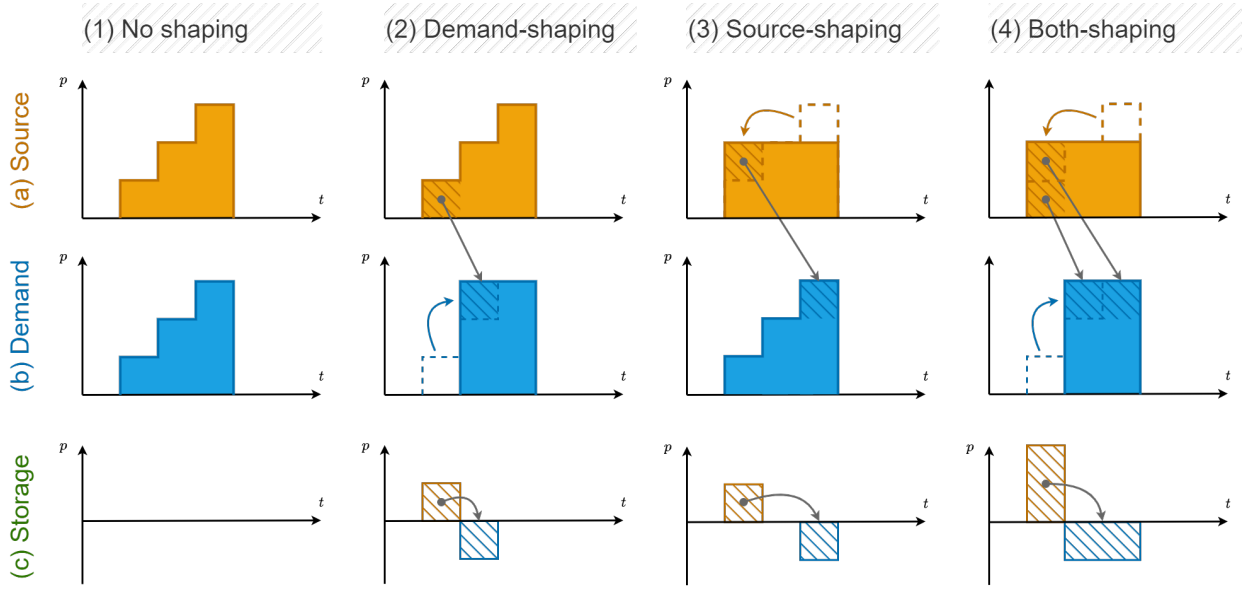

Figure 1.3: Classification of energy storage effects based on the impact on source and loads profiles, in the before-after perspective

The first column reports the reference profiles, without storage (no shaping), whereas the other ones depicts 3 possible uses, described below.

- **Demand shaping**: a storage system is used to shape the demand profile as desired, without modifying the source. For example, this effect can be leveraged to satisfy peak load increase without grid capacity upgrade, typically costly, slow and resource-intensive [17].
- **Source shaping**: a storage system is used to shape the source profile as desired, without affecting the demand. For example, this function is exploited to integrate renewable sources in power systems, enabling the fulfillment of the same load with an adjusted energy generation profile. Indeed, energy storage technologies play a pivotal role as cornerstones of dispatchable renewable power, enhancing grid flexibility and resilience [18–20].
- **Both shaping**: a storage system is used to shape both the source and the demand profile as desired, combining the two effects described above. For example, this can occur in highly flexible networks, full of controllable loads and generation systems, that may be operated by dedicated algorithms to optimize power flows and minimize losses [21].

In columns 2 to 4 of Figure 1.3 the main profiles are filled in orange and blue, whereas the reference profiles are displayed with dashed lines. The energy shifted by the storage system is represented by the hatched areas. In the last row, the input and output power profiles of the storage system are displayed, illustrating that the system substantially performs energy shifting in all three cases, regardless of the impact on the source and/or demand.

Conversely, focusing on source and demand profiles instead, different functions of storage systems can be identified, allowing a classification of every shift. it is important to note that functions refer to individual modifications of a profile, so every storage system performs at least two functions: one for charging and another for discharging. Common functions, summarized in Figure 1.4, are listed in the following, together with some real-word use case examples.

- **Peak shaving**: reducing power peaks, cutting them if they exceed a maximum limit value or profile. In power systems, peak shaving is used to prevent the increase of network capacity upon addition of peak generation. This is particularly beneficial for the integration of renewable technologies which generate maximum power output only for a limited time span [17], particularly PV.
- **Peak forming**: creating a peak over a reference flat profile. This is used to handle high power peaks adsorbed or provided by motors of electric vehicles, during acceleration and deceleration phases [22]. In such applications energy storage systems enhance traction performance providing fast response and high controllability, and enable efficient regenerative braking, unlocking significant energy and emissions savings.
- **Valley leveling**: reducing power holes, filling them if they drop below a minimum limit value or profile. This constitutes the primary function performed by traditional Uninterruptible Power Supply (UPS) systems, ensuring a continuous and reliable power supply to critical electrical loads that cannot tolerate withstand even brief interruptions in the provision of energy [23]. Additionally, valley leveling is crucial for integrating renewable sources into power systems, which are typically highly variable and non-programmable [24, 25]. In such

cases, energy storage systems with fast response times are pivotal to supply energy during intermittencies, e.g. small clouds on nearly clear days that affect PV power production.

- **Valley carving**: creating power holes when needed. This function is less common, but it is included here for a complete overview of the options. It may find application in specific scenarios requiring intermittent power flows, where temporary energy interruptions are deliberately introduced.
- **Ramp and de-ramp softening or sharping**: mitigating or exacerbating steep increases or decreases in power, relaxing or hardening them to a different rise or descent, to comply with ramping and de-ramping limits. This function can be exploited to realize an optimized coordination between traditional slow-response generation systems and highly variable renewable sources, enabling the creation of Virtual Power Plants (VPP) [26, 27].
- **Time shifting**: even though all functions perform an energy time shift, other functions not listed above, can be regarded as generic "time shifting". This applies to moving an entire part of a power profile to a different time, e.g. for standalone solar streetlights in displaced settlements [28].

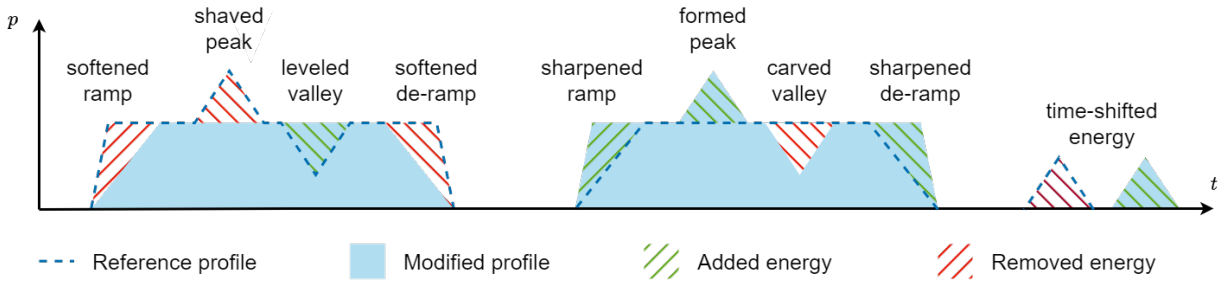

Figure 1.4: Summary of different functions performed by storage systems

Identifying the functions performed by a storage system is a critical aspect of its design phase, as it facilitates a deeper comprehension of system requirements and the intended role of the storage. This process guides the selection of appropriate technology and control strategies, tailored to the specific context and objectives. In some cases, employing a combination of multiple storage technologies, each one with its own unique attributes (discussed in the next Section) may be more suitable than relying solely on one. This approach allows each system to fulfill only the functions for which it is best suited, thereby optimizing overall performance and effectiveness.

1.3 Energy storage technologies

In the following, the major energy storage technologies are presented [29].

- **Pumped-hydro facilities** store energy by pumping water to an elevated reservoir and releasing it to generate electricity when needed. They can store large amounts of energy providing long-term storage with good efficiency, but their deployment is hindered by unfavourable topography, extended payback periods and community opposition due to their considerable landscape impact. Open-loop facilities, i.e. those receiving natural inflow to the system, outperform closed-loop systems [30]. However, recent trends indicate a growing interest in closed-loop systems due to their higher likelihood of obtaining operational licenses, as they do not interfere with local water supply security and typically have a reduced environmental impact [31].

- **Electro-chemical batteries** rely on chemical reactions to store and release electric energy. A lot of different battery technologies are being developed, but the most widely used ones (in portable devices and electric vehicles) are the traditional lead-acid and lithium-ion. Redox flow batteries are an emerging solution to meet the growing demand for large-scale energy storage systems. These batteries utilize soluble electrolytes stored in external tanks and pumped into a cell where the electro-chemical reactions occur. Such technology offer the advantage of independence between energy and power capacity [32]. Unfortunately, battery storage systems poses significant challenges in terms of safety and environmental friendliness. In fact, the release of pollutants from battery manufacturing (Cd, Co, Cr, Li, Mn, Ni, and Pb) poses significant risks to human health [33]. Moreover, the thermal runaway of batteries can lead to fires or explosions. In addition, there is an urgent issue to improve the recycling of waste batteries. Some countries have established a quite efficient recycling supply chain for lead-acid batteries, and the recovery rate has exceeded 90%, however such systems are not yet developed for lithium-ion batteries [34].

- **Supercapacitors**, called electro-chemical capacitors by some authors, leverage three effects for the storage of energy: double layer, pseudo-capacitance and faradaic processes, combined differently depending on the materials used [35]. This allows bridging the gap between batteries and conventional capacitors with regard to energy and power densities. They feature very fast response times but are limited by their high self-discharge losses, and high cost of materials for large-scale applications [22].

- **Flywheels** store energy by spinning a massive rotor at high speeds, featuring high power density and extended lifespan. Typically operated in high vacuum conditions and utilizing magnetic bearings to minimize losses, they offer advantages such as lower maintenance costs but are associated with higher initial investment. Drawbacks include structural complexity, mechanical stress and fatigue, as well as safety concerns due to the high speed of the rotor [36].

- **Compressed Air Energy Storage (CAES)** store energy by compressing air and storing it in underground caverns, releasing it into a turbine to generate electricity [37]. The main advantages of CAES include long energy storage time (more than one year), long asset life

(about 40 years) and flexible capacity range [38]. A significant challenge in constructing large-scale energy storage systems lies in identifying suitable geographic locations. Economic feasibility is typically limited to areas with access to resources such as rock mines, salt caves, aquifers, or depleted gas fields, which can lead to increased capital costs [39].

- **Superconducting Magnetic Energy Storage (SMES)** store energy using superconducting coils and magnetic fields. They are known for their high efficiency and fast response times, but they require cryogenic systems to keep the coils in a superconducting state [40]. Despite successful deployments of up to 10-20 MW scales and demonstrated effectiveness, the cost of cryogenic systems remains a significant barrier to widespread adoption. Nevertheless, advancements in high-temperature semiconductors offer promising prospects for cost reduction and improved efficiencies [41].

- **Thermal Energy Storage (TES)** store energy by heating or cooling a medium, traditionally molten salt or water, and releasing heat in the form of a Heat Transfer Fluid (HTF) [42]. Heat storage mediums can be based on latent heat, sensible heat, or chemical energy. TES is considered the most suitable means to integrate renewable energy into the grid, and it also has potential applications in waste heat recovery, solar energy utilization, and building energy conservation [39]. The main TES research efforts are directed towards the development of advanced materials, exploiting the addition of nano-particles, or combining different materials together, to improve the physical properties of the storage medium [43].

Table 1.1 summarizes advantages and disadvantages of the storage technologies presented above [39]. All of them originate as power-adding storage systems, as their primary objective is to exchange only one form of energy with the connected system. This approach is the most straightforward one, as it eliminates the need to consider multiple energy vectors. In the case of power-transfer systems, it is crucial to specify the input and output forms accepted by the technologies. Those with electric input and thermal output are regarded as "Power-to-Heat", discussed in the next section; following the same convention, calling electricity as "Power", traditional power-adding storage technologies with electrical input and output can be regarded as "Power-to-Power".

Technology	Advantages	Disadvantages
Pumped Hydro	• Mature technology • Long life cycle • High capacity	• Requires specific location • High initial cost • Lengthy construction time • Environmental concerns
Lead-acid battery	• Mature technology • High number of charge/discharge cycles • Fast response time • High recycling potential	• Short life cycle • Susceptible to sulfation • Poor performance at low temperatures
Lithium-ion battery	• High power density • High energy density • Fast response time • Not suitable for full-discharge	• Short life cycle • Highly sensitive temperature • Needs internal overcharge protection technology
Redox flow battery	• High flexibility and scalability • Low environmental impact • Long life cycle • Low maintenance cost	• Low energy density • High cost
Supercapacitor	• Fast charging time • Fast response time • High power density • Low maintenance cost	• Low energy density • High self-discharge loss • High cost for advanced materials • Needs cooling system
Flywheel	• High power density • Long life cycle • Low mantainance	• Short storage time • Risk of mechanical failure
Compressed air storage	• Long storage period • Low initial cost • High capacity	• Requires appropriate location • Limited flexibility • Limitation of fossil fuel combustion
Superconducting magnetic storage	• High power density • High efficiency • Long life cycle • Fast response time	• High cost • Low temperature operation that requires a refrigeration system • High self-discharge rate
Thermal storage	• Low cost • Long life cycle • Long storage duration	• Low efficiency • Slow response time • Needs high-temperature materials

Table 1.1: Advantages and disadvantages of widely used storage technologies

1.4 Power-to-Heat technologies

P2H technologies transform electric energy into heat, offering a sustainable alternative to fossil fuels across various sectors when the input electric energy is sourced from renewables. In the following, the most common P2H technologies are presented.

- **Electrical heating**: resistors represent the simplest solution to convert electrical energy into heat, utilizing the Joule effect within wires, bars, coils, or ribbons composed of metals (typically FeCrAl or NiCr alloys) or high-temperature semiconducting materials (e.g. SiC) [44]. These elements directly touch or irradiate the target object for heating, providing high efficiency (from 90%, even up to 99.9%). Although conductive heating predominates, inductive, high-frequency, and infrared heating systems are also widely utilized in industrial processes [45]. These alternatives are only chosen when resistive elements are impractical due to specific process requirements. Inductive and infrared heating, unlike resistive heating, do not necessitate direct contact between the heating element and the target object. Moreover, inductive heating, which operates via the Joule effect induced by eddy currents within a metal due to an alternating magnetic field, offers the advantage of controlling current penetration by adjusting the frequency of the magnetic field.

- **Heat pumps**: they are primarily employed in residential applications for space heating and/or cooling, or hot water production. Recently, heat pump technologies have been increasingly adopted in the industrial sector for the decarbonization of low-temperature processes (up to 150 °C [45]), driven by their profitable Coefficient of Performance (COP). According to IRENA, heat pumps are projected to meet 27% of the total heat demand in the EU by 2050. Hybrid configurations, combining heat pumps with resistive elements, exploit the superior COP of heat pumps to provide heating in lower temperature ranges, at the same time relying on resistors to meet heating requirements for temperatures beyond the capability of heat pumps [46]. Concurrently, some research groups are exploring "static" heat pump technologies leveraging the Peltier effect to deliver comparable energy efficiencies with enhanced reliability.

- **Power-to-gas**: electric energy can be used in electrochemical reactions to produce high-energy-density fuels, typically in gaseous form. A trending application of such technologies is power-to-hydrogen, that electrolyze water into hydrogen (and oxygen), providing a GHG-free fuel to be used in different applications, especially for moving systems, i.e. cars, buses, trains, ships, airplanes. Typical electrolyzer efficiencies range between 65 and 75% [47].

The technologies listed above do not inherently provide storage capacity, but they facilitate easy integration with other equipment to serve as storage for the output. For instance, tanks can act as storage systems, allowing the accumulation of HTF or hydrogen (e.g. during excess renewable production), to be used later when needed. However, it is important to recognize that this solution may not always be optimal, depending on the characteristics of the fluids involved. For example, certain HTFs may have unfavourable thermo-physical properties, making them impractical for storage in tanks due to their large volume requirements. In fact, the use of Power-to-Heat storage with water is restricted to its liquid form, suitable for low-temperature ranges. Regarding power-to-gas applications, hydrogen has higher energy density than diesel, but storing the same amount of

hydrogen requires a larger volume. In addition, storing gaseous hydrogen in tanks presents serious explosion risks, necessitating additional investments in security measures [48]. One approach to mitigate this risk involves storing hydrogen at atmospheric pressure by combining it with nitrogen to form ammonia. While this method eliminates the explosion hazard, it is essential to acknowledge that ammonia still poses risks to both humans and ecosystems.

The integration of tanks into a P2H system realizes a 1-port (power-transfer) storage system, as defined in Section 1.1. Here, the energy capacity depends on the tank size. The maximum input power is determined by the P2H, whereas the maximum output power is influenced by the energy density of the fluid and its maximum mass flow from the tank. This design allows for independent selection of power and energy sizing for the storage, in contrast to a significant portion of popular 2-port technologies, which typically maintain a constant power-energy ratio.

Another significant characteristic of 2-port storage systems is their ability to allow simultaneous input and output power flows. In contrast to 1-port technologies, which exhibit three operating modes (charge, storage, discharge), 2-port technologies feature an additional "direct transfer" mode. Figure 1.4 illustrates various operational scenarios of a 2-port storage system. The direct transferred energy is identified by the areas where input and output power profiles overlap.

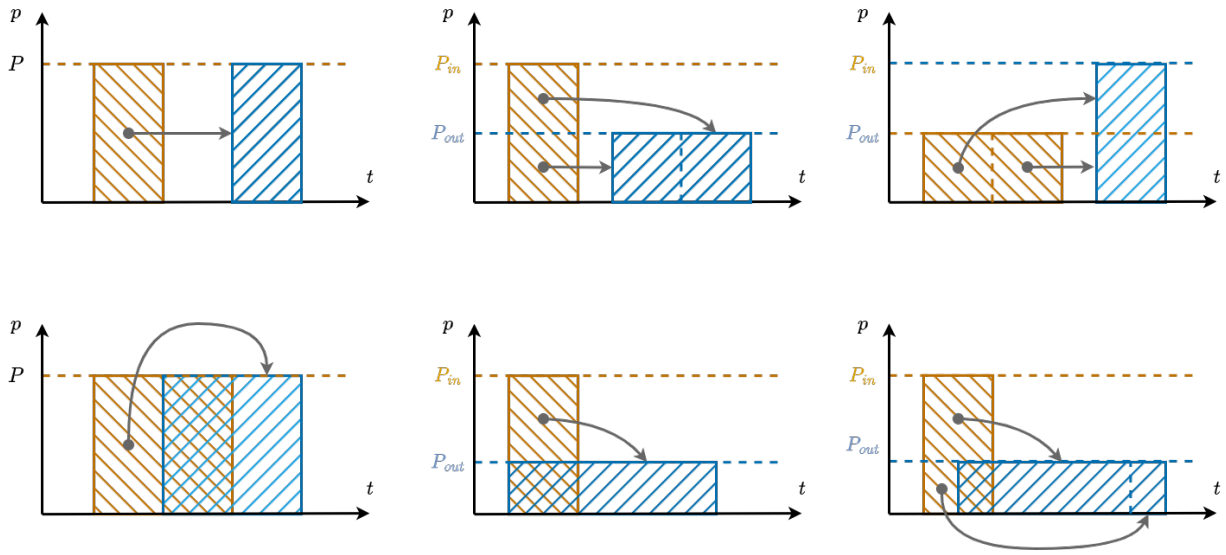

Figure 1.5: Example operation of a 2-port type storage system, showing scenarios with and without direct transfer

1.5 Optimization algorithms

1.5.1 Purpose

Optimization plays a pivotal role for the deployment of storage systems, and energy systems in general, since it enables remarkable improvements over different phases of storage projects, as detailed below.

- **Design**: optimization-augmented research and development on storage technologies enables manufacturers enhancing the technical performance of their products, e.g. increasing efficiency and reducing costs per unit power or energy, gaining market competitivity over other producers.
- **Sizing**: for a given case study, energy storage integrators can leverage optimization algorithms to select the best technologies and sizes for every application, ensuring noteworthy resources allocation and cost savings, both on CAPital EXpenditure (CAPEX) and OPerational EXpenditure (OPEX). Given the unique advantages brought by every technology, in most applications optimization results reveal attractive combinations of different energy storage systems, also providing valuable information about how to combine them effectively.
- **Operation**: optimal energy management and real-time control of storage systems enable the minimization of OPerational EXpenditure (OPEX), e.g. energy cost supply, emissions, maintenance, for a system with fixed size. This type of optimization is commonly performed by Energy Management System (EMS)s, that continuously compute the optimal working conditions of the system and control power flows accordingly, based on past, present, and future environmental conditions, evaluated using real-time data and forecasts.

In a nutshell, every party that interact with energy storage systems can greatly benefit from optimization. For this reasons, several optimization methods for energy systems have been studied in the literature, in order to achieve accurate results, with reasonable computation time and complexity.

1.5.2 Methods

In general, optimization algorithms can be classified into different groups [49], presented in the following.

- **Mathematical methods** encompass a broad range of techniques, relying on mathematical formulations and algorithms to find the optimal solution within given constraints, often yielding precise and deterministic results. The most used mathematical optimization algorithms are presented further on.
- **Meta-heuristic methods** offer a flexible and efficient approach to optimization by simulating natural processes or heuristic strategies to explore solution spaces. These algorithms iteratively improve candidate solutions, often providing near-optimal solutions for complex problems with large search spaces and no exact mathematical formulation.
- **Fuzzy methods** address problems involving uncertainty in decision-making by employing fuzzy logic to model vague or ambiguous information. These methods can effectively handle real-world optimization problems with incomplete or uncertain data, quantifying uncertainty through fuzzy sets.
- **Artificial neural networks** utilize interconnected nodes inspired by biological neurons to learn complex patterns and relationships from data. Through iterative training processes, neural networks can optimize decision-making tasks by approximating non-linear functions and adapting to changes in input data, making them suitable for various optimization problems without exact mathematical formulation, but a lot of available data.
- **Model predictive control** integrates optimization techniques with control theory to optimize system performance while considering constraints and dynamics. By solving optimization problems in real-time or with predictive horizons, such algorithms can adjust control actions to achieve desired objectives while accounting for system dynamics and constraints.
- **Multi-agent systems** employ distributed decision-making among autonomous agents, coordinating interactions and information exchange between the agents. Multi-agent systems can achieve efficient solutions in decentralized environments while adapting to changing conditions.

1.5.3 Mathematical methods

Below is a non-exhaustive list of the most used mathematical methods and approaches [49].

- **Linear Programming (LP)** enables the minimization or maximization of linear objective functions, for optimization models with continuous variables and linear constraints. A linearization approach is often used to optimize non-linear systems, e.g. for load flow equations of power networks, to reduce model complexity and shorten computation time.
- **Mixed Integer Linear Programming (MILP)** is an extension of LP that includes also binary or integer variables into the models, to take into account the discrete states of components, such as grid-connected/islanded mode for microgrids or energy storage charging/discharging states. Typically, the resolution of Mixed Integer Linear Programming (MILP) problems involves a linear relaxation of integer variables, then restored to match the solution of the relaxed problem to the original one, requiring additional computation time.
- **Non-linear Programming (NLP)** is embraced when LP approximation lacks sufficient accuracy, requiring the inclusion of non-linear constraints or objective function. A popular subset of NLP is Quadratic Programming (QP), mostly employing linear constraints and a quadratic objective function, commonly used to adopt quadratic models for thermal generators production cost.
- **Dynamic programming** breaks down optimization problems into simpler sub-problems to reduce complexity, then solves sub-problems separately. This approach is particularly useful for problems with sequential decision-making and time-dependent variables.
- **Stochastic programming** addresses uncertainty dealing with random variables and uncertain parameters, optimizing the objective function over a set of possible scenarios, each one with its associated probability, in order to compute the solution that best balances risk and reward. This approach
- **Robust optimization** considers uncertainty in LP models focusing on worst-case scenarios, ensuring that solutions are robust against variations in input parameters, i.e. minimizing the risk of poor performance due to uncertainty.

1.5.4 Energy storage systems optimization

The literature contains numerous studies about the optimization of energy storage systems for the integration of renewable energy sources, especially in micro-grids [49].

A large number of research papers regard electric-only storage technologies, analyzing the system by an electric point of view, i.e. focusing on electrical energy flows, control of power converters, stability and inertia [50], thus taking into account only power-adding (1-port) storage technologies. This approach is justified by the evident superiority of electricity as a convenient energy form to transfer power, especially over distance, but the use of only one energy vector represents a substantial limitation of such studies.

A lot of research papers regarding the optimization of TES and hydrogen storage focus on Power-to-Power (P2P) applications [51], thus utilizing heat and hydrogen only for energy storage, not for power transfer. In this perspective, storage systems are modeled just as black boxes exposing a connection with the electric network, i.e. power-adding storage systems.

Conversely, other studies examine the optimization of energy hubs, i.e. multi-energy systems that involve various energy carriers, such as electric, thermal, gas, and hydrogen. A major advantage of energy hubs is the fully exploitation of the potential of the technologies allowing energy conversion between different forms. To achieve this, both 1-port and 2-port storage technologies are considered. [52] reviews different optimization algorithms regarding planning, operation, and energy trading into energy hubs, showing that most research is based on mathematical methods.

The most widely used method for energy hub optimization is MILP, given the frequent need to include both integer and continuous variables [52]. Despite their complexity, MILP algorithms have become increasingly efficient, even for large-scale problems, thanks to modern solvers and optimization techniques. However, its computational complexity can pose challenges, especially with problems with a large number of integer variables, which may require significant computational resources and time, making it impractical for certain real-time or online applications. Moreover, MILP problems with non-convex objective functions or constraints can be difficult to solve optimally, potentially leading to suboptimal solutions or infeasibility. In addition, overly complex problem formulations can result in modeling inefficiencies.

Accordingly, the author chose MILP for MGTES optimization, falling back to LP to solve problems that would have required an excessive computation time.

1.6 Forecasting algorithms

Forecasting algorithms play a crucial role in various fields, including meteorology, energy, and finance, providing valuable insights and predictions. These algorithms are used to anticipate factors such as weather conditions, energy prices, electricity generation, and consumption patterns. Two fundamental approaches to forecasting, compared below, can be identified.

- **Model-based algorithms, relying on simulations**: they are employed in the context of weather forecasting, especially for predicting variables like solar irradiance and wind speed and direction, to calculate photovoltaic and wind power generation. Such algorithms involve Computational Fluid Dynamics (CFD) simulations, using complex mathematical models to simulate the physical behavior of atmospheric conditions. While these models offer a deep understanding of the underlying physics, they demand substantial computational power and resources.
- **Data-based algorithms, employing neural networks**: they have gained popularity for their ability to capture complex patterns and relationships in historical data, without the need of a model. For forecasting tasks involving markets or human decisions it is not possible to create proper simulation models, thus the data-based approach is the only possible option. In fact, data-based algorithms are commonly used for the forecasting of energy prices and load demand, showing great performance due to their adaptability and data-driven nature, enabling them to handle volatility and uncertainties in energy markets. However, they are also suitable to predict photovoltaic and wind power generation [53]. In this field, the research area receiving the most attention in the last years has been hybrid forecasting methods, i.e. very complex frameworks that are composed of several algorithms [54].

Among data-based algorithms, the most used are Artificial Neural Networks (ANN), that have evolved from one variant to another, e.g. Convolutional Neural Networks (CNN), Recurrent Neural Networks (RNN) and Deep Neural Networks (DNN). In particular, RNNs produce sequential information from time series data, maintaining past information in their internal state, regularly updating it with new data. Thanks to their unique structure, RNNs perform well in time series applications, but require complex training algorithms. In order to address this weakness, Long-Short Term Memory (LSTM) and Gate Recurrent Unit (GRU) have been proposed. These two networks are variants of RNN capable of learning long-term dependencies to generate sequential information from time-series data [55]. Beyond the type of model used, the research on forecasting methods explored the use of multiple models at once, via ensemble learning techniques. Such methods use one dataset to create more than one model, then merged at the end of the procedure. Since they explore more than one way to improve the prediction model, they result in more robust and accurate predictions than traditional methods. The ensemble learning methods are generally categorized into three main groups: bagging, boosting, and stacking [55].

Despite the advancements in forecasting algorithms, it is essential to acknowledge their limitations: one of the significant challenges in forecasting is predicting extreme events. For instance, such algorithms are not able to predict extreme price fluctuations resulting from geopolitical conflicts or financial crises.

Chapter 2

Magaldi Green Thermal Energy Storage

2.1 Overview and components

Magaldi Green Thermal Energy Storage (MGTES) is a TES technology consisting of an insulated tank containing fluidized sand that can be heated using electrical resistors via Joule Effect (Power-to-X applications) or by a hot fluid (Heat-to-X applications), typically steam or hot gases. Stored energy is extracted, when required, in the form of superheated steam or hot air, to be used directly for industrial purposes (X-to-Heat applications) or, when connected to a power block, to generate electricity (X-to-Power applications) [56].

Current research efforts, including this thesis, are directed to P2H applications (Figure 2.1), that use resistors supplied by local renewable sources and/or the power grid as electrical input, and provide superheated steam as thermal output, supplying mid-temperature industrial processes, as partial or total replacement for gas boilers. Therefore, applications other than P2H will not be considered in the following. Neverthless, the software developed for this research, thanks to its flexibility, has the ability to simulate and optimize systems comprising MGTES with any type of input and output, thus virtually covering all its applications.

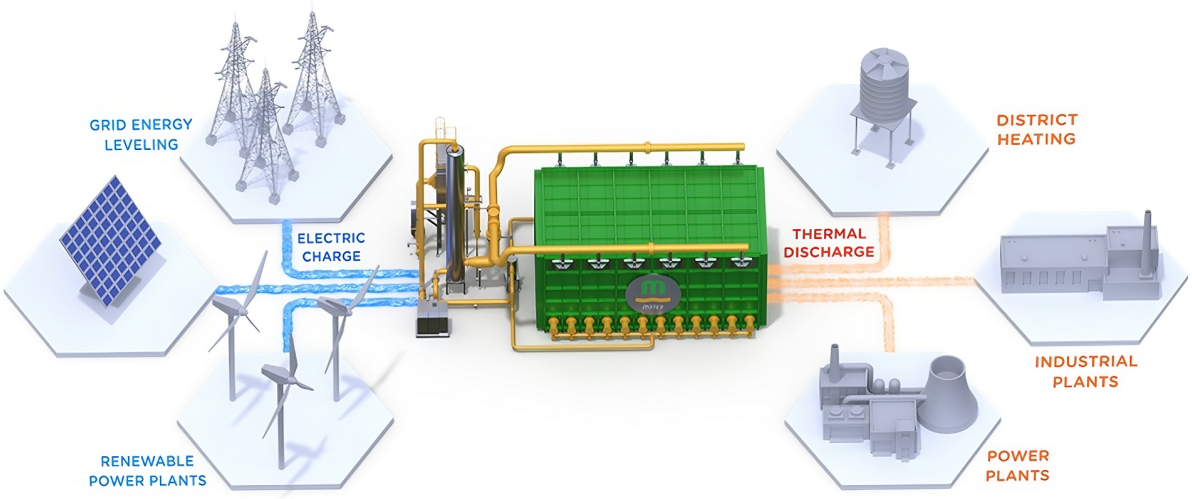

Figure 2.1: MGTES usage in Power-to-Heat applications

Tipically, the size of a MGTES module ranges from 125 to 500 tons of sand, and its thermal storage capacity is between 12 and 48 MWh, depending on the sand mass and its working temperatures (up to 1000 °C without degradation). A first semi-industrial scale-size prototype has been built in Magaldi production facilities near Buccino (SA), Italy.

The main components of a MGTES module are outlined in the following.

- **Sand bed**: simple silica sand (chosen for its environmental friendliness and low cost), contained in a big metal tank, with thermally insulated walls to minimize thermal losses. The bed is equipped with several sensors at different locations and heights: thermocouples to check temperature uniformity and monitor the amount of stored energy, and immersed pressure transmitters to supervise the fluidization state of the bed.

- **Fluidization system**: a compressor blows air into the sand bed through dedicated injection nozzles installed at the bottom of the tank. A fan extracts the air from the upper part of the tank, and conveys it into a filter to remove sand residuals, before it is released to the outside. Compressor and fan are controlled together to ensure proper air speed and pressure, to ensure that the sand bed transitions to a fluidized state, when needed. Such state allows immersed metal elements to freely expand without problems. To increase the efficiency of the fluidization system, an air-to-air heat exchanger pre-heats the (cold) air blown into the tank, transferring heat from the (hot) air extracted from the tank.

- **Steam generation system**: several heat exchangers immersed inside the sand bed and connected in series or in parallel depending on the application. A pump forces a Heat Transfer Fluid (HTF) circulating through the exchangers to adsorb heat from the sand bed. A dedicated control system keeps the output HTF temperature and pressure constant, as required by the industrial process to supply.

- **Electrical heaters**: resistive elements inside the tank, supplied by local renewable sources and/or the electrical grid. A dedicated power control system adjusts the power adsorbed by the resistors, depending on renewable sources availability and grid prices.

MGTES was born as a variant of a similar technology: Solar ThermoElectric Magaldi (STEM) [57], developed by the same company. STEM systems are composed by the same components as MGTES, except for the charging system. In fact, every STEM module has an opening on the top, and acts as a solar receiver, placed in the center of a field of 2-axis tracking mirrors (heliostats) that reflect the sunbeams onto a secondary reflector (beam down), which concentrates the solar radiation into the module, heating the fluidized sand bed, thus charging the storage. In recent years, two STEM prototypes have been built in Italy: a first prototype (500 kWh th) in Buccino (SA), then a bigger one (2 MWh th) in San Filippo del Mela (ME) [58].

Given its great flexibility, the software developed for this research will be easily configured and employed to simulate and optimize also STEM systems.

2.2 Operation

The fluidization system of MGTES (but also STEM) systems, makes their operation different from other storage technologies. Essentially, the sand bed can have two states:

- **Packed**: no air is blown into the bed, so the sand noes not move. This "idle" state is optimal to store energy for a long time without any significant power exchange with the external environment, i.e. only a small power loss occurs through the tank walls.
- **Fluidized**: the bed features excellent thermal diffusivity and heat transfer properties, making this "active" state optimal for energy exchange with the external environment. Keeping the sad bed in such state involves "fluidization losses", due the warm air released to the outside, and the electric power required to supply the air compressor and fan.

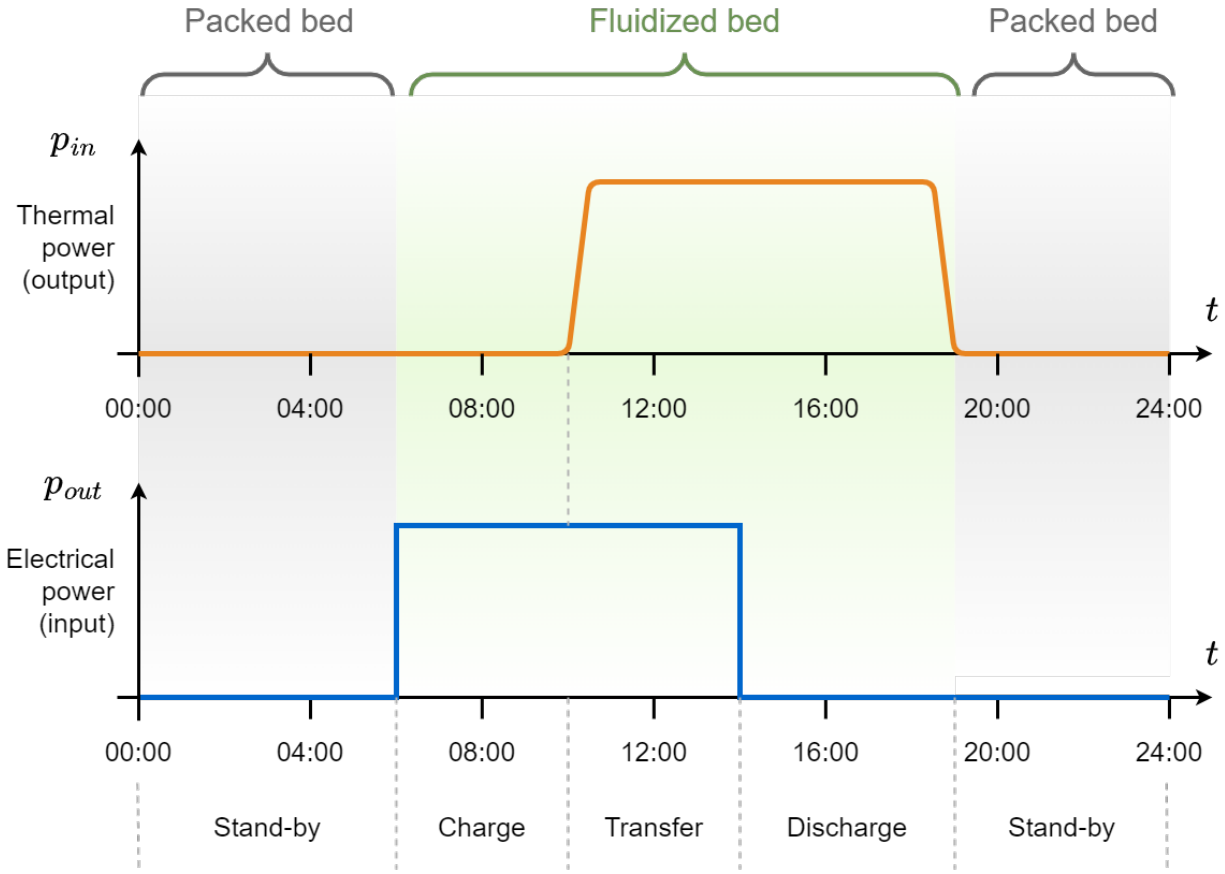

Figure 2.2: Example operation of a MGTES module

An intermediate almost-fluidized state has no advantages, since features low thermal diffusivity, poor heat exchange with immersed elements, and involves fluidization losses. Therefore, the control system of compressor and fan ensures that such state occur only during the transition from packed to fluidized state. The transition from fluidized to packed state is not critical, since it only requires to turn off the compressor and fan.

To minimize losses and maximize MGTES efficiency, the fluidization system is turned on only when needed, i.e. when the electrical heaters are providing thermal power to the sand (charging)

or when the HTF is flowing through the heat exchangers to transfer heat from the sand to supply the industrial process (discharging). It should be noted that, as shown in Figure 2.2, charge and discharge may take place at the same time.

In terms of power, fluidization losses remain constant regardless of the heat power transferred between the bed and heaters or exchangers, so that the only way to minimize the total fluidization losses in terms of energy is to to reduce the time the fluidization system is on. This can be achieved maximizing charging power, to minimize charging time, for the same amount of input energy, and the same holds for discharging. Similarly, charging and discharging simultaneously involves higher efficiency than charging and discharging separately. Undoubtedly, operating MGTES with low input power should be avoided, since in such conditions a considerable portion of the thermal energy dissipated by the heaters is wasted due to fluidization losses.

2.3 Benefits

One of the remarkable strengths inherent to MGTES lies in its remarkable sustainability, characterized by limited environmental and social impact. Specifically, this sustainability encompasses both the landscape perspective and the choice of materials, primarily sand and steel, which are non-polluting, non-hazardous, readily available, and cost-effective. This commitment stands in contrast to traditional TES systems utilizing molten salts and diathermic oils, which come with notable environmental drawbacks [59, 60]. Such materials tend to be corrosive, harmful, and environmentally polluting, creating challenges for disposal at the end of their life cycle [61]. In contrast, MGTES offers a fully recyclable solution: sand can be easily repurposed in the construction sector, while steel components find new life in various industrial and civil applications.

Another significant advantage that MGTES holds over traditional molten salt systems is its ability to store energy over extended periods without significant energy losses. Unlike molten salt systems, which necessitate constant heating to maintain the storage medium at high temperatures and prevent freezing [62], MGTES operates without this demanding requirement.

Beyond sustainability, MGTES features simplicity in construction and modular adaptability. These systems can be tailored to fit any scale, accommodating diverse energy requirements and available spaces, e.g. serving independent installations meeting the energy needs of isolated communities, or larger facilities. Furthermore, this modularity not only enhances reliability but also ensures energy supply continuity, even during module maintenance. This design approach simplifies industrialization, accelerates cost reductions, and facilitates the widespread adoption of the technology, reinforcing the competitiveness of MGTES in the thermal energy storage landscape.

When compared to other P2H technologies like heat pumps and electrical boilers, MGTES offers major advantage through its built-in energy storage capability [63], allowing to achieve high levels of decarbonization. In fact, as explained further on, P2H technologies without storage can be cost-effectively integrated only in specific cases, and moreover, with limited decarbonization potential remains limited. Moreover, despite the impressive efficiency of heat pumps, boasting coefficient of performance values of up to 3 or 4, their heating capabilities are confined to temperatures up to 150 °C. Consequently, heat pumps find their primary use in residential settings, often in conjunction with hot water storage solutions [45].

2.4 Power-to-Heat usage scenarios

MGTES technology can be integrated in industrial processes accomplishing different decarbonization levels, based on the ratio between the thermal energy E^{PR} required by the process and the GHG-free thermal energy E^{MG} provided by MGTES. Thus, three main decarbonization levels are outlined in the following.

- **Partial decarbonization** ($E^{MG} \ll E^{PR}$): only a small part of the total thermal energy required by the process is provided by MGTES. In such scenario the process still relies on fossil fuels to fulfill its heat demand, but the existing non-renewable heat generation systems can work at lower power (with lower emissions). MGTES can always work at its maximum potential and the addition of other modules cost-effectively decreases the emissions.
- **Almost-total decarbonization** ($E^{MG} \sim E^{PR}$): the industrial process is supplied mostly with renewable heat from MGTES. As before, the storage capacity is exploited at its maximum for most of the time. The existing fossil-fuel heat generation systems can be partially decommissioned or maintained as a backup.
- **Total decarbonization** ($E^{MG} = E^{PR}$): the industrial process is supplied solely by MGTES. The system needs to be slightly oversized and redundant to fulfill the heat demand even in the least favorable scenario, i.e. highly cloudy weeks, involving a considerably high investment cost. In this last case, the existing non-renewable heat generation systems can be totally decommissioned.

Thanks to the modularity of MGTES technology, an increasing number of modules can be progressively integrated into a process to achieve progressive decarbonization, from partial to total, by spreading initial costs over a longer period of time.

Real-world industrial processes can have very complex daily heat demand profiles, but in the first instance, it is useful to group them into two categories: "baseload" processes, that require (approximately) constant power over the whole day, and "peakload" processes, that require power only in some hours of the day, and no power during the rest of the time.

Peakload processes can be further split into three categories, presented below, depending on "source-demand simultaneity", i.e. if process heat is required when low-price electric power (from renewable sources or the grid) is available. This categorization is not rationale if considering energy supply by wind, since its production lacks the temporal regularity of solar source.

- **Peakload simultaneous**: processes that require heat only when power is (generally) available from PV, i.e. during mid hours of the day.
- **Peakload partial-shifted**: processes requiring heat in moments when generally available, but also in other moments where not available.
- **Peakload shifted**: processes requiring heat only in moments when power is not generally available, i.e. during the night.

Combining the 4 process categories (baseload plus 3 peakload) and the 3 decarbonization levels presented above, 12 scenarios are possibile, shown in Figure 2.3.

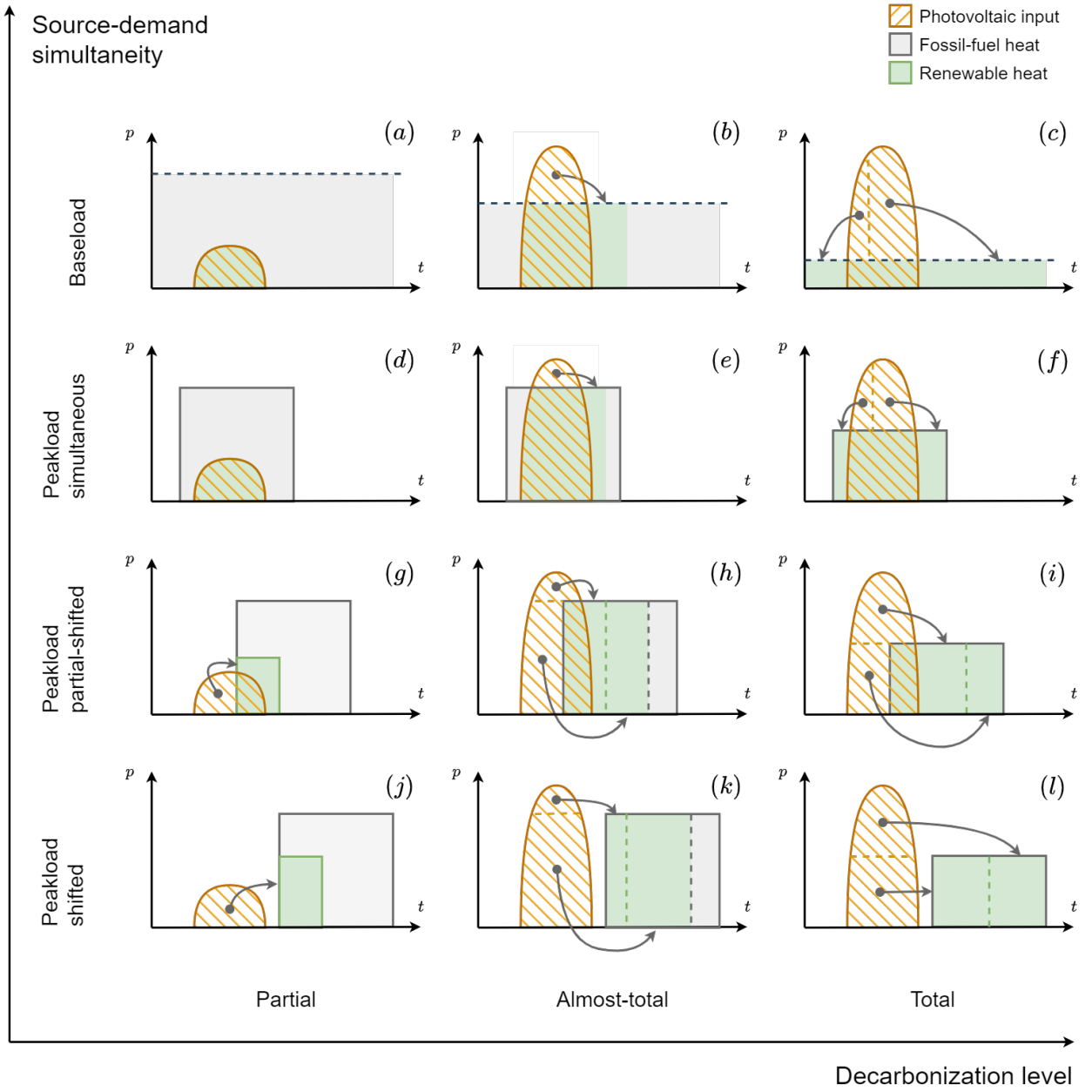

Figure 2.3: Classification of different MGTES usage scenarios based on decarbonization level and source-demand simultaneity

It should be noted that the above classification takes into account only the temporal overlapping of source and demand, without considering the amount of available and needed energy.

In general, as shown in Chapter 1 (Figure 1.5), the overlapping area between source and demand profiles identifies the power directly transferred, i.e. not exploiting storage capabilities. MGTES technology is best suited when the application really needs for storage capacity; if not, alternative P2H technologies, e.g. electrical boilers, may be cheaper for those applications.

As shown in Figure 2.3, baseload and peakload simultaneous scenarios involve total overlapping (of the grey process heat demand profile over the yellow renewable power source profile) only for partial decarbonization levels (scenarios a and d). In such cases, no energy shift is required, thus storage is not needed. All the other 10 scenarios include energy to be shifted, especially j, k, and l, where no overlap exists.

2.5 Grid services

The storage capability of MGTES, which is not common among other P2H technologies, enables the decoupling of input and output power profiles, as discussed in Chapter 1. This creates opportunities for providing ancillary services to the power grid, particularly active power reserve. This involves modulating the electrical power absorbed by the heaters from the grid, as requested by the Transmission System Operator (TSO) according to power system needs, such as grid frequency control. For simplicity, this section describes ancillary services provision by MGTES supplied only by the grid; however, most considerations are also valid for systems supplied both by the grid and local renewable sources.

From a thermal perspective, the substantial thermal capacity of resistive elements allows them to be turned on or off without temperature shocks that may cause the accelerated ageing of the heating elements. This confines the slow response of the air fluidization system (which requires a few minutes to bring the sand bed into the fluidized state) only to the power output, allowing for a rapid electrical response.

On the electrical side, the absorbed active power can be adjusted by acting on the power control devices described in Chapter 3. Different control performances can be achieved depending on the chosen devices and configurations. As described later, simpler devices with limited control ability are associated with lower capital costs, but they may not meet the resolution requirements needed to provide ancillary services. Therefore, the expected revenue from grid services provision should be considered when selecting such devices.

It should be noted that the demand for ancillary services, and the associated economic reward, strongly depends on the location of the grid connection point to which the plant is connected. In fact, various countries, including Italy, adopt a nodal model for its ancillary service market, making it essential to study the impact of grid services for individual case studies. For instance, the use of inverters may enable the system to exchange reactive power with the grid, providing voltage support. However, regulations are still evolving to allow this type of contribution, and accurately quantifying the potential economic revenue from such services is not yet possible.

Regarding active power reserve, it can be provided by either increasing or reducing resistor load, when possible. This depends on the system having sufficient power and energy margins based on current operating conditions. Figure 2.4 illustrates some basic MGTES operation scenarios, showing in blue the baseline power to charge the storage system, and highlighting in red the power reserve band that the heaters can provide to the grid. Two working states of the heaters are considered in the figure, named "L" (Low power) and "H" (High power). The "high power" does not necessarily correspond to the maximum power that can be absorbed by the heaters, to reserve some margin for power increase, and the same holds for "low power", which may not be zero to provide margin for power decrease.

Traditionally, power generators adopt a symmetric power reserve band, offering the TSO the ability to increase or decrease their production by the same amount of power. This implies that if no upward margin is available (when power is maximum), no downward reserve can be provided. Similarly, if no downward margin is available (when power is zero), no upward reserve can be provided. This standard approach is considered in the scenarios depicted in the left part of Figure 2.4.

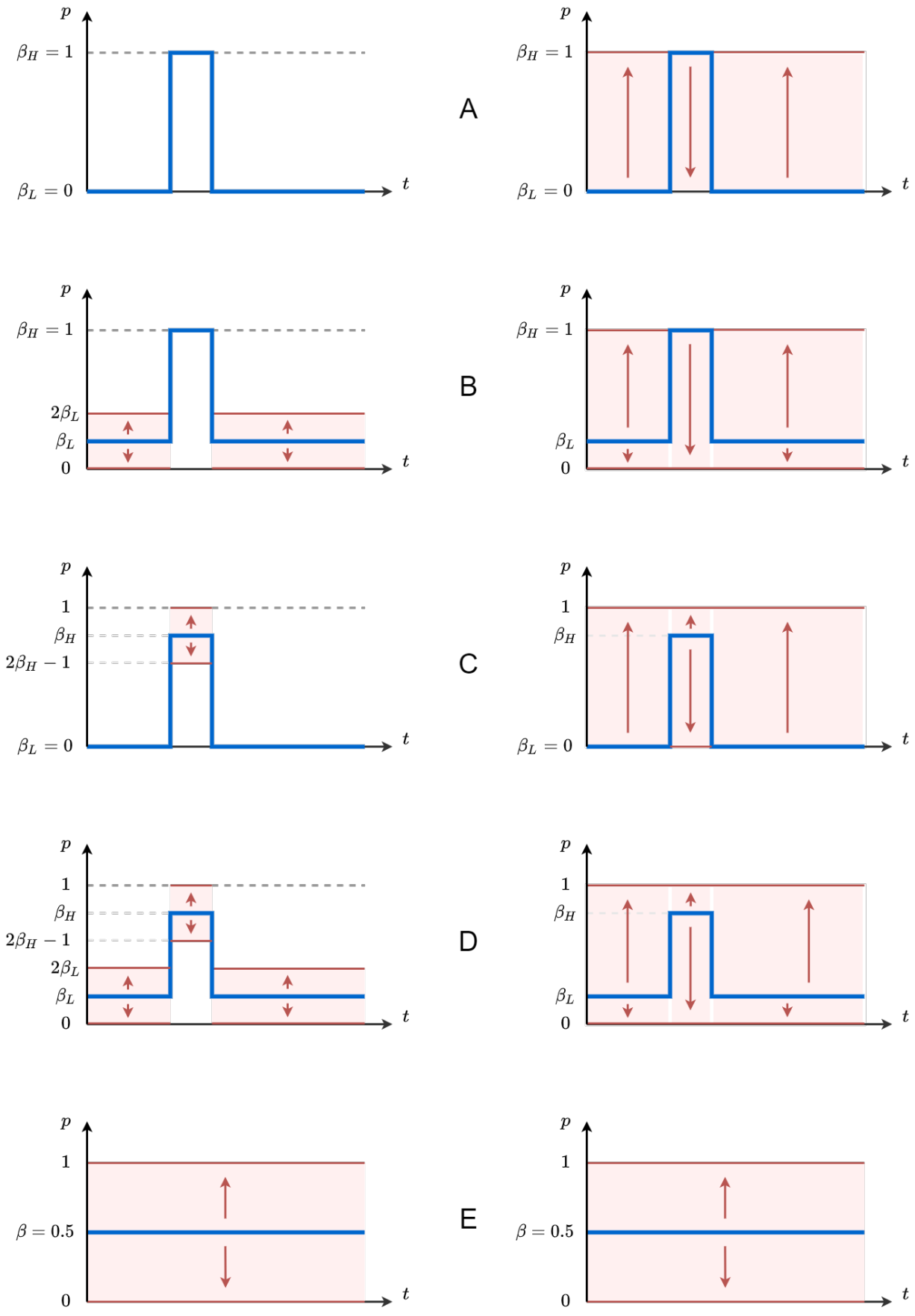

Figure 2.4: Possible basic operation scenarios for grid services provision by MGTES resistors: symmetric power reserve (left) and asymmetric power reserve (right)

Nevertheless, the significant increase in renewable power capacity in recent years has led to increased interest in opening ancillary services markets to non-conventional generation systems and loads [64]. This aims to expand grid flexibility resources to enhance power system reliability and reduce prices of ancillary services. An effective modification to traditional network regulation to facilitate this process is asymmetrical power reserve [65], allowing renewable power plants (or loads) to operate at their maximum power, only providing reserve in one direction. This approach is considered for MGTES in the scenarios depicted in the right part of Figure 2.4.

With asymmetrical reserve, the system is always able to provide its full power margin, whereas the exploitable margin remains limited in most cases with symmetrical reserve. In the following, the five scenarios with symmetrical power reserve are analyzed.

β_L and β_H indicate the absorbed power by the heaters in L and H states respectively, normalized to the maximum power, i.e. $\beta = 0$ corresponds to resistors off and $\beta = 1$ means resistors fully on. In general: $0 \leq \beta_L \leq \beta_H \leq 1$.

- **Scenario A.** $\beta_L = 0$, $\beta_H = 1$: the heaters are controlled only off or fully on, optimized for energy provision without considering ancillary services, operating during low-energy price hours and switched off otherwise. Symmetric reserve cannot be provided.
- **Scenario B.** $\beta_L > 0$, $\beta_H = 1$: the heaters are turned fully on during hours with low energy prices but never switched off completely, providing a symmetric power margin during the rest of the day.
- **Scenario C.** $\beta_L = 0$, $\beta_H < 1$: the heaters are never turned on at maximum power, providing a symmetrical reserve during hours with low prices. In this scenario, the MGTES provides ancillary services only for a few hours per day.
- **Scenario D.** $\beta_L > 0$, $\beta_H < 1$: this scenario combines B and C, always offering symmetric reserve but still taking advantage of low energy prices to collect energy for storage. Such operation may be optimal if the TSO requires a minimum symmetrical reserve amount for the whole day.
- **Scenario E.** $\beta_L = \beta_H = 0.5$: the heaters are always on at half power. This working condition provides the maximum possible power margin in both directions, making it the preferred option when the remuneration for ancillary services is high and well-balanced between upward and downward reserve.

Scenarios B and D are not ideal for MGTES, as they both have $\beta_L > 0$. As mentioned in Section 2.2, since fluidization auxiliaries absorb the same amount of power regardless of the operating conditions of the heaters, turning them on at low power reduces system efficiency. However, such situations could be economically favorable depending on prices of energy and ancillary services. In fact, during periods of high renewable penetration, energy prices are likely to be low (or even negative), but services may be highly rewarded due to the significant power reserve required by the system to handle the large uncertainty associated with massive renewable production.

2.6 Charging process modeling

The mathematical modelling of MGTES charging process is a fundamental step to achieve a proper optimization and control of the system, as it allows to calculate all the relevant quantities in advance. In particular, the knowledge of the time evolution of sand temperature $T_S(t)$ and transferred thermal power $P(t)$, as well as the calculation of the charging time Δt_{ch}, is derived in the following, analyzing the heat transfer between the electrical resistors and the storage medium.

The model will be used in Chapter 3, as a starting point for the optimization of MGTES heaters control, and the design of hardware involved to adjust electrical input power.

2.6.1 Model assumptions

In the model described in the following, the fluidized sand is considered isothermal, at the time-varying temperature T_S, so every portion of the bed is considered at the same temperature; the heaters are also modeled as isothermal, but their temperature T_H is considered constant with time and independent from T_S. The discharging system is not included in the model, i.e. the steam circuit is assumed to be off, since the focus is on the electrical charging system. As the walls of the MGTES module are properly insulated, all the heat losses are neglected, therefore the heat transfer occurs solely from the heaters to the sand.

The specific heat of sand is assumed as constant with good approximation, allowing to consider a linear relationship between the sand bed temperature T_S and the stored energy E. Defining $C = dE/dT_S$ as the heat capacity of the bed (constant by assumption), the total charging time Δt_{ch} can be calculated as follows in (2.2), where t_0 and $t_{100\%}$ are the charging start and end times, and T_0 and $T_{100\%}$ the corresponding sand temperatures.

$$dE = C\,dT_S = P\,dt \quad \rightarrow \quad dt = \frac{C\,dT_S}{P} \tag{2.1}$$

$$\Delta t_{ch} = t_{100\%} - t_0 = \int_{t_0}^{t_{100\%}} dt = \int_{T_0}^{T_{100\%}} \frac{C\,dT_S}{P} \tag{2.2}$$

Solving the integral for each heating mode yields the analytical expression of the charging time, from 0 to 100% of the total storage capacity. The same expression is valid also from t_0 to a generic time instant t, with generic sand temperature T_S. Then, the equation can be inverted to obtain the sand temperature profile over time $T_S(t)$, then the input heat power as in (2.3).

$$P(t) = dE/dt = C\,T_s'(t) \tag{2.3}$$

Actually, any heat transfer process always involves all heat transfer modes (conductive, convective, irradiative), but in a lot of cases is possible to identify a predominant mode. In this context, only the predominant mode will be considered, in order not to overcomplicate the model.

2.6.2 Conductive and convective heat transfer

With conduction and convection heating system (metal elements in contact with sand), the power can be approximated as proportional to the difference between the temperature of the heaters T_H and the temperature of the sand T_S, via Fourier's law (2.4).

$$P = k_C(T_H - T_S) \tag{2.4}$$

In this case, the calculation of charging time, achieved substituting (2.4) in (2.2), temperature and power evolution in time is straightforward.

$$\Delta t_{ch} = \int_{T_0}^{T_{100\%}} \frac{C dT_S}{P} = \int_{T_0}^{T_{100\%}} \frac{C\, dT_S}{k_C(T_H - T_S)} = \tag{2.5}$$

$$= -\frac{C}{k_C} \left[\ln\left(T_H - T_S\right)\right]_{T_0}^{T_{100\%}} = \frac{C}{k_C}\, \ln \frac{T_H - T_{100\%}}{T_H - T_0} \tag{2.6}$$

Inverting (2.6), solving for a generic T_S as a function of a generic time instant t, the well-known exponential expressions for temperature (2.7) and heat power transfer (2.8) of thermal transients are obtained, so the sand temperature T_S raises to the asymptotic value of T_H and the transferred power P decays asymptotically to zero.

$$T_S(t) = T_H - (T_H - T_0)e^{-(t-t_0)k_C/C} \tag{2.7}$$

$$P(t) = k_C(T_H - T_0)e^{-(t-t_0)k_C/C} \tag{2.8}$$

2.6.3 Irradiative heat transfer

If the heat transfer from the heaters to the sand occurs predominantly by radiation, the transferred power P is a function of the fourth power of the temperature of the heaters T_H and that of the sand bed T_S, in accordance with Stefan-Boltzmann's law (2.9), with k_I dependent on various factors (surface area of the emitting bodies and other characteristics). Compared with the previous case, k_I is a totally different quantity from k_C (also in terms of units of measurement).

$$P = k_I(T_H^4 - T_S^4) \tag{2.9}$$

With irradiative heat transfer the calculation of charging time (2.10) is less obvious: the integral in (2.10) can be solved remembering (2.11) whose Taylor expansion in $x = 0$ is (2.12).

$$\Delta t_{ch} = \int_{T_0}^{T_{100\%}} \frac{C\, dT_S}{P} = \int_{T_0}^{T_{100\%}} \frac{C\, dT_S}{k_I(T_H^4 - T_S^4)} = \frac{C}{k_I} \int_{T_0}^{T_{100\%}} \frac{dT_S}{T_H^4 - T_S^4} \tag{2.10}$$

$$\int \frac{dx}{a^4 - x^4} = \frac{tan^{-1}x/a + tanh^{-1}x/a}{2a^3} + c \tag{2.11}$$

$$\frac{1}{a^3}\left(\frac{x}{a} + \frac{1}{5}\left(\frac{x}{a}\right)^5 + \frac{1}{9}\left(\frac{x}{a}\right)^9\right) + o(x^9) \tag{2.12}$$

For $x/a < 0.7$ the only first-order term approximates the exact function with adequate accuracy;

it is advisable to include also the other two terms for values of x/a up to 0.8 and 0.9 respectively. In this context a first-order approximation will be adopted, since for the working temperatures of MGTES heaters and sand the condition $x/a < 0.7$ is always guaranteed.

$$\Delta t_{ch} \approx \frac{C}{k_I}\left[\frac{T_S}{T_H^4}\right]_{T_0}^{T_{100\%}} = \frac{C}{k_I}\frac{(T_{100\%} - T_0)}{T_H^4} \tag{2.13}$$

$$T_S(t) \approx T_0 + \frac{T_H^4 k_I}{C}(t - t_0) \tag{2.14}$$

$$P(t) = \frac{dE}{dt} = C\frac{dT_s}{dt} \approx T_H^4 k_I \tag{2.15}$$

Equation (2.13) shows that, in this approximation, the charging time is approximately linear with the total variation in sand temperature, which means the heat power is considered constant (2.15), i.e. independent of T_S. In fact, the same expression for the charging time can also be obtained by simplifying the original equation (2.10), directly neglecting T_S^4 with respect to T_H^4, yielding (2.16).

$$\Delta t_{ch} = \int_{T_0}^{T_{100\%}} \frac{C}{k_I(T_H^4 - T_S^4)} dT_S \approx \int_{T_0}^{T_{100\%}} \frac{C dT_S}{k_I T_H^4} == \frac{C}{k_I T_H^4}\left[T_S\right]_{T_0}^{T_{100\%}} = \frac{C}{k_I}\frac{(T_{100\%} - T_0)}{T_H^4} \tag{2.16}$$

As mentioned before, these equations will be used in Chapter 3, for the optimization of MGTES heaters control, and the design of the hardware involved to adjust its eletrical input power.

Chapter 3

MGTES power supply hardware

The design of MGTES power supply hardware, described in this Chapter, has been performed taking into account the requirements of loads and sources, considering various aspects, including maturity, cost, reliability and control capability of available technologies.

After a preliminary analysis of loads and sources (Section 3.1), some possible hardware architectures for MGTES electrical distribution system are presented and compared (Section 3.2), addressing reliability aspects and drawing conclusions about topological and redundancy characteristics (Section 3.3).

Afterwards, the attention focuses on heaters, particularly on their control (Section 3.4), and how this impacts on the sizing of MGTES power supply hardware (Section 3.5). Then, different power control devices and schemes are examined (Section 3.6), highlighting their strengths and weaknesses, describing different solutions to achieve different types of control, including a novel solution proposed by the author. A mathematical method is derived to optimize the control to minimize charging time (Section 3.7); finally, the method is applied to the proposed solution to achieve a discrete power control with reduced cost and proper resolution (Section 3.8).

3.1 Loads and sources

The electrical loads included in a MGTES system are listed in the following.

- **Electrical heaters**: they are the most relevant electrical loads, whose power may range from about 2 to 10 MW per module, depending of the sand mass in the tank.
- **Fluidization and steam auxiliaries**: air compressor and fan, HTF pump, valves and sensors. They adsorb a limited power with respect to electrical heaters (between 2 and 3%) and, depending on process requirements, they may be backed-up by a diesel generator or other emergency energy source to ensure continuous steam supply for the industrial process.
- **Control auxiliaries**: industrial computers and logic controllers to collect sensor data and supervise the whole system. They are supplied by dedicated UPS systems.

Possible sources to supply MGTES loads are also listed in the following.

- **The electrical grid**: due to the relatively high power demand of the heaters, a dedicated connection to the HV grid is typically necessary. This implies additional construction costs, but it also enables the provision of grid services to the transmission network.
- **A local renewable power plant**, i.e. a PV field and/or a wind farm. As explained earlier, only a PV plant is considered in the following.

According to the number of available sources to supply MGTES heaters, the possible configurations can be classified into "1-source configurations", which adsorb power either from the grid or renewable sources, and "2-source configurations", which can adsorb power from both [66]. Additional energy storage systems such as batteries are not considered as a source. This classification considers only the energy sources for the heaters, without taking into account an eventual connection to the local public MV distribution grid, that may supply only MGTES auxiliaries. Following this rule, a configuration employing solely a PV field to supply the heaters and the public MV grid only for auxiliaries, is considered 1-source.

Even though the 2-source configuration is the most flexible and effective, it is still worth considering also the 1-source options. Occasionally, the access to energy sources can be particularly difficult or expensive due to several types of practical problems, such as limited available space, authorization problems, opposition of local communities, or long distance to the closest primary substation. Therefore, it might not be possible to obtain both sources, thus having to settle for only one of the two. However, for the sake of generality, 2-source configurations are considered in the following for the design of MGTES electrical hardware.

3.2 Hardware architecture

Due to the modular nature of the PV and MGTES technologies, two system architectures are possible for the electrical connection between PV and heaters, depending on the voltage level used.

- **Point-to-point (LV)**: every PV string supplies a small group of heaters (heater bank), using short indipendent Low Voltage connections.
- **Centralized (MV)**: energy flows from every PV string to the same Medium Voltage system, then to the heaters.

If the PV system is far from the module, it is convenient to switch to MV, to lower capital costs and joule losses. In addition, for megawatt-scale PV systems the choice of the centralized architecture is mandatory: in fact, even placing the module in the middle of the field, the solar panels on the sides would be too far from the heaters. For this reason, only the centralized architecture is suitable for MGTES.

In this case the MV part of the system can be easily connected to the grid, that may act as a backup energy source, providing power when the renewable source is not available. The MV part of the system can be either AC or DC, with the heaters supplied accordingly, to minimize the total number of AC/DC conversions.

Figure 3.1 shows the MVAC configuration, where the PV strings are connected to the MV system through DC/AC inverters and transformers. Other transformers connect the MV system to the AC heaters, whose power is adjusted by some power control components, further described later. The other subsystems are supplied just as before.

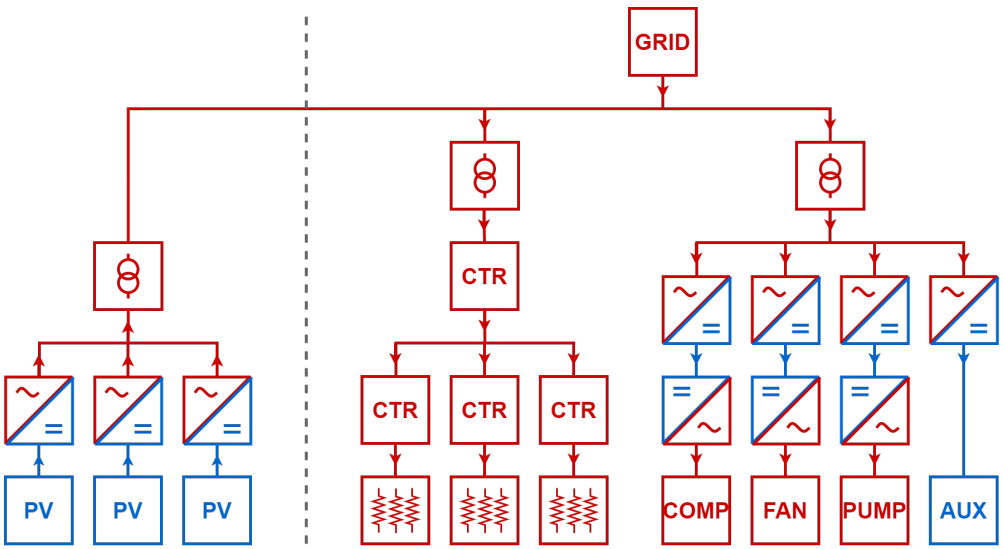

Figure 3.1: MVAC configuration schematic, chosen as the standard one for MGTES

The simpler electrical system architectures for MGTES is the point-to-point (LV) solution, where every heater bank is supplied separately by a set of PV strings and the other subsystems (air fluidization compressor and fan, steam pump, etc.) are supplied by the grid. This architecture can be convenient only if the PV system has limited power and it is located very close to the module, so that the Joule losses in the power cables are negligible.

Figure 3.2 shows a LVDC configuration, where DC/DC converters are used for the coordinated control of PV strings (MPPT) and the heaters power. In the dual solution, point-to-point with AC heaters (LVAC), a full-bridge solar inverter is needed to supply every AC heater bank, but this configuration is not competitive with respect to the DC one, since the cost of DC/AC inverters per unit power is considerably higher if compared with DC/DC converters.

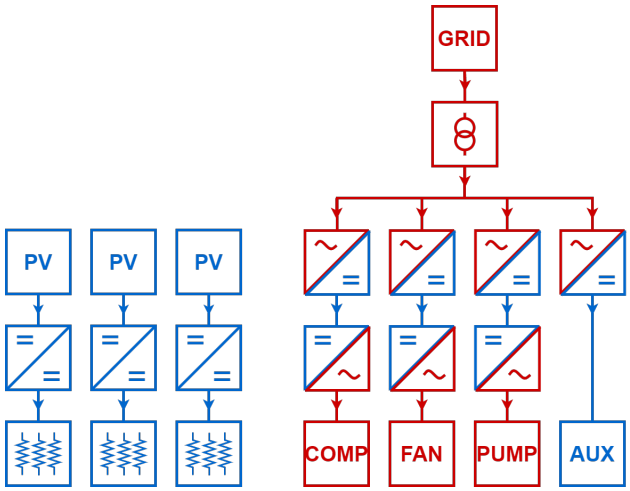

Figure 3.2: LVDC configuration schematic (point-to-point), with DC/DC converters used for the coordinated control of PV strings (MPPT) and heaters

The centralized architecture can be realized also in DC, using dedicated step-down or step-up DC/DC converters for the MV/LV connections between every subsystem (PV, heaters, other) and the MVDC system; as shown in Figure 3.3, PV strings and heaters banks are individually controlled through smaller DC/DC converters. In this configuration, a medium voltage AC/DC inverter is required for the grid connection.

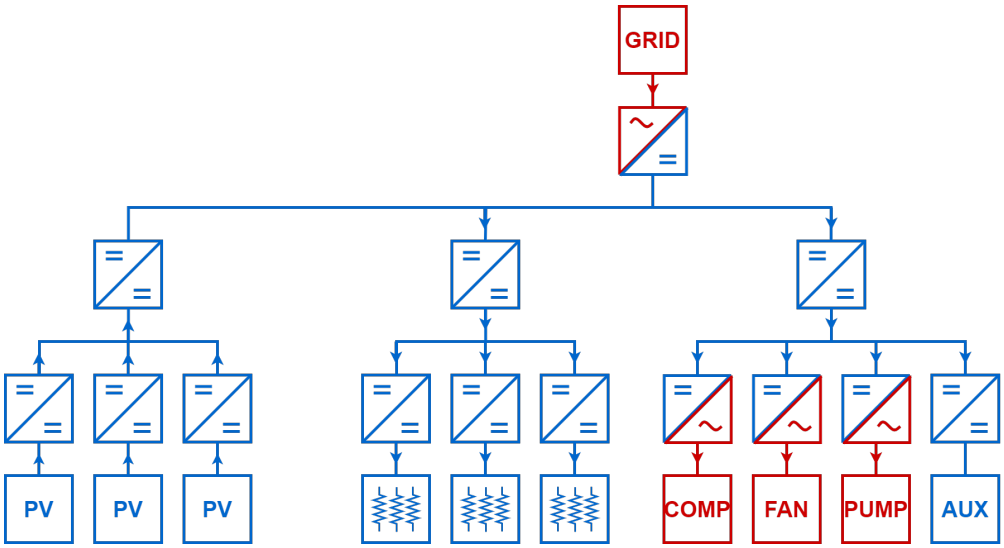

Figure 3.3: MVDC configuration schematic, employing MV AC/DC and DC/DC converters

It should be noted that MVDC technology is still in development and not well consolidated, in fact its cost is quite high if compared to traditional MV equipment. For this reason, the MVAC configuration has been chosen as the standard one for MGTES systems.

3.3 Resistors supply reliability

An important aspect to consider during the design of MGTES power supply hardware is the robustness of the system to various type of faults. In fact, depending on the application, different robustness levels may be appropriate, modifying the base setup with oversized or redundant components, to avoid economic loss in case of malfunction or failure in the system. In this perspective, the optimal reliability level lies in the balance between the increased capital costs associated with oversizing/redundancy, and the reduction in additional costs stemming from failures.

In general, two impacts, discussed in the following, should be considered for every possible fault.

- **Thermal impact**: inability to provide steam to the industrial process. The severity of thermal impact depends on the size of additional (fossil fuel) heat generation capacity contributing in the system, thus on the decarbonization level of the process. In fact, when a fault pertaining MGTES interrupts or limits heat power provision, the process can still be supplied by other sources, if sufficient.

- **Electric impact**: inability to adsorb power and provide ancillary services to the power grid. This impact can be mitigated oversizing heaters and the whole electrical distribution system.

Faults pertaining fluidization or control equipment have both thermal and electrical impacts, since MGTES sand bed cannot be charged nor discharged effectively in the packed state. Such faults are the most severe ones, so redundant fluidization and control components (and backup power sources for them) may be the best choice for a large number of applications. Fortunately, since they adsorb a limited power with respect of the total, the additional cost for increased reliability remains limited.

Regarding the heaters, since the proper supply reliability depends on the decarbonization level, the MV distribution grid topology shall be chosen accordingly, to accomplish the right balance between supply reliability and electrical equipment cost. In the following, one optimal grid topology is presented for every reliability (decarbonization) level. In some cases, other configurations could be more suitable, depending on the available backup (fossil fuel) heat generation capacity, fuel prices and electrical equipment cost.

- **For partial decarbonized processes**, where no special reliability is required, the distribution system shall be radial. For 1-source configurations, MGTES MV distribution grid is trivially a single MV connection from the source to the main MV switchboard. For 2-source configurations, the MV distribution grid consists of two connections, to supply the main switchboard from both sources (Figure 3.4).

- **For almost-decarbonized processes**, the distribution system can be split into two separate sections, so that a single fault on a MV cable only affects a half of the system (Figure 3.5 without dashed switchboard couplers). Each cable is sized considering the nominal power, without any redundancy.

- **For total-decarbonized processes**, the distribution system topology should be dual-fed radial (Figure 3.5), oversizing every cable by 100%. Below is a concise list of what happens in case of fault on one cable.

1. **The breakers open**: this leads to the disconnection of 50% of resistors. Such condition persists for a few minutes or hours, depending on the availability of on-site trained personnel.
2. **The system is reconfigured (manually)**: operators act on the disconnectors and close the proper switchboard couplers (dashed lines in Figure 3.5) to restore the supply to the disconnected part of the grid.
3. **The fault is fixed**: the faulty cable gets replaced and the system is restored to its initial state, with open switchboard couplers.

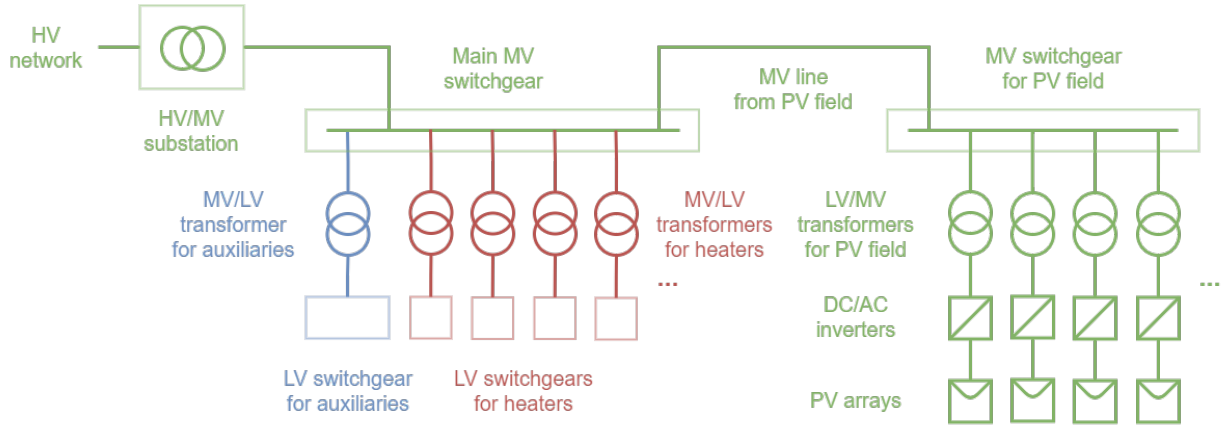

Figure 3.4: MGTES electrical distribution system in 2-source configuration and simple radial topology, suitable for partial decarbonized processes.

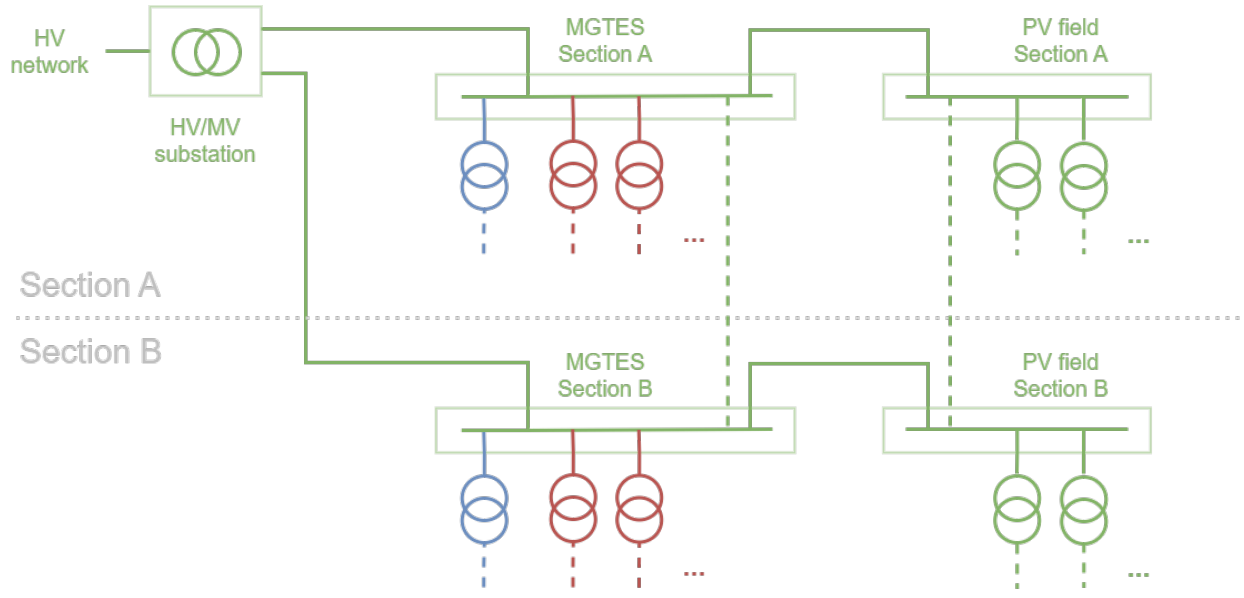

Figure 3.5: MGTES electrical distribution system with dual-fed radial topology (the optimal one for total-decarbonized processes). The optimal configuration for almost-decarbonized processes is the same, removing the switchboard couplers (green dashed lines).

It should be noted that, for 2-source configurations, a fault on a MV cable connecting the main MV switchboard to the grid will not allow to feed the heaters only from the PV field. In fact, most grid-connected photovoltaic DC/AC inverters are "grid-following", i.e. they are not able to work

in island mode, so they have to be shut down upon such fault. Conversely, a fault on a MV cable connecting the main MV switchboard to the PV field, would not harm the grid connection (if the faulty cable is correctly identified by the protection relays and isolated by the breakers).

Electrochemical batteries or other similar types of energy storage systems can be connected to the distribution system in two ways:

- **AC switchboards** through DC/AC inverters and one or more dedicated MV/LV transformers to let them act as harmonic filters. This keeps the other LV grids passive, and allows to use simple protection systems for all LV loads.
- **PV DC-links** through dedicated DC/DC converters, sharing the same inverters of the PV field. This option can be cheaper than the other (lower cost of DC/DC converters with respect to DC/AC inverters), but it requires proper coordination between the converters, thus involving additional complexity in their control systems.

For the AC option, any MV switchboard can be used to connect batteries, without significant difference. Anyway, other practical aspects shall be taken into account when selecting the connection point, such as available space and fire hazard, especially if using Li-ion batteries. If connecting a considerable battery power, demanding a lot of space, a dedicated additional MV switchboard could be needed.

Figure 3.6 summarizes the MV distribution grid topology depending on the decarbonization level (reliability) and available sources. The dark points represent MV switchboards, and the small squares represent couplers; transformers and converters are not shown. Thicker lines indicate +100% cables oversizing.

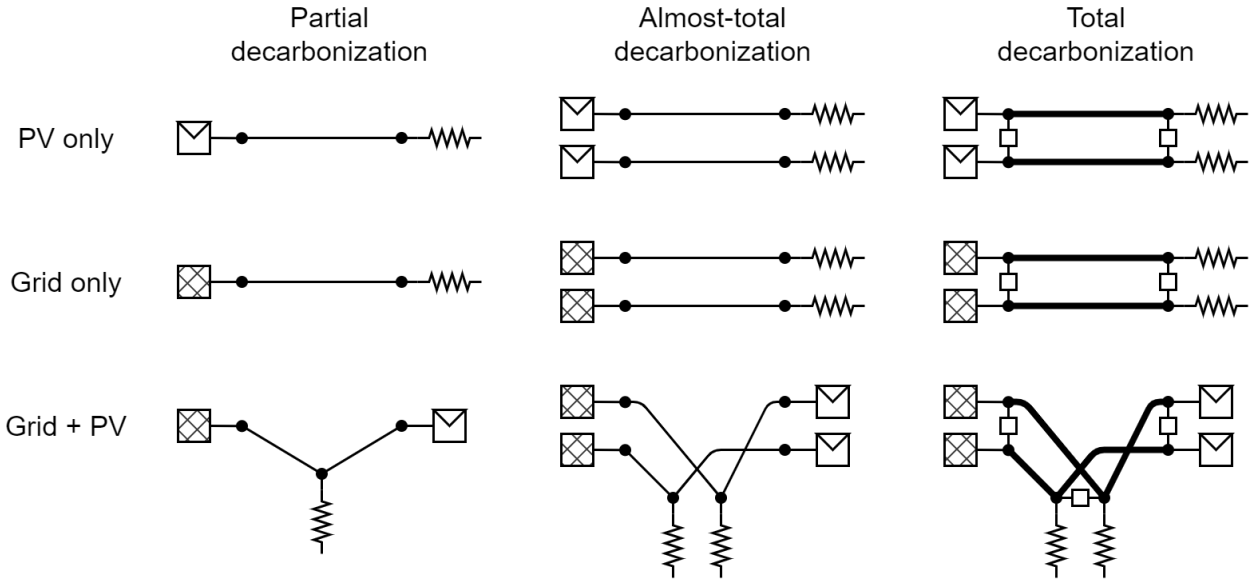

Figure 3.6: MGTES MV distribution grid topology, based on decarbonization level and available sources.

3.4 Heaters power control

3.4.1 Control constraints

The main purpose of MGTES control system is adjusting the input thermal power provided by the charging system to the storage, controlling the electrical power absorbed by the heaters. In order to guarantee the correct operation of the system and maximize its performance, the control system shall operate to meet two types of constraints, classified as internal or external.

- **Internal constraints** are related to the technical limits of the storage components (heaters, sand, electrical distribution system). The compliance with these constraints is crucial: in fact, the violation of the internal ones can result in physical damage to the components due to over-temperatures.
- **External constraints** are related to energy and cash flows exchange between MGTES and its energy sources. The power dissipated into the storage should follow the power produced by the renewable power plant feeding the heaters, and the energy exchange with the grid must respect the scheduled power profiles bid on the energy market. The violation of the external ones results in abnormal power flows, with possible grid imbalances, associated with economic penalties.

The behavior of the control system can be explored form its P-T capability diagram, which shows the limits of the maximum transferable heat power P as a function of sand temperature T_S. Figure 3.7 illustrates two examples of MGTES capability diagram. Each operating point of the system corresponds to a point on the diagram; the grey region, delimited by the curves representing the technical constraints, correspond to the set of the allowed MGTES operating points, that satisfy all constraints.

Unlike the internal constraints, constant over time, the energy source availability depends on solar radiation (or wind), which varies with the time of the day and possible weather disturbances; similarly, the power exchanged with the grid is not constant. Therefore, only the internal constraints are included in the P-T diagram.

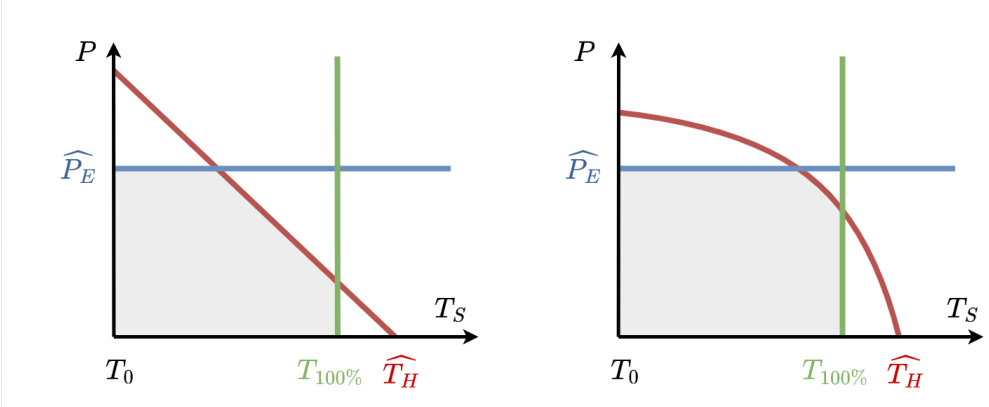

Figure 3.7: Example of MGTES P-T capability diagrams (left: CHT, right: IHT)

Typical MGTES P-T capability diagrams consist of three curves, one for each internal constraint, listed below.

- **Maximum storage temperature (red curve)**: sand temperature must be limited to avoid damaging the casing materials. This curve follows Fourier's law (2.4) for conductive/convective heaters, and Stefan-Botzmann's law (2.9) for radiative heaters.
- **Maximum heaters temperature (green vertical line)**: must be limited to preserve the nominal yield strength of the material.
- **Maximum power of the distribution system (blue horizontal line)**: the thermal limits of the electrical components (transformers, cables, protection devices, etc.) must be respected.

3.4.2 Operating modes

MGTES electrical heaters can work in three operating modes: constant power mode, constant temperature mode, power-tracking mode.

During the initial phase of charging, the heaters can be turned on at the maximum permitted power $\widehat{P_E}$, fully exploiting the thermal limit of the distribution system. Under this condition, the control operates in constant power mode, so the sand temperature rises linearly. The temperature of the heaters T_H raises as well, until reaching the maximum allowed value $\widehat{T_H}$; at this point, the control system switches to constant temperature mode, gradually decreasing the input power keeping the heaters at $\widehat{T_H}$. In this operation mode, the time profiles of sand temperature and heat output follow the equations obtained in Section 2.6. Finally, the heaters must be turned off when the sand reaches its maximum temperature $T_{100\%}$, i.e. when the storage is fully charged. If at some time the PV plant (or other energy source) feeding the system is unable to provide the power required by the heaters, the system switches to power-tracking mode, reducing the input power and controlling the heaters to absorb the whole power produced by the source.

In the above, a totally controllable system is assumed, however, this is possible only equipping the system with proper control devices. In general, 3 control types are possible, listed in the following.

- **Continuous power control** allows to precisely adjust the adsorbed power to the desired set-point, with high resolution. This control type is deepened in Section 3.6.1.
- **Discrete power control** allows to set the adsorbed power to a limited number of pre-defined power values, with low resolution. This control type is deepened in Section 3.6.2.
- **ON-OFF power control** allows only to turn heaters on or off. In contrast to the other ones, this very simple control type will be mentioned but not deepened.

It should be noted that constant temperature and power tracking operation modes can be achieved only with continuous power control, capable of rapidly adjusting the heating power to an arbitrary value. In the case of discrete power control, only constant power operation with pre-defined values can be achieved; when a heat power adjustment is required, the control system settles at a lower power, choosing the pre-defined value closest to the desired heat power. In the case of ON/OFF power control, no adjustment is possible, so the charging system is shut down in the event that the heaters reach the maximum temperature or the available power is insufficient.

3.5 Resistors power supply sizing

During the design phase, it is important to perform a proper sizing of the system, taking into account the P-T capability to achieve an adequate coordination of the technical constraints. The maximum temperature of the heaters is a fixed technological constraint, and the range of the working sand temperatures is chosen according to the characteristics of the required output steam. Instead, a degree of freedom exist for the power of the power supply, which can be used to optimize MGTES toward a flexible, high-performance, yet expensive solution or a simple and cheap one, seeking the best technical-economic trade-off matching the needs of individual applications [67].

The highest flexibility (and cost) is achieved sizing the power supply as to provide the maximum heat power transferable by the heaters to the sand, which is accomplished only with full discharged storage, i.e. sand at its minimum temperature T_0. Continuous power control ensures the freedom to fully exploit the P-T capability (Figure 3.8). In this case, the power supply is oversized if compared to its average usage; the heaters, on the other hand, always operate at their maximum temperature (constant temperature operation mode), except when power-tracking operation is needed.

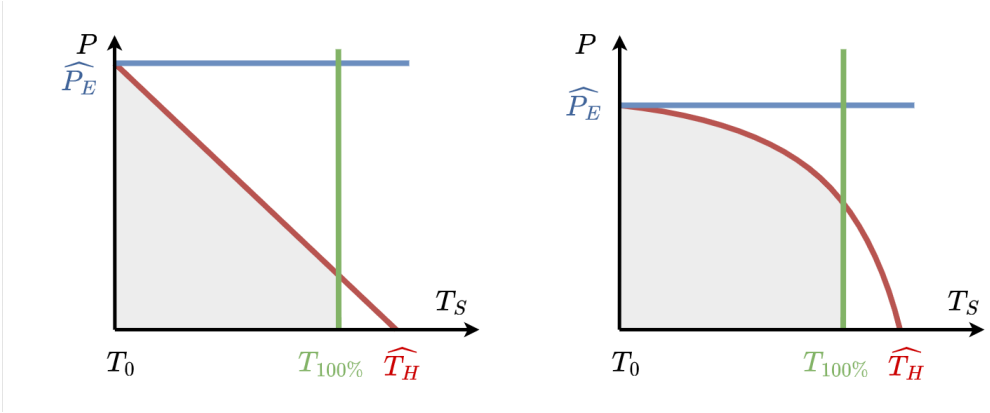

Figure 3.8: MGTES P-T capability with continuous power control (left: CHT, right: IHT)

A cheaper and simpler system can be realized sizing the power system to the maximum transmissible power of the heaters when the sand is at its maximum temperature $T_{100\%}$, i.e when the storage is fully charged. Compared to the previous case, the P-T capability is reduced considerably, losing its upper part, highlighted in yellow in Figure 3.9. On the other hand, the power supply operates always at its maximum power, thus discrete control or ON/OFF control can be used without significant loss in system performance, if permitted by the power tracking needs required by the application. It should be noted that, focusing on the red curves in the diagrams of Figure 3.7, since in CHT the heat power is linear with the sand temperature, the max temperature limit is represented by a line in the left P-T capability and the heat power decrease is constant along the diagram. On the other hand, in IHT the heat power exhibits a slow decrease for low values of sand temperature, but decreases faster near higher temperatures, due to the fourth powers in the Stefan-Boltzmann equation (2.9). This results in higher loss of capability in the CHT mode, resulting in longer charging times if compared to IHT.

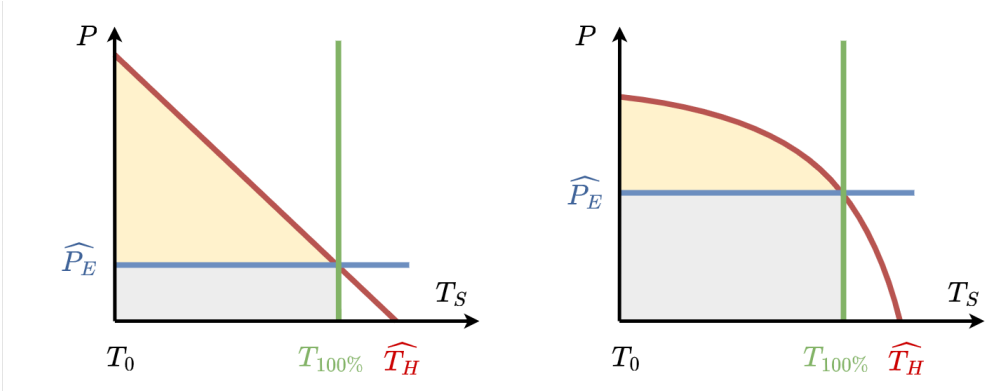

Figure 3.9: MGTES P-T capability with ON/OFF power control (left: CHT, right: IHT)

A balanced solution can be achieved sizing the power supply system at an intermediate power between the previous cases, with P-T capabilities shown in Figure 3.10. In this case, it may be convenient to employ a discrete power control, which, with respect to continuous control allows less flexibility at lower costs. This solution will be studied in detail in Sections 3.6.2, 3.7 and 3.8, optimizing power steps and presenting some hardware solutions that realize this control.

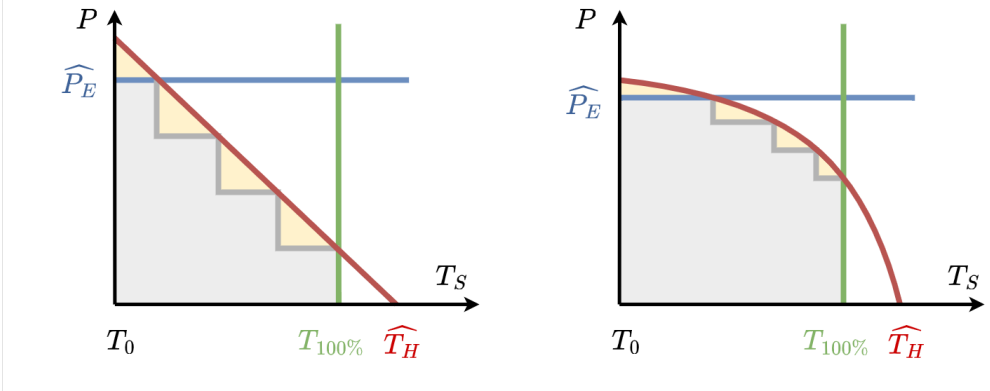

Figure 3.10: MGTES P-T capability with discrete power control (left: CHT, right: IHT)

3.6 Power control devices

As anticipated in Section 3.4, the electrical power adsorbed by MGTES heaters can be controlled using different devices, achieving 3 control types: continuous, discrete or ON/OFF control.

ON/OFF control to is the simplest and straightforward control type, achieved connecting or disconnecting individual heater banks to its supply through mechanical contactors. Despite being the least flexible solution, it should not be ruled out a priori, as it may be the most convenient in some cases where fine power control is not required. In fact, contactors have longer technical life than other control technologies, with fast response time and no Electro-Magnetic Compatibility (EMC) problems.

The next sections delve into the description of the other two types, describing the devices that can be employed to achieve them, along with a comparison of the main advantages and disadvantages of every technical solution. Table 3.1 summarizes the key differences between the components included in the analysis: power electronics, transformers with On-Load Tap Changers (OLTC), and mechanical contactors.

Technology	Power electronics	OLTC	Contactors
Control mode	Continuous	Discrete	Discrete / ON-OFF
Resolution	High	Medium	Medium / Low
Response time	Fast (∼ms)	Slow (∼s)	Fast (∼ms)
Technical life	5-10 years	15-20 years	25-30 years
EMC problems	Yes	Transient	No

Table 3.1: Comparison of different devices for MGTES heaters power control

3.6.1 Continuous power control solutions

Continuous control allows to adjust the power adsorbed by MGTES heaters to the desired set-point, with high resolution. It is undoubtedly the most flexible control type and can be easily achieved with different power electronic devices. In the scientific literature, consistent research efforts have been directed to the development of several types of power electronic systems for different context, ranging from long-distance high-power transmission to low-power consumer applications. Focusing on industrial energy intensive industrial processes, most applications involve electro-chemical reactions, requiring high DC currents, provided by high-power rectifiers. This applications include example aluminum smelters (primary production of aluminum), chlor-alkali processes (production of common industrial chemicals), and electro-winning (production of copper, zinc, and other non-ferrous metals) [68]. A trending application requiring high-power rectifiers is water electrolysis for green hydrogen production, using excess renewable energy.

Most studies on power electronic converters collectively support the utilization of newer power electronics technologies to achieve faster control, higher power factor, and reduced harmonics in the grid. For instance, in [69], the author compares different types of converters (used for hydrogen production via electrolysis), showing that while simpler designs are cost-effective, they exhibit more harmonics. Similarly, (for the same application) [70] proposes an AC/DC conversion system using diodes and IGBTs with improved power quality performances. Other energy intensive industrial

applications involve heating and welding, not requiring DC current, thus sometimes using cheaper power control solutions such as thyristor-based AC regulators or cycloconverters. These solutions usually require dedicated filters to tackle EMC issues, to avoid disturbing other loads or interference with near electronic equipment.

For the MGTES scale-size prototype in Buccino (Italy) thyristor-based AC regulators have been installed, solving EMC problems using a Zero Voltage Switching (ZVS) modulation, achieving a fast and flexible continuous power control.

Such solution can be used also in full-scale MGTES systems, making sure to employ delta connections for the primary windings of the transformers supplying the resistors. This ensures low equivalent zero-sequence impedance at the secondary side, reducing harmonics and switching over-voltages, thus increasing transformers life. Figure 3.11 shows a comparison of two simulations involving different connection types for the primary winding of the transformer. The simulation has been performed using Simscape Eletrical, modeling a test system with star-neutral connected resistors, supplied by a distribution transformer (6% short circuit impedance) sized on the nominal current of resistors. The solution with star-connected primary winding (leftmost charts) exhibits asymmetrical currents and distorted line voltages, whereas the delta connection (rightmost charts) significantly contributes to current balancing and voltage harmonics limitation.

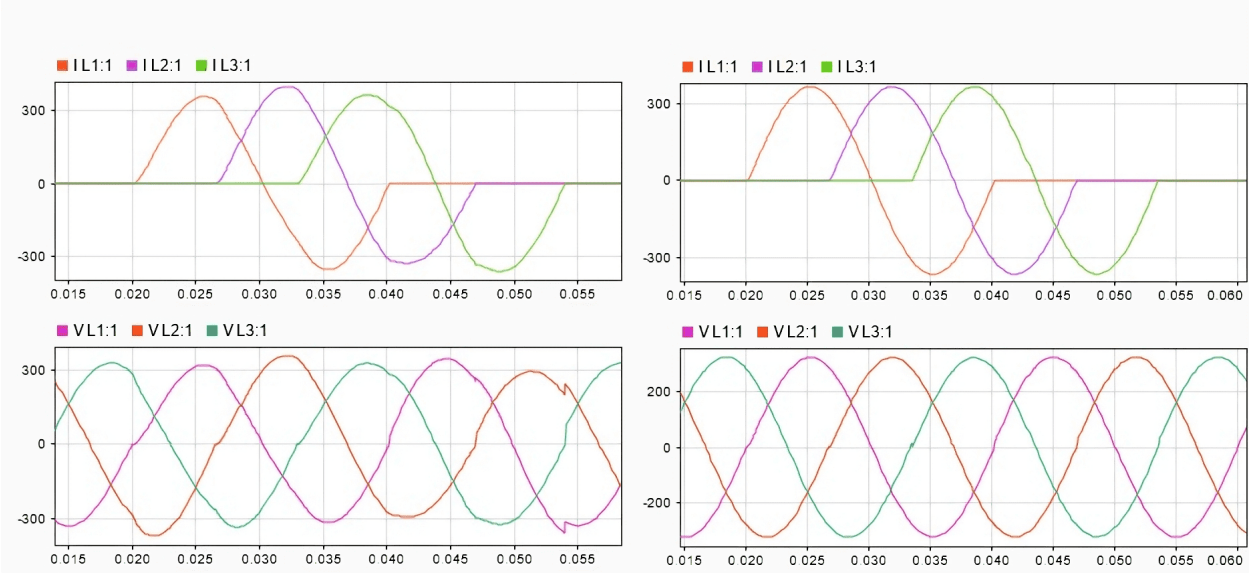

Figure 3.11: Comparison of line currents (top) and secondary voltage (bottom) of an MGTES transformer, using different connections for primary winding: star without neutral (left) and delta (right).

In general, power electronic systems pose problems of rapid component obsolescence and difficulties in the procurement of semiconducting materials, leading to higher costs. On the other hand, such a rapid and accurate control can be obtained with no other solution, so enough to be the preferred technology in several applications. Since MGTES technology developement aims towards cost reduction, high reliability and recyclability, solutions based on power electronics are not preferable where not strictly necessary. Therefore, different technical solutions for power control have been investigated, and described in the next Section.

3.6.2 Discrete power control solutions

Discrete control allows to set the adsorbed power to a limited number of pre-defined power values, with low resolution. It can be achieved in different ways, employing star-delta reconfiguration techniques, using OLTC for heaters transformers, or both.

Star-delta contactors represent a robust and economical solution to achieve discrete control, but they allow to set only two power values for each heater bank: 100% (delta) or 33% (star). Figure 3.12 shows the P-T capabilities of MGTES system with discrete power control achieved using star-delta contactors.

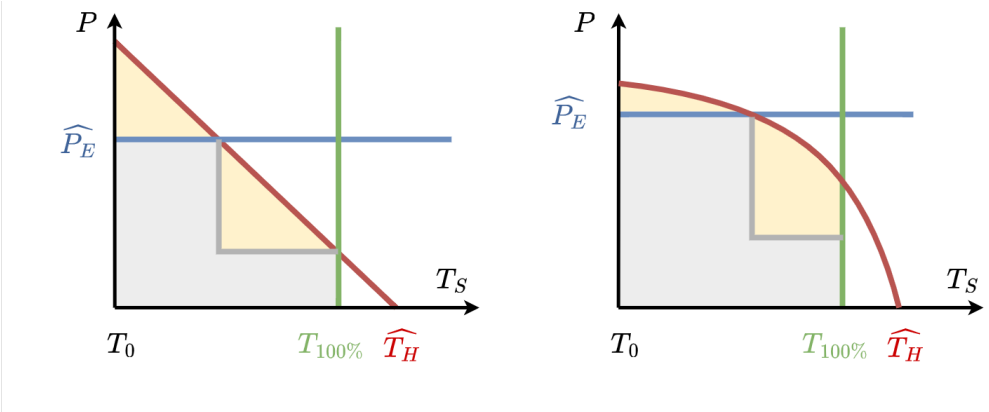

Figure 3.12: MGTES P-T capability with discrete power control achieved using star-delta contactors (left: CHT, right: IHT)

Another potential solution to adjust the power adsorbed by MGTES resistors is the use of transformers with OLTC, commonly used in power systems to adjust grid voltage. Compared to power electronics, OLTCs represent a more robust, reliable and established technology, due to their widespread use in power systems.

Regardless its advantages, discrete power control with OLTCs has limited flexibility, as the tap change process is quite slow, with commutation times in the order of seconds. To fasten tap change, solid-state OLTC solutions have been proposed in the literature [71]. A major problem, found both in mechanical [72] and electronic tap changers [73], are switching over-voltages generated during commutation between taps, which stress the transformer insulation and the other electrical components connected to the system. In addition, voltage regulation can only be performed in a relatively small range around the nominal value (e.g. ±10-20%), and one OLTC acts on all the heaters supplied by the same MV/LV transformer, without individual power control on smaller load groups.

Traditionally, OLTCs are responsible for changing the connection between the taps of the transformer primary windings and the variable-voltage supply network, in order to adjust the secondary voltage to a constant value. It should be noted that, when using a tap changer on the primary windings, the magnetic flux in the transformer core is approximately proportional to the secondary windings voltage. In this case, the magnetic flux is kept constant by the the secondary voltage control performed by the OLTC. On the other hand, OLTCs for MGTES heaters control should have the opposite purpose: varying the secondary voltage, with constant primary voltage.

Unlike the traditional case, in an MGTES system the control performed of OLTCs varies the magnetic flux with the voltage applied to the heaters; in order to achieve wider voltage control

ranges (e.g. ±50%), the flux variability requires oversizing the core to avoid its saturation, leading to higher material usage, thus to additional costs for the transformer. The transformer oversizing could be solved using a tap changer acting on the secondary windings; however, such devices are not widespread, so it may be hard to find them on the market with competitive prices. Using commercial OLTCs connected to LV secondary windings is not cost-effective, since the OLTCs would have an oversized (MV) insulation with respect to their effective working conditions (LV) in MGTES systems.

3.6.3 Discrete power control solutions using CSTS

The author addressed the problems related to OLTCs proposing a custom configuration: Contactors as Secondary Tap Selector (CSTS), which employ transformers with multiple taps on the secondary windings, using contactors to connect the heaters to the desired tap. Contactors must be interlocked to avoid connecting the same heaters bank to multiple taps at the same time, realizing a short circuit between taps at different voltages.

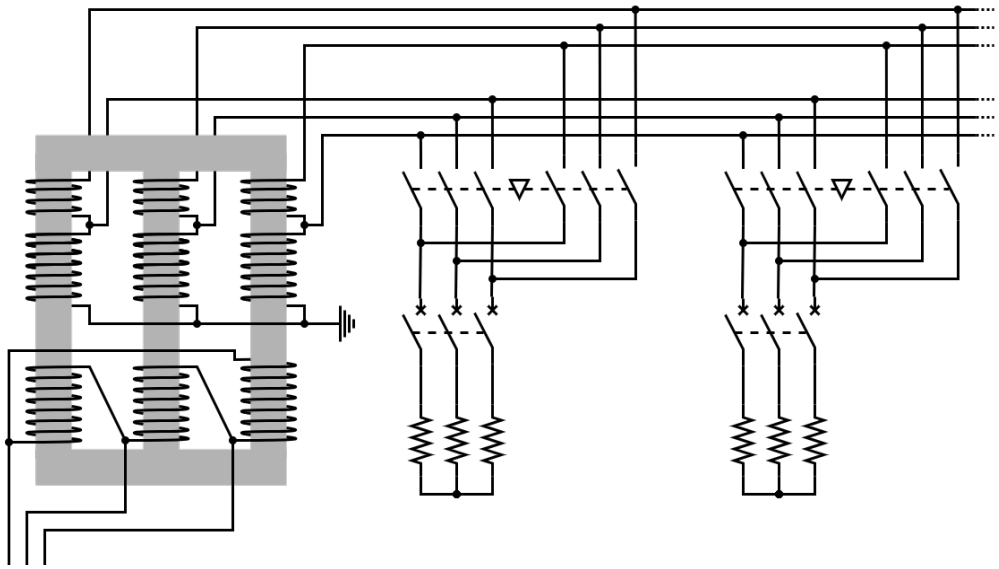

Figure 3.13: Basic schematic of a simple CSTS configuration with two taps, for two resistor banks

With respect to OLTC, the CSTS solution imposes lower insulation stress on transformers and, for the same number of taps manufactured on the transformers, CSTSs allow for higher resolution than OLTCs. In fact, as shown in Figure 3.13, several independent CSTS systems can be used for each transformer, one for each heaters bank. Unfortunately, the CSTS solution requires the construction of non-standard transformers, and their cost could raise significantly with the number of taps. Moreover, the control at low power values can be problematic, since the reduction in the supply voltage modifies fault currents, posing selectivity problems for the protection system. Nevertheless, it remains an interesting solution, as it allows to achieve a discrete control over an arbitrary set of power steps.

For a single resistors bank, the CSTS solution requires one transformer tap and one contactor for every power step, thus resulting in an equal number of contactors N_C, taps N_T and power steps N_S ($N_T = N_C = N_S$).

As shown in Figure 3.14, the CSTS configuration can be combined to star-delta contactors to double the number of power steps ($N_S = 2N_T$), since the resistors can connected to every tap in two ways (star and delta). This "advanced CSTS" configuration introduces two additional contactors for every heaters bank ($N_C = N_T + 2$). This results in fewer contactors and taps, for the same number of power steps, reducing contactors cost, and transformer complexity and cost compared to the "simple CSTS" solution described before, as shown in Table 3.2.

In addition, power steps with star connection involve lower current in cables, reducing power losses, and higher short circuit current, mitigating selectivity problems. This benefit alone is worth adopting the advanced CSTS solution even when an equal number of contactors is needed, i.e. $N_T = 2, N_C = 4, N_S = 4$.

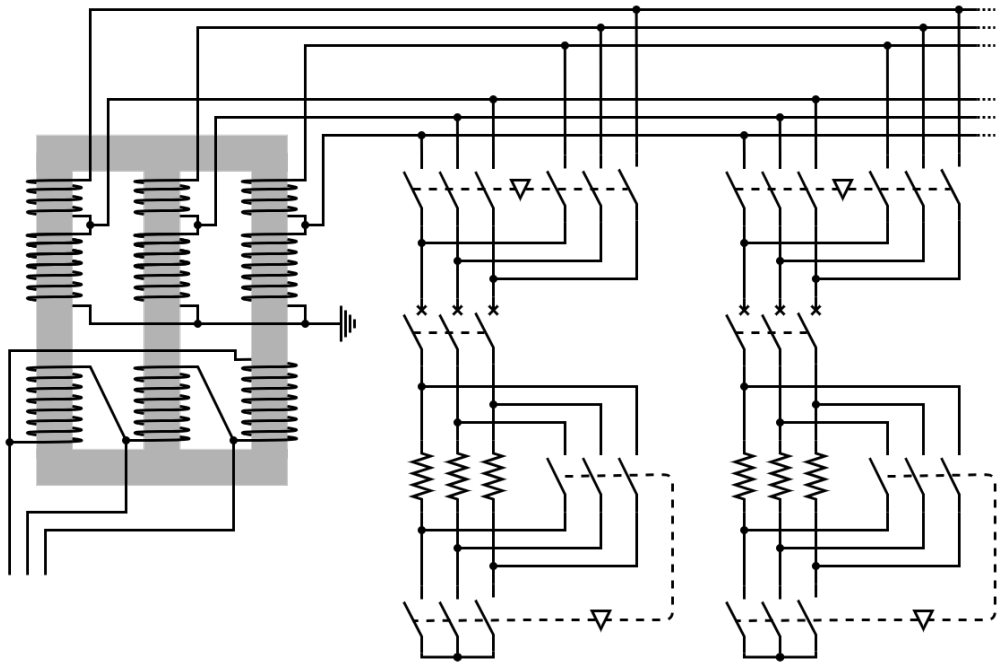

Figure 3.14: Basic schematic of the advanced CSTS configuration with two taps, for two resistors banks

		Simple CSTS				**Advanced CSTS**			
Number of power steps	N_S	2	4	6	8	2	4	6	8
Number of contactors	N_C	2	4	6	8	2	4	5	6
Number of taps	N_T	2	4	6	8	1	2	3	4

Table 3.2: Comparison in the number of contactors, taps and power steps between simple and advanced CSTS solutions for discrete power control of a single heaters bank

3.7 Discrete control steps optimization

If employing a discrete control, the electrical heaters can adsorb only a specific pre-determined set of n power values $P_1, ...P_k, ..., P_n$. For each power value P_k, a corresponding sand temperature value T_k has to be defined, so that the power control system can set $P = P_k$ when $T_{k-1} < T_S < T_k$. Since discrete control does not allow to exploit the full capability, the system can benefit a lot from the optimization described in the following, aiming to find the P_k and T_k values that allow minimizing the charging time, that corresponds to the maximization of the average adsorbed power. For sure, the optimal points must be on the capability curve, to maximize the power adsorbed for each step and reduce the capability loss (yellow area). As shown in figure 3.15, the first power step P_1 can be set to the maximum power of the power supply $\widehat{P_E}$ and the last power step P_n can be set so $T_n = T_{100\%}$. The other $n-2$ points $P_2, ..., P_j, ..., P_{n-1}$ must be chosen to minimize the total charging time $\Delta t_{ch} = \sum_{k=1}^{n} \Delta t_k$, calculated as the sum of the charging times Δt_k for each step, where $T_{k-1} < T_S < T_k$, so (2.2) becomes (3.1).

$$\Delta t_k = \int_{T_{k-1}}^{T_k} \frac{C dT_s}{P} = \frac{C(T_k - T_{k-1})}{P_k} \quad \rightarrow \quad \Delta t_{ch} = \sum_{k=1}^{n} \Delta t_k = C \sum_{k=1}^{n} \frac{T_k - T_{k-1}}{P_k} \tag{3.1}$$

Since the optimal power values depend on the heaters capability, they are different if using conductive/convective or irradiating heat transfer. Both cases are considered below.

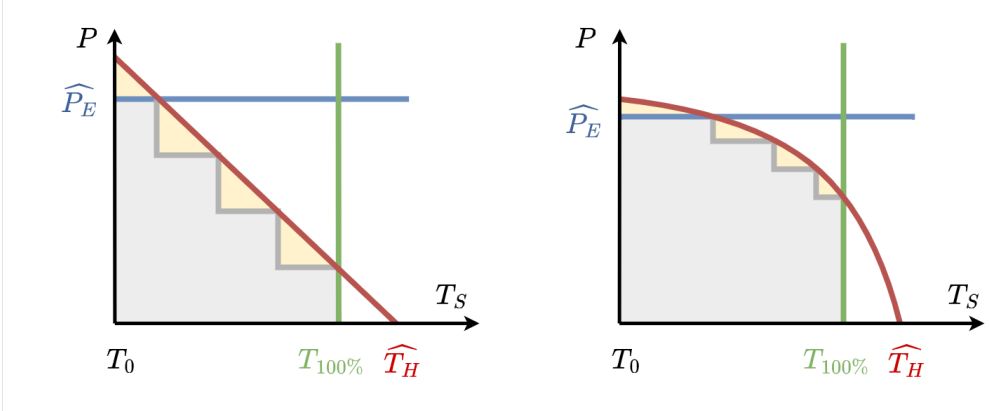

Figure 3.15: MGTES P-T capability with discrete power control (left: CHT, right: IHT)

3.7.1 Conductive/Convective Heat Transfer (CHT)

As described in Section 5, in this mode the transferred heat power is linear with the sand temperature, hence (2.4) can be rewritten as (3.2), then substituted into (3.1) to obtain (3.3).

$$P_k = k_C(T_H - T_k) \quad \rightarrow \quad T_k - T_{k-1} = -\frac{1}{k_C}(P_k - P_{k-1}) \tag{3.2}$$

$$\Delta t_{ch} = -C \sum_{k=1}^{n} \frac{P_k - P_{k-1}}{k_C P_k} = \frac{C}{k_C} \left(\sum_{k=1}^{n} \frac{P_{k-1}}{P_k} - n \right) \tag{3.3}$$

For a given n, the minimization problem for Δt_{ch} (3.3) can be simplified and rewritten without the constant positive quantities C, k_C, n as (3.4).

$$min_{P_j} \frac{C}{k_C} \left(\sum_{k=1}^{n} \frac{P_{k-1}}{P_k} - n \right) \rightarrow \min_{P_j} \sum_{k=1}^{n} \frac{P_{k-1}}{P_k} \tag{3.4}$$

The solutions of the minimization problem (3.4) can be found calculating the partial derivatives of the quantity to minimize, with respect to the unknown variables P_j, and equalling them to zero, yielding (3.5).

$$\frac{\partial}{\partial P_j} \sum_{k=1}^{n} \frac{P_{k-1}}{P_k} = 0 \qquad j = 2, ..., n-1 \tag{3.5}$$

Since P_j appears in the summation terms of (3.5) only for $k = j$ and $k = j + 1$, they are the only ones with non-vanishing derivative, to be considered for the optimization, giving (3.6).

$$\frac{\partial}{\partial P_j} \left(\frac{P_{j-1}}{P_j} + \frac{P_j}{P_{j+1}} \right) = -\frac{P_{j-1}}{P_j^2} + \frac{1}{P_{j+1}} = 0 \quad \rightarrow \quad \frac{P_{j-1}}{P_j} = \frac{P_j}{P_{j+1}} \tag{3.6}$$

$$\frac{P_{j+1}}{P_j} = r \quad \rightarrow \quad P_{j+1} = P_j r \tag{3.7}$$

Equation (3.7) shows that the charging time is minimized if, for each power value P_j, the ratio between the previous one and itself is the same of the ration between itself and the next one. Since this is true for every step, the ratio r between two contiguous values should be always the same, i.e. the optimal power steps follow a geometric progression. As a consequence, P_j can be calculated directly as is (3.8).

$$r = \sqrt[n-1]{\frac{P_n}{P_1}} \qquad P_j = P_1 r^{j-1} \tag{3.8}$$

3.7.2 Irradiative Heat Transfer (IHT)

As described in Section 5, in this mode the transferred heat power is not linear with the sand temperature, so a different approach is required to solve the optimization problem. In this case it is convenient to define the optimization problem on T_k rather than P_k, yielding (3.9), and calculate the derivatives with respect to T_j, giving (3.10). Just as in the previous case, in (3.10) T_j appears in the summation terms with $k = j$ and $k = j + 1$, giving (3.11).

$$\Delta t_{ch} = C \sum_{k=1}^{n} \frac{T_k - T_{k-1}}{P_k} = C \sum_{k=1}^{n} \frac{T_k - T_{k-1}}{k_I (T_H^4 - T_k^4)} \tag{3.9}$$

$$\frac{\partial}{\partial T_j} \sum_{k=1}^{n} \frac{T_k - T_{k-1}}{T_H^4 - T_k^4} = 0 \qquad j = 2, ..., n-1 \tag{3.10}$$

$$\frac{\partial}{\partial T_j} \left(\frac{T_j - T_{j-1}}{T_H^4 - T_j^4} + \frac{T_{j+1} - T_j}{T_H^4 - T_{j+1}^4} \right) = 0 \quad \rightarrow \quad \frac{T_H^4 + T_j^3 (3T_j - 4T_{j-1})}{(T_H^4 - T_j^4)^2} - \frac{1}{T_H^4 - T_{j+1}^4} = 0 \tag{3.11}$$

$$\frac{T_H^4 - T_j^4 + 4T_j^3(T_j - T_{j-1})}{T_H^4 - T_j^4} = \frac{T_H^4 - T_j^4}{T_H^4 - T_{j+1}^4} \tag{3.12}$$

Approximating $2T_j^2$ to $(T_j^2 + T_{j-1}^2)$ and $2T_j$ to $(T_j + T_{j-1})$, the numerator of the first member of (3.12) becomes $T_H^4 - T_{j-1}^4$, yielding (3.15).

$$-T_j^4 + 4T_j^3(T_j - T_{j-1}) = -T_j^4 + (2T_j^2)(2T_j)(T_j - T_{j-1}) \approx \tag{3.13}$$

$$\approx -T_j^4 + (T_j^2 + T_{j-1}^2)(T_j + T_{j-1})(T_j - T_{j-1}) = -T_j^4 + (T_j^4 - T_{j-1}^4) = -T_{j-1}^4 \tag{3.14}$$

$$\frac{T_H^4 - T_{j-1}^4}{T_H^4 - T_j^4} = \frac{T_H^4 - T_j^4}{T_H^4 - T_{j+1}^4} \tag{3.15}$$

Substituting back P_k into (3.15), the same result as the previous case is achieved, i.e. the optimal power steps follow a geometric progression.

$$\frac{T_H^4 - T_{j-1}^4}{T_H^4 - T_j^4} = \frac{T_H^4 - T_j^4}{T_H^4 - T_{j+1}^4} \quad \rightarrow \quad \frac{P_{j-1}}{P_j} = \frac{P_j}{P_{j+1}} \tag{3.16}$$

3.7.3 Result interpretation

Equation (3.8), valid for both heat transfer modes, shows that, fixing the number of power steps, an optimal power control is achieved using lower resolution at the beginning of the charging process and higher resolution at the end. Therefore, a higher resolution it is desirable near the lowest power values.

In fact, as evidenced by the right chart in Figure 3.16, when the sand temperature approaches the maximum allowed value, i.e when the system is close to the full charge, a variation in the slope of sand temperature curve has a more pronounced impact on the charging time compared to the initial stages of charging, where the curve slope is steeper. Since in this representation the slope is proportional to the heat power, higher power resolution close to the the set-point temperature allows for a higher control over the charging time, offering the potential for its minimization.

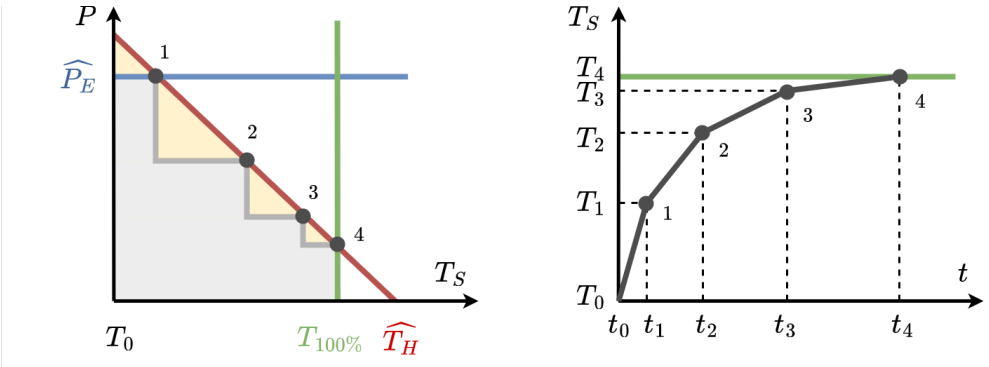

Figure 3.16: MGTES P-T capability with optimized discrete power control (left) and corresponding sand temperature time evolution (right)

3.8 Optimized discrete power control hardware

Equation (3.8) can be applied to CSTS solutions, to calculate the optimal voltages of secondary taps, in order to minimize the charging time of the storage system. For simple CSTS, the optimal voltages for taps $(V_1, ..., V_j, ..., V_n)$ can be calculated as (3.17), since the power dissipated by resistors is proportional to the square of the voltage applied to their terminals.

$$P_j = P_1 r^{j-1} \quad \rightarrow \quad V_j = V_1(\sqrt{r})^{j-1} \tag{3.17}$$

For the CSTS solution, the optimal discrete power control can be achieved choosing tap voltages so that the first $N_S/2$ steps are realized with delta connection, and the remaining $N_S/2$ with star connection. The ratio between two consecutive power steps can be calculated as (3.18), rewriting (3.8) with $n = N_S/2 + 1$:

$$r = \sqrt[N_S/2]{\frac{P_{(N_S/2)+1}}{P_1}} = \sqrt[N_S/2]{1/3} \tag{3.18}$$

A suitable balance between hardware complexity and power control resolution is achieved with two taps ("high tap" at V_1 and "low tap" at V_2), with $N_T = 2, N_C = 4, N_S = 4$, resulting in (3.19).

$$r = \sqrt[2]{1/3} \approx 0.577 \qquad V_2 = V_1 \sqrt[4]{1/3} \approx 0.760\, V_1 \tag{3.19}$$

Table 3.3 shows, for every power step, the state of the four contactors involved, together with some key working conditions, e.g. cable current, affecting Joule losses.

Power step name	High delta	Low delta	High star	Low star	Off
High tap contactor	Closed	Open	Closed	Open	Open
Low tap contactor	Open	Closed	Open	Closed	Open
Delta contactor	Closed	Closed	Open	Open	-
Star contactor	Open	Open	Closed	Closed	-
Resistor voltage	100 %	76.0 %	57.7 %	43.9 %	0 %
Resistor current	100 %	76.0 %	57.7 %	43.9 %	0 %
Cable voltage	100 %	76.0 %	100 %	76.0 %	0 %
Cable current	100 %	76.0 %	33.3 %	25.3 %	0 %
Power	**100 %**	**57.7 %**	**33.3 %**	**19.3 %**	**0 %**

Table 3.3: Optimized discrete power control obtained with advanced CSTS solution, with two taps and four contactors

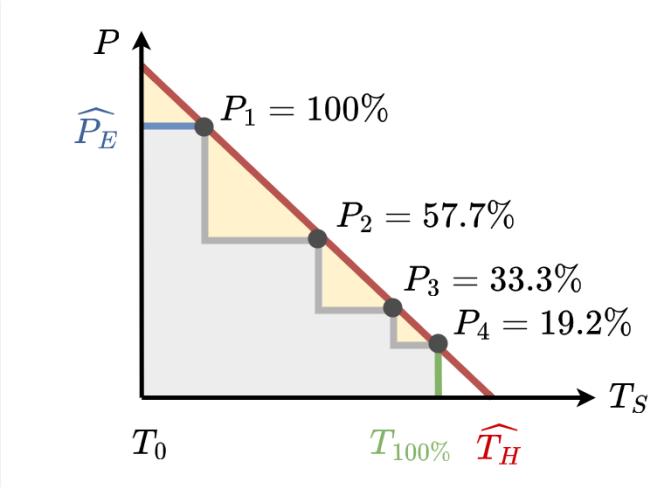

Figure 3.17: MGTES P-T capability with optimized discrete power control, achieved using star-delta contactors and CSTS with two taps

Chapter 4

MGTES optimization software

4.1 ESTESO

To perform the optimization of energy systems comprising MGTES technology, an integrated multi-purpose software has been developed. It's the Elastic Software for Thermal Energy Storage Optimization (ESTESO).

The name of the software has been chosen with precision to reflect its purpose, essence and capabilities. Three out of the six letters in "ESTESO" are "TES", since it includes models to optimize Thermal Energy Storage systems. However, the remaining half of the name ("E" and "SO") goes beyond this specific domain and refers to its broader capacity for optimization in general. The inclusion of "Elastic" in the name highlights the flexibility and adaptability of the software, reflecting the fact that ESTESO modelling framework has been intentionally designed to be generic and versatile. While it currently addresses TES optimization, the framework's architecture and capabilities are not constrained solely to this application, so that it has the potential to be extended and tailored for a variety of optimization purposes in the future.

The software has been written in Python and takes advantage of various open source libraries, listed in Appendix B. ESTESO can run on different operating systems, allowing to use it locally on personal computers, or installing it onto a cloud environment, and accessing it remotely. This last option allows to share between different users high computational power for calculations, and at the same time it ensures an efficient way to share data between team members, thus fostering collaboration.

4.2 One-model, one-tool approach

Optimization tools have the valuable ability to discover how to lower costs and maximize performance of energy systems. Such tools can be leveraged in different ways, during both system design (sizing), and real-time operation (management).

Despite the system remains the same, different purposes require distinct models, based on the context and the purpose of the study. For instance, the optimization of individual components usually involve detailed and complex models, whereas system optimization benefit from simpler models to increase computational speed, especially if quick real-time actions must be taken.

A common approach is to develop different models (usually with different software) and use them separately. Such workflow is simpler and easier to setup, but harder to maintain: since models are decoupled, every update of the system requires the manual update of both models. This "multi-tool" approach becomes more limiting and inefficient if employed into a continuous improvement context, where real-time data from existing plants are used to improve the design of new plants. In fact, the need to exchange data between different tools and models may take time and resources, possibly leading to errors, and constituting an avoidable complication.

These problems can be solved adopting a "one-tool approach", that unifies models (and data) in a central place, leveraging an automated mechanism to read general information of the system, and create a model tailored to perform the desired task, according to users' needs. Figure 4.1 highlights the benefit of using a one-tool approach. The block colored in red represent the actions performed by the user, whereas those in grey the automated actions executed by the computer. The one-tool approach leaves less tasks to the user, speeding up the process and minimizing human mistakes in the process.

ESTESO has been realized with the aim of (gradually) switching to a one-tool approach for the development of MGTES systems, to collect all models and data into a unique place, and manage them consistently, streamlining the workflow to boost the continuous improvement of the technology.

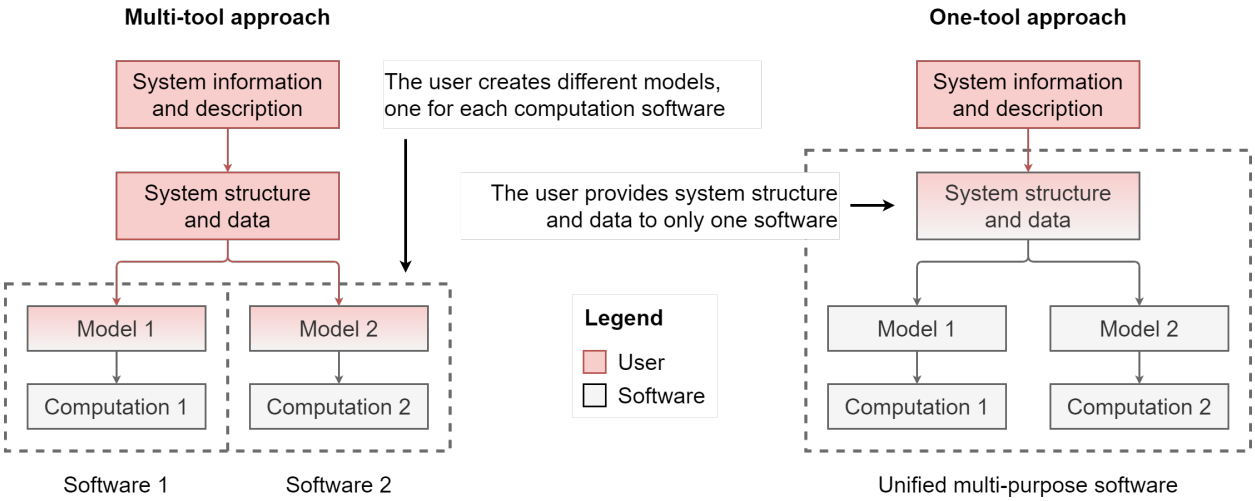

Figure 4.1: Workflow comparison between multi-tool approach and one-tool approach

4.3 Design and operation optimization

The one-tool approach adopted for ESTESO development had the primary aim of exploiting the same software for design (sizing) and operation (management) optimization of energy systems comprising MGTES.

In fact, ESTESO generates model variables and equations based on input data, treating quantities as input parameters for the model if their value is specified, or marking them as variables to optimize if no value is provided. This allows to easily cover the use cases described below.

- **Operation optimization** aims to identify the optimal management strategy for an existing system. In ESTESO, this is achieved setting all information about system sizing, specifying values for operational limits of every component, e.g. maximum power or energy capacity. With these input data, the solver calculates the optimal management strategy, i.e. power profiles in every part of the system for every time-step considered, that minimize or maximize the chosen objective quantity. The results are influenced by different factors, particularly components usage-dependent costs, e.g. energy prices.

- **Design optimization** aims to the determination of the optimal size for all components. In ESTESO, this is achieved not specifying components sizes, in contrast to the previous case. These (incomplete) input data leaves to the solver the choice of the operational limits for every component, to minimize or maximize the chosen objective quantity. Unlike management optimization, the results are also influenced by size-dependent usage-independent costs (e.g. CAPital EXpenditure (CAPEX)). Given the higher number of unknown variables to be optimized by the solver, optimizing design requires longer computation time than optimizing operation.

Operation optimization can be performed in two ways, described below.

- **Offline operation optimization** involves including all the considered timesteps in a single big optimization problem, so the solver finds an optimal management strategy in a single run. This optimization type is usually performed during system design, to evaluate the performance of different sizing solutions to compare in a known scenario, typically exploiting past data, e.g. energy prices of previous years.

- **Online operation optimization** consists of the continuous determination of the optimal management of a working system, exploiting real-time data to generate an optimized schedule of system operation. The solver adopts data collected from sensors as initial conditions, and performs optimizations over a rolling horizon, e.g. the following 48 hours, periodically updating system schedule with its results. Then, the system undertakes the first action of the schedule, and the optimization is repeated, using updated real-time data. This type of optimization requires the integration with a forecasting system, predicting the input scenario for the optimization. During the operation the forecasting system may leverage newly collected data to improve its prediction model, constantly adapting to the changes in the environment.

For now, only the first type is supported by ESTESO, but the other one is planned to be added in the future, enabling the software to act as an EMS for real energy systems comprising MGTES, fully realizing the one-tool approach envisioned for the software.

4.4 Software architecture

ESTESO is composed by three main parts, briefly presented below, summarized in Figure 4.2, and described in detail in the following sections.

- **Modelling framework**: stores the structure and the data of the system to be studied, generating its equations from available information. It acts as the core of the software, connecting together the other parts. It also handles saving and loading data from files.
- **Computation plugins**: perform calculations (simulations, optimizations, parametric sweeps, etc.) on input data, using the equations provided by the modelling framework, adapting model details according to the specific need of the computation to run, e.g. linear approximations for optimization using linear programming.
- **User interface**: allows the user to inspect and edit input data, system models and equations, run computations, and analyze output data thanks to various interactive visualizations.

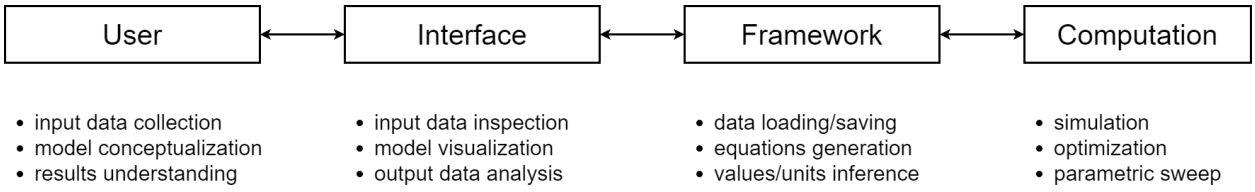

Figure 4.2: General architecture of ESTESO software

The modelling framework is based on 5 key concepts presented in the following, with the help of an example (Figure 4.3) showing a very simple model for two cascaded unidirectional power converters.

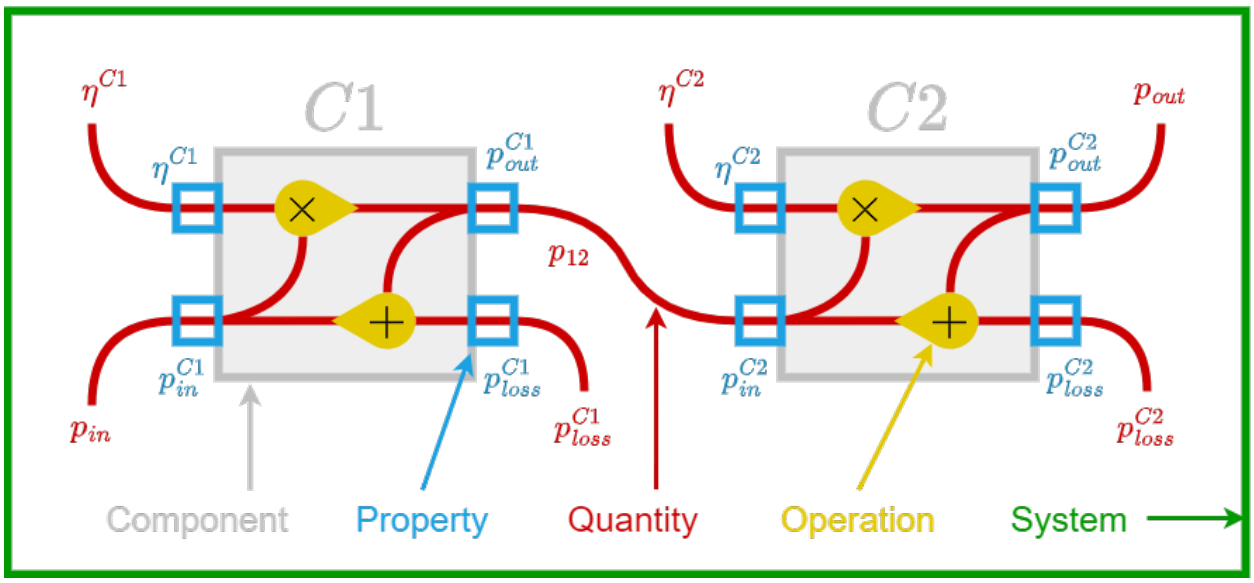

Figure 4.3: Basic example model of two cascade converters using ESTESO framework

- `System`: main container of the system to study (green frame).
- `Component`: basic block of the system, each one identified by a unique code, composed by uppercase letters. The example in Figure 4.3 comprises 2 components: $C1$ and $C2$ (grey blocks), one for each converter. Converters can be created from templates so they share the same internal structure.
- `Property`: variable of a component. In the example, since both converters have been created from the same template, they share the same 4 properties (blue squares): efficiency η^{Ck}, input power p_{in}^{Ck}, output power p_{out}^{Ck}, power losses p_{loss}^{Ck}. Properties can be time-varying, named with a lowercase letter (e.g. p_{in}), or static (i.e. scalar), named with an uppercase letter.
- `Quantity`: relevant variable of the system to study. It represents a specific physical quantity, with a value (if known) and a unit of measure. During model setup, every property is always linked to a quantity. The same quantity can connect together two or more properties, setting an interaction between components. The connection can be direct or through mathematical operations. In the example, every property (blue squares) has its own quantity (red links), with the same name, except for properties p_{out}^{C1} and p_{in}^{C2}, that are linked to the same quantity p_{12}.
- `Operation`: mathematical operation between properties or quantities, to define equations. In the example, the properties (blue squares) of each component are connected by operations (yellow drop-like shapes) to form the equations $\eta^{Ck} p_{in}^{Ck} = p_{out}^{Ck}$ and $p_{in} = p_{out} + p_{loss}$. Supported operations in ESTESO are summation, difference, multiplication, integral, derivative, equality, inequality. Every component can define its operations to define both "internal" equations, i.e. between its own properties, or "external" equations, i.e. with properties of other components.

The diagram presented in Figure 4.3 resembles a printed circuit board, where the entire system mirrors the board itself, components are chips, properties are their pins, quantities are links between chip pins, and operations resemble logic gates. In fact, this framework has been designed to empower users to assemble intricate systems, with the ease of employing pre-made components, just like electronic chips. Diverging from this analogy, the ESTESO framework offers the flexibility to inspect the internal functionality (properties and operations) of existing components, to tailor them to precise requirements or craft custom components from scratch to address specific needs.

It is very important to note that there are no predefined input or output properties (pins). In fact, as explained in more detail in the following sections, during model setup the software writes the equations in the correct form, inverting the operations based on the available data. For instance, $p_{out}^{C1} = p_{in}^{C1} \eta^{C1}$ is left unchanged if p_{in}^{C1} and η^{C1} are known and p_{out}^{C1} is unknown, but the equation is rewritten as $p_{in}^{C1} = p_{out}^{C1} / \eta^{C1}$ if p_{out}^{C1} and η^{C1} are known and p_{in}^{C1} is unknown. This behaviour is one of the simple yet powerful mechanisms of ESTESO that lets the user focusing on the system, not on the model and its computation.

4.5 Standard properties and containers

All components (except some edge cases) have the same set of standard properties, used to model common aspects considered in the field of energy systems, or engineering in general, e.g. the size of a component, its activation over time, its cost, lifetime. Table 4.1 summarizes the standard properties, along with the equations defined between them. For instance, CAPEX and OPEX costs properties define simple equations to calculate the total expenditure linked to the component over its entire lifespan. In addition, the framework offers some basic components to model simple elements of energy systems: sources and loads, converters, and others, listed in Table 4.2.

Given the high number of components that may be included in one system, properties are judiciously employed only if needed. For instance, properties pertaining to CAPEX are included in the model exclusively when an associated cost is supplied. This discerning approach ensures that the system is not cluttered with superfluous properties and equations, enhancing its efficiency and relevance.

Property	Usage	Equations
`limit`	Sizing constraint	$x \leq X$
`on`	Component activation state	$x = X\ s$
`target, unbal`	Desired profile to follow	$\tilde{x} = \hat{x} - x \geq 0$
`capexCost`	Fixed size-dependent cost	$M = X\ C$
`lifetime`	Time to amortize CAPEX	$M = X\ C\ T/T_{life}$
`opexCost`	Usage-dependent cost	$m = \int x\ c\ dt$
`unbalCost`	Cost of not respecting the target	$\tilde{m} = \int \tilde{x}\ \tilde{c}\ dt$
`money`	Total costs	$\mathbb{M} = M + m + \tilde{m}$

Table 4.1: Available standard properties for each component

Name	Connections	Example	Equations
`Container`	As needed	MGTES	$x^{(C)} = \sum_i x^{(Ci)}$
`Source`	Only 1 output	Generator	$E_{out} = \int p_{out}\ dt$
`Demand`	Only 1 input	Load	$E_{in} = \int p_{in}\ dt$
`Transfer`	1 input and 1 output	Resistor	$p_{out} = \eta\ p_{in}$
`Loss`	Only 1 input	Wall loss	$L = \int l\ dt$
`Storage`	Bidirectional connection	Battery	$p = -\partial_t(e)$
`Node`	Many inputs and outputs	Hub	$\sum_i x_{in}^{(i)} = \sum_i x_{out}^{(i)}$
`Totals`	None	Totals	$x_{tot} = \sum_i x^{(i)}$

Table 4.2: Some available components types in the modelling framework

The examples showcased in the preceding sections served as a fundamental demonstration, intentionally simplified to illustrate fundamental concepts. In practice, addressing real-world challenges demands the construction of intricate models, with numerous components and properties. Such complexity can be effectively managed by strategically breaking down the system into smaller, more manageable subsystems. Within ESTESO framework, multiple components can be nested

within a container component, which can include specific properties tailored to reveal the most pertinent quantities of the inner components. This approach streamlines the understanding and manipulation of complex systems, enhancing their usability and coherence.

Figure 4.4 shows how the components $C1$ and $C2$ from the previous example can be included in a CX container component, exposing some properties (input, output, efficiencies) directly, and others (losses) with operations.

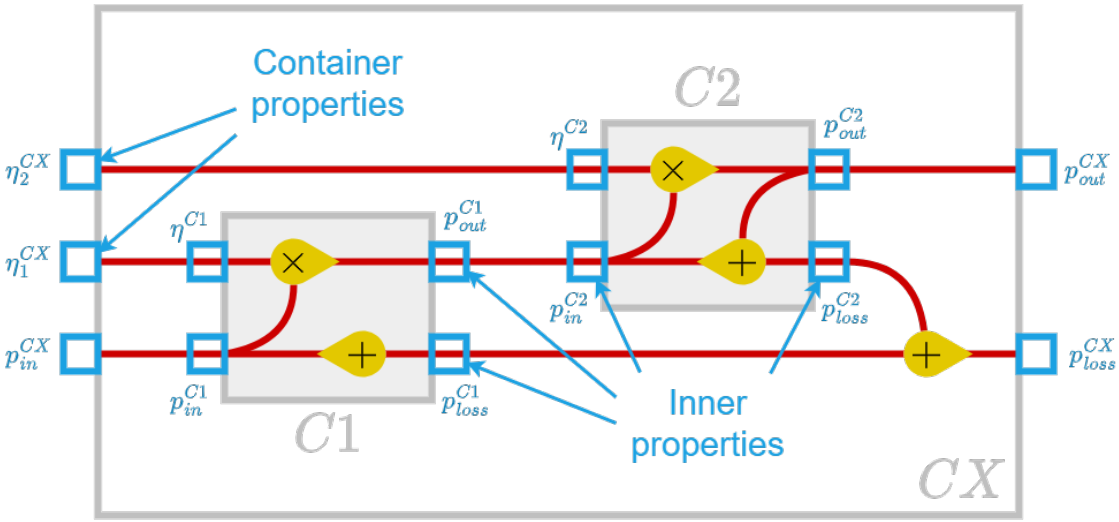

Figure 4.4: Basic example of a container component for two cascade converters using the ESTESO framework

4.6 User interface

ESTESO interface aids the user through all the steps of the computation process, as outlined below.

- **System structuring**: the user can explore the system and its components, viewing their properties and the connections between them.
- **Data input and review**: input values are shown in interactive tables for easy visualization and manipulation, for quick review before starting the computation.
- **Model inspection**: the interface shows all the equations used in the model. Given the high number of equations involved, a filter feature has been implemented to view only the equations regarding specific components, or those including specific variables, to simplify model exploration.
- **Computation configuration and supervision**: simulation and optimization parameters (e.g. cost function) can be tweaked directly through the interface. Solver errors can be inspected in the interface, simplifying and speeding up debug process in case of wrong problem formulation.
- **Results analysis**: output values are shown in tables and different types of interactive charts, for quick visualization with easy navigation.

Figure 4.5 shows the system graph navigation page, providing to the user a rich representation of the objects involved. Components are drawn as circles, static properties as rectangles, and time-varying properties as database shapes. Input quantities are highlighted with a solid shade. Figure 4.6 depicts the system equations page, allowing to inspect the model generated by ESTESO. Figure 4.7 shows one of the interactive chart pages to explore the results. Appendix C shows some other screenshots of ESTESO main pages.

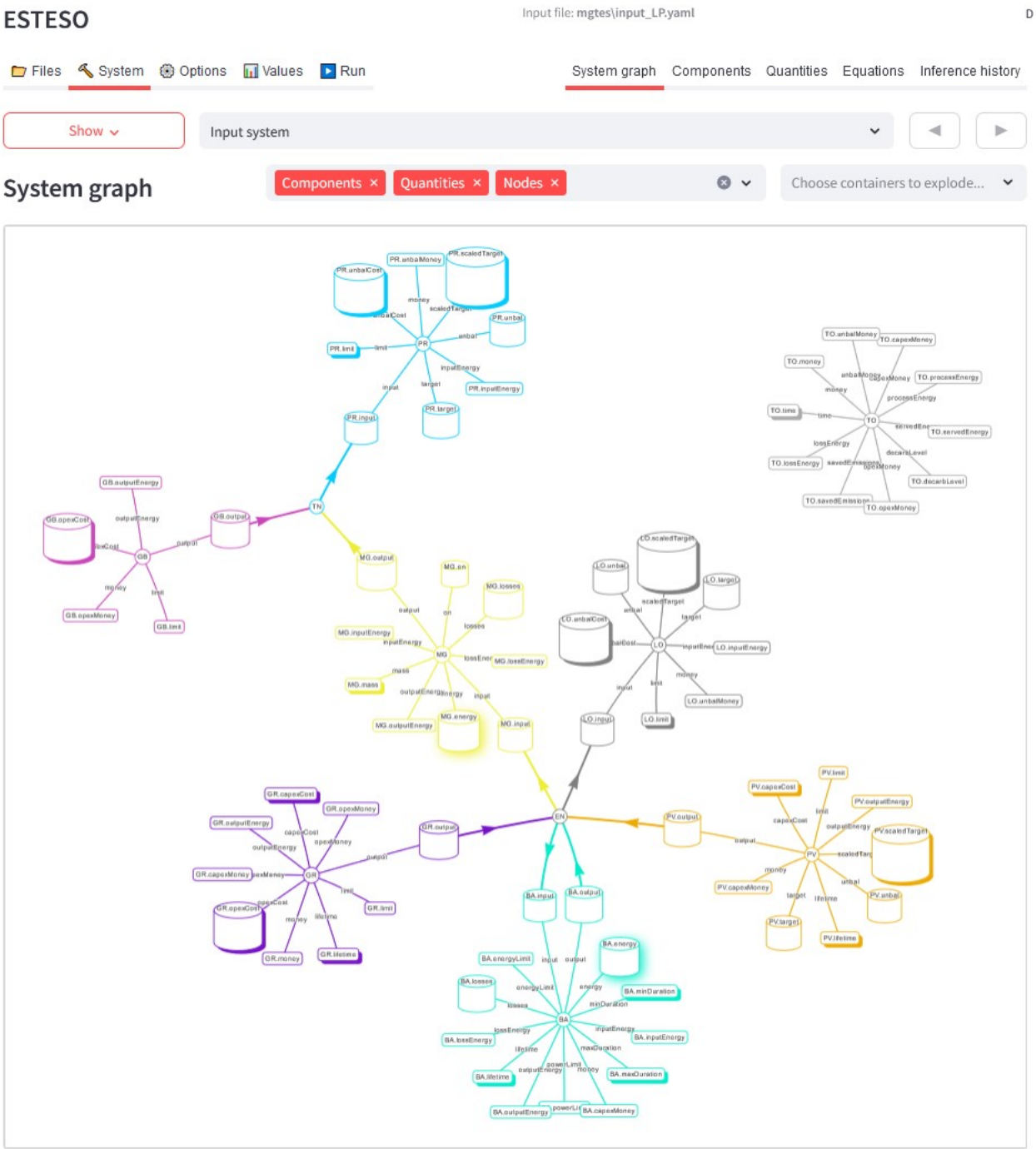

Figure 4.5: ESTESO system graph exploration page

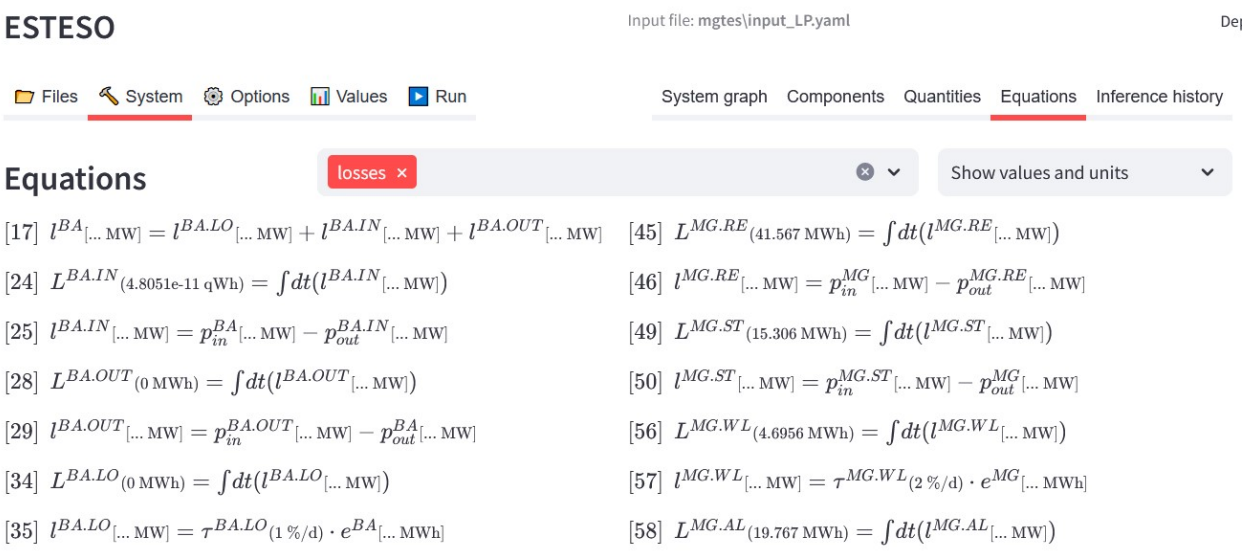

Figure 4.6: ESTESO system equations inspection page

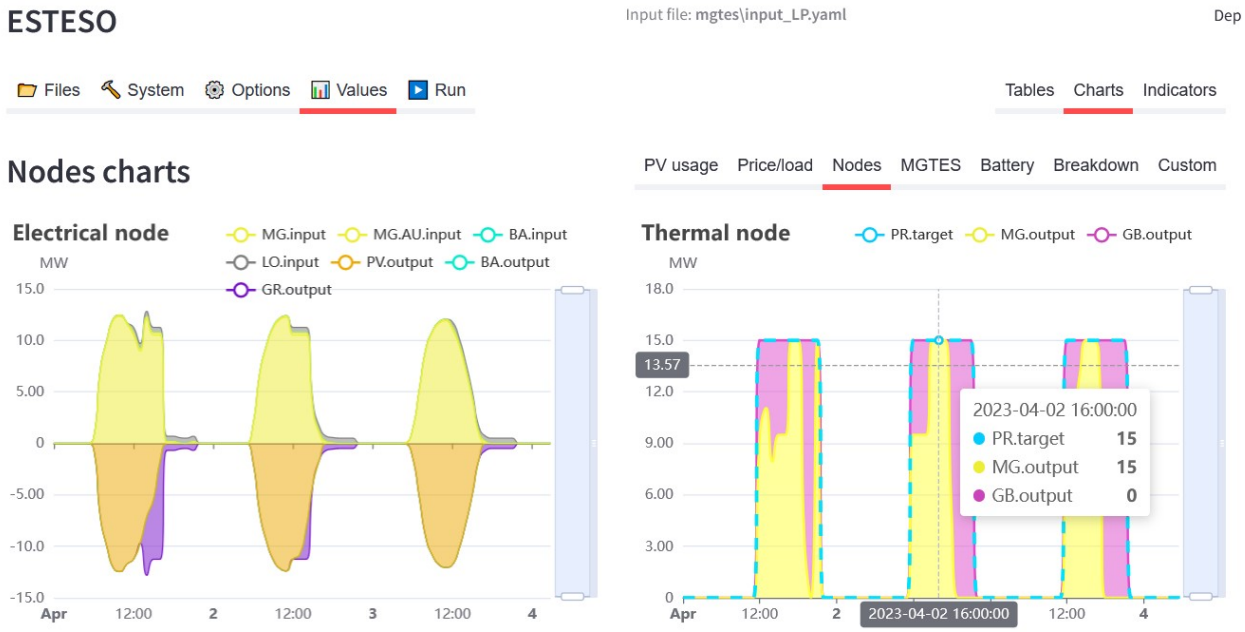

Figure 4.7: ESTESO energy nodes chart exploration page

For data management in ESTESO, CSV and YAML file formats have been chosen, for their on conciseness and human readability, achieving ease of debug, manual modification, and version control. Another relevant aspect considered was portability, given the need to use the software on different environments; in fact, CSV has been preferred as open standard in contrast to proprietary formats. CSV is used vector data, especially for long time-series of input and output variables, whereas YAML is used for configuration, scalar data, and small vector data. A linking feature allows to reference CSV and YAML files inside other YAML files, enabling loading complex data structures from multiple files, and reuse common data between different case studies, minimizing data repetition and enhancing consistency.

4.7 Computation steps

The steps followed by ESTESO to perform a computation are described in the following.

1. **Structure loading**: the system is constructed loading structure data from file. This includes names and types of all components, and how they are nested.

2. **Input values loading**: known values are assigned to corresponding properties.

3. **Equations writing**: ESTESO writes the equations of the model, depending on the settings of the study, thus linking components one another by connecting their properties together though operations. Some equations are written in any case, whereas other ones are "conditional", i.e. they are written only if some specific quantity has an assigned a value or is used in other equations. For instance, the equation of total CAPEX money of a component is written only if CAPEX cost is specified; similarly, losses are calculated only if the efficiency of the component is specified (100% efficiency is assumed otherwise). When any equation is written, its terms are marked as "used", triggering the writing of other conditional equations, that marks other quantities as used, and so on. Equation terms are marked also as "input" if they have values, or as "output" if not. For example, the quantity representing the peak power of a PV plant will be marked as input if the power is specified; if instead the peak power is not set, the quantity will be marked as output, and its value will be optimized by the solver.

4. **Static/time-varying inference**: ESTESO tries to determine if quantities are static or time-varying, to determine if equations and unknown quantities should be treated as scalars or vectors in the optimization. The inference process starts from quantities with known values (or unknown quantities already marked as static or time-varying), and uses equations to infer if the other terms are static or not. For example, analyzing the equation $a + b = c + d$, if a is time-varying, $(a+b)$ will be inferred as time-varying as well; then, the equation will be inferred as time-varying, and so the other side of the equation $(c + d)$. At this point we know that at least one of c and d is time-varying, but it's not possible to know which one, so the inference stops. Once a quantity has been inferred, ESTESO tries to exploit this new information to infer other quantities, analyzing the equations where the quantity is present, until no more inference can be performed.

5. **Values inference**: before starting the optimization, ESTESO tries to perform all the trivial (or almost-trivial) calculations, processing equations that can be solved simply by inverting the operations. This helps eliminating some non-linear terms from equations, also reducing the number unknown quantities in the systems, thus speeding up the computation process.

6. **Units inference**: the inference is repeated considering only the units of measurements. This step is not strictly necessary from an algorithmic point of view, but ensures that all quantities (both known and unknown) have a defined unit before starting the computation, enabling the identification of dimensional errors in the equations before computation start.

7. **Model conversion**: written equations and known quantity values are converted to the format accepted by the solver.

8. **Solver run**: the solver calculates the unknown values, using the algorithm configured for the study. This is the step that takes most of the time.

9. **Data retrieval**: the data calculated by the solver, i.e. the values of unknown quantities, are converted and copied back to the system, post-processed, and saved to a file, if configured.

Every computation can be batch-repeated multiple times, using different values for some selected quantities at every run. For example, the same system can be simulated with different time steps, at different times of the year. This can be done with any number of parameters, but the most common cases are 1-parameter and 2-parameter sweeps. This feature is particularly useful also to assess the performance of the model, visualizing the computation time for every run.

Chapter 5

Power-to-Heat optimization model and results

5.1 System components

A typical industrial P2H system has been modeled in ESTESO, to study the impact of MGTES in terms of decarbonization and cost. MGTES is modeled as a container including various components: resistors, sand, steam tubes, wall losses, air losses, and auxiliaries. In the system, the thermal process is supplied by a gas boiler and MGTES, whose resistors are supplied by the grid, a PV plant, and a battery storage. The battery is modeled as a container including: an input component, an output component, a storage component, and a loss component. An electric load has been included in the system, representing auxiliary consumption linked to the thermal process.

Figure 5.1 shows a simplified diagram of the system and Table 5.1 lists the components (and sub-components) included in the model, reporting for each one a code of two letters, used as superscript in the equations. Each component has its own color, used in ESTESO charts.

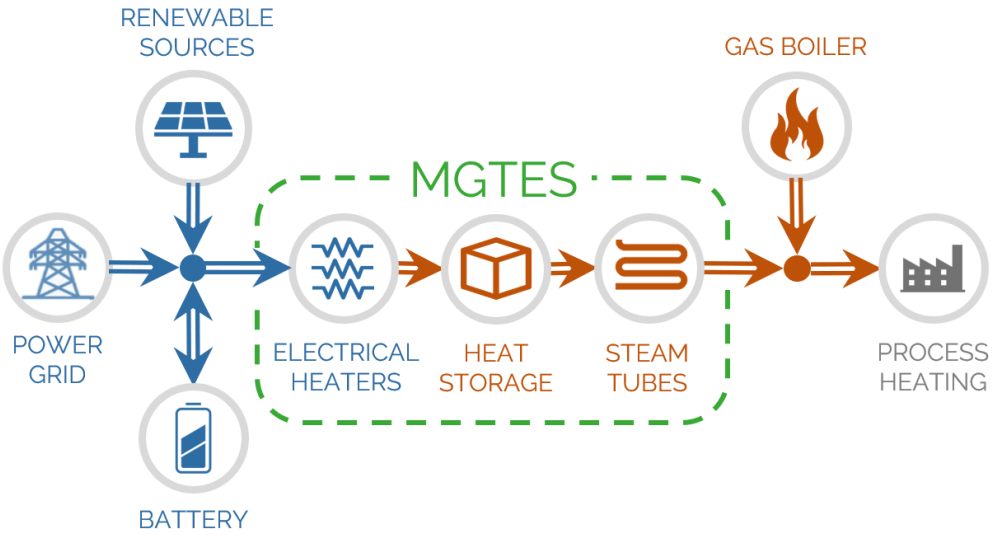

Figure 5.1: P2H system modeled in ESTESO software

Name	Code	Type	Color	Container
Grid	GR	Source	Purple	
Photovoltaic	PV	Source	Orange	
Electrical node	EN	Node		
Load	LO	Demand		
Battery	BA	Container	Aqua	
Battery input	BA.IN	Transfer		Battery
Battery output	BA.OUT	Transfer		Battery
Battery storage	BA.STO	Storage		Battery
Battery loss	BA.LO	Loss		Battery
Battery node	BA.NO	Node		Battery
MGTES	MG	Container		
Resistors	MG.RE	Transfer	Brown	MGTES
Sand	MG.SA	Storage	Yellow	MGTES
Steam tubes	MG.ST	Transfer	Blue	MGTES
Wall loss	MG.WL	Loss		MGTES
Air loss	MG.AL	Loss		MGTES
Auxiliaries	MG.AU	Demand		MGTES
Thermal node	TN	Node		
Gas boiler	GB	Source	Fucsia	
Process	PR	Demand	Sky	
Totals	TO	Totals		

Table 5.1: Components used to model the system in ESTESO

5.2 Components modeling

The rich set of ESTESO standard properties allowed to model easily almost every part of the system, except for MGTES, whose peculiarities (linked to the fluidization system) have been included in the model exploiting the flexibility of the software, adding custom properties and equations to the system.

Table 5.2 summarizes the standard properties automatically added to every component of the system, and Appendix D reports the full list of the equations generated for the model.

Name	Code	limit	target	unbal	capex	opex	money
Grid	GR	✓			✓	✓	✓
Photovoltaic	PV	✓	✓	✓	✓		✓
Electrical node	EN						
Battery	BA				✓		✓
Battery input	BA.IN	✓			✓		✓
Battery output	BA.OUT	✓					
Battery storage	BA.STO	✓			✓		✓
Battery loss	BL						
Battery node	BN						
Load	LO	✓	✓	✓			✓
MGTES	MG						
Resistors	MG.RE	✓					
Sand	MG.SA	✓					
Steam tubes	MG.ST	✓					
Wall loss	MG.WL						
Air loss	MG.AL	✓					
Auxiliaries	MG.AU	✓					
Gas boiler	GB	✓				✓	✓
Process	PR	✓	✓	✓			✓
Thermal node	TN						
Totals	TO				✓	✓	✓

Table 5.2: Standard properties used by ESTESO for the modeled P2H system

In the first instance, only linear models have been used for this study; in the future, the equations will be refined and enriched to include non-linearies, thus modeling the system even more accurately. This will require the addition of a non-linear solver into ESTESO.

The maximum energy stored by MGTES E^{MG} is linearly dependent on sand mass Λ^{MG} (for a fixed interval of working temperatures of sand), as in Equation 5.1. The same holds for the maximum power of resistors and steam tubes (Equations 5.2), i.e. maximum input and output power of MGTES.

$$E^{MG} = \Lambda^{MG} K^{MG.SA} \tag{5.1}$$

$$P_{in}^{MG} = \Lambda^{MG} K^{MG.RE} \qquad P_{out}^{MG} = \Lambda^{MG} K^{MG.ST} \tag{5.2}$$

As described in Section 2.2, MGTES fluidization system must be turned on in order to allow an effective thermal power transfer between the sand and resistors, or between the sand and steam tubes. To model this behavior in ESTESO, three binary decision variables have been introduced, representing the boolean activation state (0 = off, 1 = on) of MGTES resistors, steam tubes, and fluidization system: $s^{MG.RE}$, $s^{MG.ST}$, and s^{MG} respectively. As in Equation 5.3, resistors and steam tubes can exchange energy only if active ($s = 1$); as in Equation 5.4, the fluidization system is activated if resistors `OR` steam tubes are on.

$$p_{in}^{MG.RE} \leq P_{in}^{MG.RE} s^{MG.RE} \qquad p_{in}^{MG.ST} \leq P_{in}^{MG.ST} s^{MG.ST} \tag{5.3}$$

$$s^{MG} \geq s^{MG.RE} \qquad s^{MG} \geq s^{MG.ST} \tag{5.4}$$

As in Equation 5.5, MGTES air loss, i.e. thermal power lost in the exhaust hot air coming out of the module, is approximately constant, linearly dependent on sand mass, and arising only when the fluidization system is active. Similarly, the electrical loads pertaining to the fluidization system, i.e. air compressor and fan, adsorb constant power, when the fluidization system is active (Equation 5.6).

$$l^{MG.AL} = \Lambda^{MG} K^{MG.AL} s^{MG} \tag{5.5}$$

$$p_{in}^{MG.AU} = \Lambda^{MG} K^{MG.AU} s^{MG} \tag{5.6}$$

Power losses (l) of the battery and MGTES walls have been modeled as dependent on the stored energy (e), by a constant factor (τ), expressed in percent per day, as in Equation 5.7.

$$l = e\,\tau \tag{5.7}$$

It should be noted that, in Equations 5.5 and 5.6, the multiplication between sand mass Λ^{MG} and the activation variable s^{MG} makes the problem non-linear if trying to optimize sand mass, i.e. MGTES energy capacity. The same applies to Equations 5.3, causing an analogous issue with the maximum power of resistors and steam tubes, i.e. MGTES charging and discharging capacity. However, the optimal MGTES size for a given system can be discovered even keeping the problem linear, exploiting the parametric sweep feature of ESTESO, by solving the optimization problem multiple times, with different fixed input values for MGTES energy (or power) capacity, then selecting the best option depending on the computed values for the objective quantity.

5.3 Objectives and post-processing

ESTESO offers the flexibility to fully configure computation parameters, with the possibility to choose any quantity as optimization objective, to be minimized or maximized by the solver. The default objective (to minimize) is total system cost $\mathbb{M}$, comprising CAPEX M, OPEX m, and unbalance costs $\tilde{m}$ of all components (Equation 5.8).

$$\mathbb{M} = M + m + \tilde{m} \tag{5.8}$$

Additional quantities have been defined to expand the set of objectives to select: saved CO_2 emissions and decarbonization level. Saved emissions Γ (Equation 5.9) are evaluated observing that, with the same total energy required by the process, MGTES output replaces the energy provided gas boiler, thus reducing gas consumption. A gas-CO_2 conversion factor $K_\Gamma = 0.18$ tCO_2/MWh has been assumed [74].

$$\Gamma = E_{out}^{MG} K_\Gamma \tag{5.9}$$

Another useful indicator related to emission is the decarbonization level D, defined as the fraction of process energy supplied by renewable sources. In this context, we consider MGTES output energy as totally renewable, yielding Equation 5.10.

$$D = \frac{E_{out}^{MG}}{E_{in}^{PR}} = \frac{\int p_{out}^{MG}\, dt}{\int p_{in}^{PR}\, dt} \tag{5.10}$$

It should be noted that in the above definition, the unknown variable p_{in}^{PR} in the denominator makes the problem non-linear, requiring the use of a dedicated solver if using D as objective or constraint for the optimization. To avoid this issue, the input energy of the process E_{in}^{PR} has been replaced by its target value $\bar{E}_{in}^{PR} = \int \bar{p}_{in}^{PR}\, dt$, yielding Equation 5.11. In fact, since the target profile of process input power $\bar{p}_{in}^{PR}$ is known, the target input energy of the process $\bar{E}_{in}^{PR}$ is calculated by ESTESO during the value inference step of the computation, before model conversion for the solver, that sees the quantity as a known constant value.

$$D = \frac{E_{out}^{MG}}{\bar{E}_{in}^{PR}} = \frac{\int p_{out}^{MG}\, dt}{\int \bar{p}_{in}^{PR}\, dt} \tag{5.11}$$

The same issue (optimization variables in the denominator) rose also for other quantities, such as round-trip efficiencies of battery and MGTES (Equation 5.12), but could not be solved, so ESTESO has been set to calculate such supplementary quantities in the post-processing step of the computation.

$$\eta = E_{out}/E_{in} \tag{5.12}$$

Another key quantity calculated in the post-processing step is the decarbonization cost γ, i.e. the total money spent for decarbonization (CAPEX and OPEX of all components, except the gas boiler) over the saved emissions, as in Equation 5.13.

$$\gamma = \frac{\mathbb{M} - m^{GB}}{\Gamma} \tag{5.13}$$

5.4 Usage-independent components costs

Online datasets have been utilized to extract the size-dependent usage-independent component costs used in the model, summarized by Table 5.3 and described in the following sections. For battery and PV, construction costs plus fixed yearly O&M costs have been considered. Dollar prices have been converted to euros considering an average currency exchange of 1.08 €/$.

Component	CAPEX	Source	Ref	Year	Notes
PV field	2.4 M€/MW	NREL ATB	[75, 76]	2023	
Grid	0.65 k€/MW	e-distribuzione	[77]	2024	MV connection
		Terna	[78, 79]	2023	HV connection
Battery	1.5 M€/MW + 0.45 M€/MWh	NREL ATB	[80, 81]	2023	Estimated with linear model

Table 5.3: Summary of CAPEX (usage-independent) costs used in this study

5.4.1 PV field costs

For the estimation of PV costs, two datasets have been used (Figure 5.2): an utility-scale 100 MW 1-axis tracking PV field [76], and a commercial 500 kW PV plant [75]. A technical life of 25 years has been considered to include O&M along with construction cost (Table 5.4). For this study, expecting a PV field in the range 1-20 MWp, an average value between utility-scale and commercial sizes has been adopted: 2.4 M€/MW.

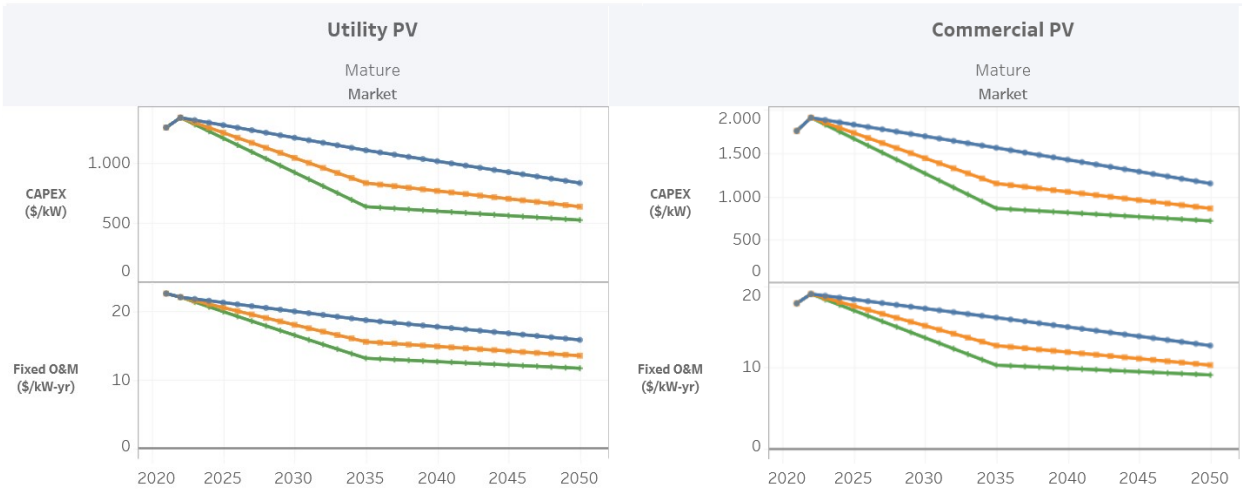

Figure 5.2: Construction cost of a PV field in 2023, with projected cost reduction over the next years

	Contruction	O&M	Size cost (power)	
	M$/MW	M$/MW/y	M$/MW	M€/MW
Utility-Scale PV	1.61	22.2	2.17	2.34
Commercial PV	1.85	18.8	2.32	2.51

Table 5.4: PV size-dependent usage-independent cost estimation

5.4.2 Grid connection costs

For the grid connection, 1-20 MW power range has been considered. This range comprises the border value of 10 MW, that in Italy discriminates the voltage level for the connection. For this reason, both MV and HV connection cases have been analyzed, with 10 MW of power and different distances from the existing grid: 5, 15, 30 km.

MV grid connection prices have been estimated using data from e-distribuzione [77], the major Italian public MV distribution network operator. The connection cost requested by e-distribuzione for a new MV connection point is determined by a power term of 61.7 k€/MW plus a distance term of 0.52 k€/km.

Power	MW	10	10	10
Power term	k€	616.9	616.9	616.9
Distance	km	5	10	15
Distance term	k€	2.6	5.2	7.7
Total cost	k€	619.5	622.1	624.6
Connection price	k€/MW	61.95	62.21	62.46

Table 5.5: MV grid connection cost estimation

HV grid connection prices have been estimated using data from Terna, the Italian TSO [78]. Unlike the previous case, connection costs are not standardized, since they are strongly dependent on the actual connection solution (overhead lines or cables, air or gas insulation for substations). The connection cost requested by Terna from the user is only a fraction of the total costs incurred for the realization of the new lines and substations, since the same infrastructure may serve also other uses in the future [79]. The conventional power for 150 kV connections is 325 MW, e.g. for a connection of 32,5 MW the user pays 10% of the total costs. HV/MV transformers and their HV switchgear are payed entirely by the user.

Given the increasing difficulties in the realization of overhead lines, the estimation has been performed considering aluminum cables, costing 1.6 M€/km. For the substation, air insulation has been chosen, with one busbar system (150 kV Italian standard). For a 10 MW connection, the user pays 3.1% of total costs.

Distance	km	5	10	15
Cable line	k€	8000	16000	24000
Line switchgear (both sides)	k€	878	878	878
Substation busbars system	k€	1780	1780	1780
Total cost	k€	10 658	18 658	26 658

Table 5.6: HV grid connection costs, payed by the user only for a fraction

Distance	km	5	10	15
Cable line	k€	246	492	738
Line switchgear (both sides)	k€	27	27	27
Substation busbars	k€	55	55	55
Transformer HV switchgear	k€	60	60	60
Transformer (16 MVA)	k€	200	200	200
Total user cost	k€	588	834	1080
Connection price	k€/MW	58.8	83.4	108.0

Table 5.7: HV grid connection costs payed by the user

In constrast to MV, HV grid connection costs have a higher variability with the connection distance, due to the elevated cost of cable lines. For the study, an average CAPEX value of 0.65 k€/MW has been assumed.

5.4.3 Battery storage costs

Since storage systems can have different C-rates, battery cost has been modeled as the sum of a power temr (€/MW) and an energy term (€/MWh), taking into account construction costs and O&M costs for both terms. In general, battery costs are usually reported as dependent only on size or energy, specifying storage duration case by case. Therefore, the cost terms have been calculated fitting the cost model with available data. As for the PV, two dataset have been used, referring to different power ranges: an utility-scale 60 MW battery with duration from 2 to 10 hours [81], and a commercial 300 kW battery with duration from 1 to 8 hours [80].

Figure 5.3 shows the construction cost of batteries used to fit the data, and Table 5.8, Table 5.9, and Figure 5.4 report a comparison of the real costs and those estimated by the model.

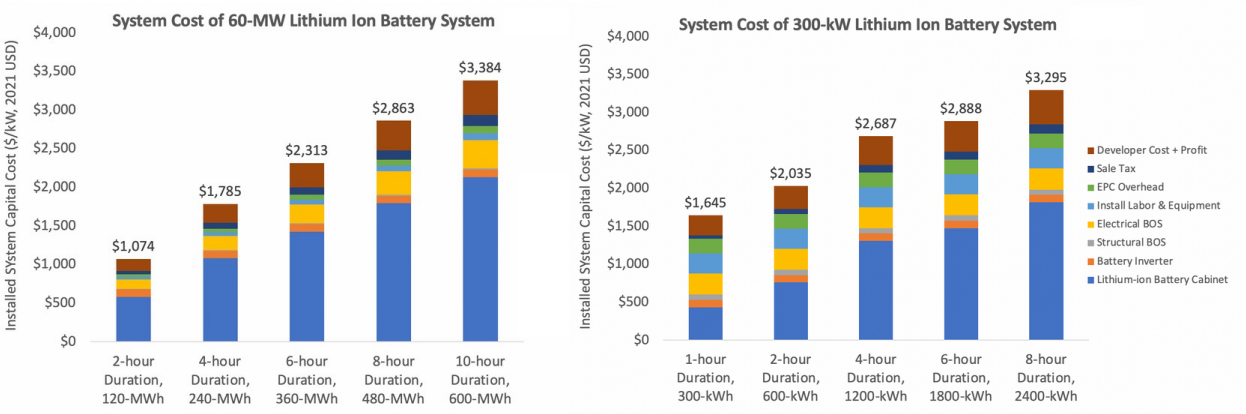

Figure 5.3: Battery construction costs breakdown for different sizes and C-rates

Power	Energy	Duration	Price	Real cost	Estimate
MW	MWh	h	k$/MW/y	M$/y	M$/y
60	120	2	28.3	1.70	1.70
60	240	4	47.7	2.86	2.87
60	360	6	67.0	4.02	4.03
60	480	8	86.4	5.18	5.20
60	600	10	105.7	6.34	6.36

Table 5.8: Comparison between real and estimated construction costs of different utility-scale batteries

Power	Energy	Duration	Price	Real cost	Estimate
kW	kWh	h	$/kW/y	k$/y	k$/y
300	300	1	40.4	12.1	12.2
300	600	2	48.9	14.7	14.7
300	1200	4	65.9	19.8	19.8
300	1800	6	82.8	24.8	24.9
300	2400	8	99.7	29.9	30.0

Table 5.9: Comparison between real and estimated construction costs of different commercial batteries

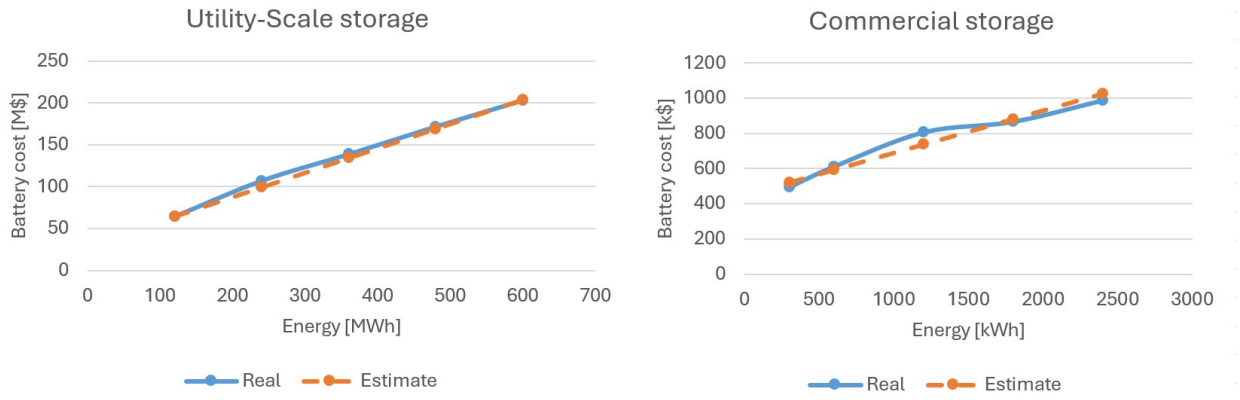

Figure 5.4: Comparison between real construction costs for batteries and construction costs estimated through the model

The same process has been repeated for O&M costs, fitting data from batteries with different charge/discharge times (Figure 5.5) into the model, as shown in Table 5.10, Table 5.11, and Figure 5.6.

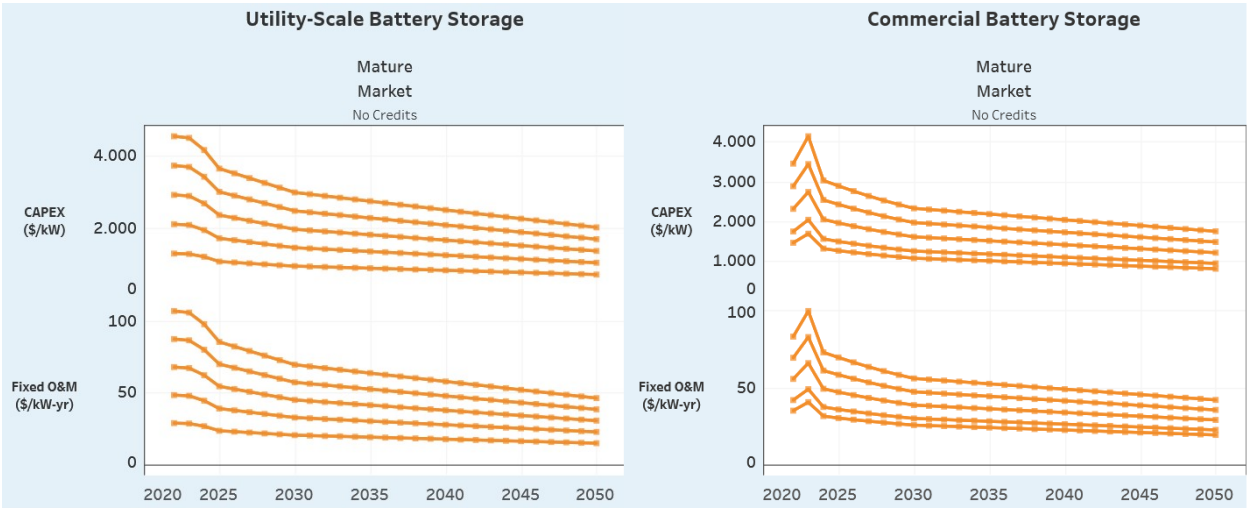

Figure 5.5: Battery O&M costs in 2023, with projected cost reduction over the next years

Power	Energy	Duration	Price	Real cost	Estimate
MW	MWh	h	k$/MW/y	M$/y	M$/y
60	120	2	28.3	1.70	1.70
60	240	4	47.7	2.86	2.87
60	360	6	67.0	4.02	4.03
60	480	8	86.4	5.18	5.20
60	600	10	105.7	6.34	6.36

Table 5.10: Comparison between real and model-estimated O&M costs of different utility-scale batteries

Power	Energy	Duration	Price	Real cost	Estimate
kW	kWh	h	$/kW/y	k$/y	k$/y
300	300	1	40.4	12.1	12.2
300	600	2	48.9	14.7	14.7
300	1200	4	65.9	19.8	19.8
300	1800	6	82.8	24.8	24.9
300	2400	8	99.7	29.9	30.0

Table 5.11: Comparison between real and model-estimated O&M costs of different commercial batteries

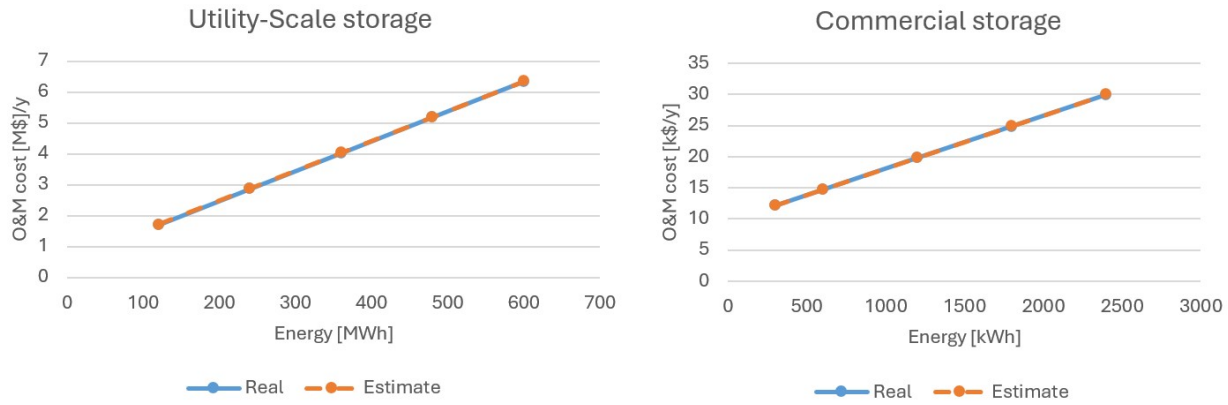

Figure 5.6: Comparison between real O&M costs for batteries and O&M costs estimated through the model

For both utility-scale and commercial sizes, yearly O&M costs have been merged to construction costs considering a technical life of 15 years. For this study, expecting to include battery systems of a few megawatts, intermediate values between utility-scale and commercial size have been used: 1.5 M€/MW for power, and 0.45 M€/MWh for energy. Battery energy conversion efficiency has been set to 95%, corresponding to a round trip efficiency around 90% [82].

	Construction	O&M	Battery power cost	
	M$/MW	M$/MW/y	M$/MW	M€/MW
Utility-scale storage	0.5	9	0.64	0.69
Commercial storage	1.5	32	1.98	2.14

Table 5.12: Battery power size-dependent usage-independent cost estimation

	Construction	O&M	Battery energy cost	
	M$/MWh	k$/MWh/y	M$/MWh	M€/MWh
Utility-Scale storage	0.29	9.7	0.44	0.47
Commercial storage	0.24	8.5	0.37	0.40

Table 5.13: Battery energy size-dependent usage-independent cost estimation

5.5 Usage-dependent components costs

As reported previously in Table 5.2, the model includes usage-dependent costs (€/MWh) for the gas boiler and the grid, i.e. money for the provision of natural gas and electric energy from the public networks. All simulations have been carried considering the system as located in Buccino (Magaldi's industrial production facility), in the province of Salerno, Italy; therefore, Italian markets have been considered, employing day-ahead hourly prices of electricity [83] and daily prices of natural gas [84] from the Italian energy markets operator: Gestore Mercati Energetici (GME). Unless explicitly specified, prices of year 2023 have been considered in the simulations.

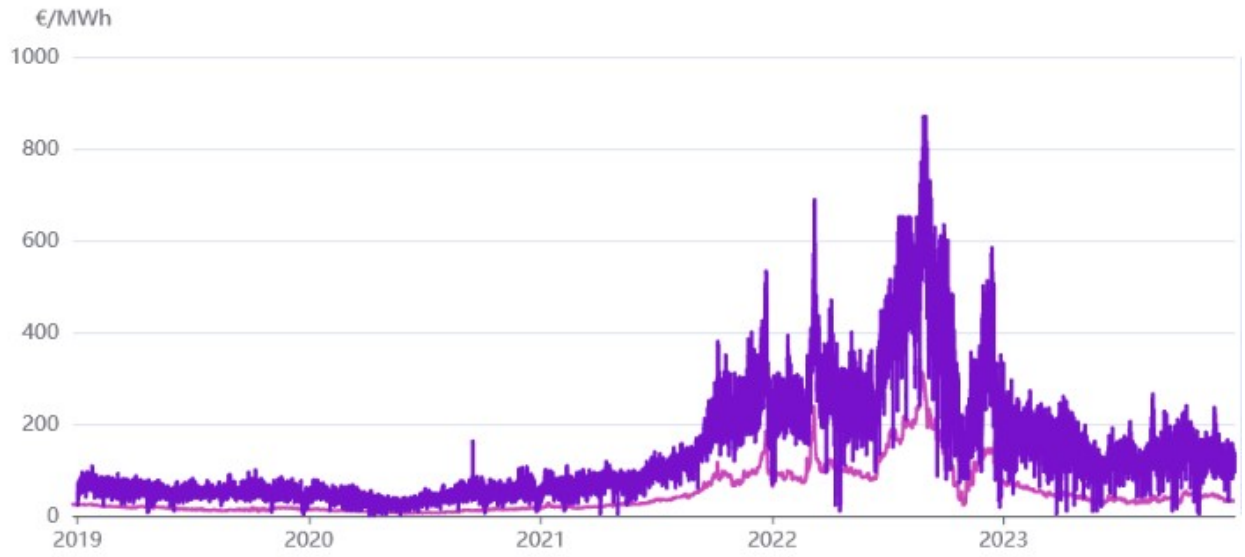

Figure 5.7: Hourly prices of electricity and daily prices of natural gas in day-ahead Italian market

5.6 PV production profile and other input data

For the PV plant, no usage-dependent cost has been considered, given the great advantage of exploiting (free) solar source. Data from PVGIS 5.2 [85] have been employed as target power profile for the PV plant ($\bar{p}_{out}^{PV}$); since PVGIS 5.2 offers data from 2010 to 2021, ESTESO has been set to use the data of the closest available year for computations before 2010 and after 2021.

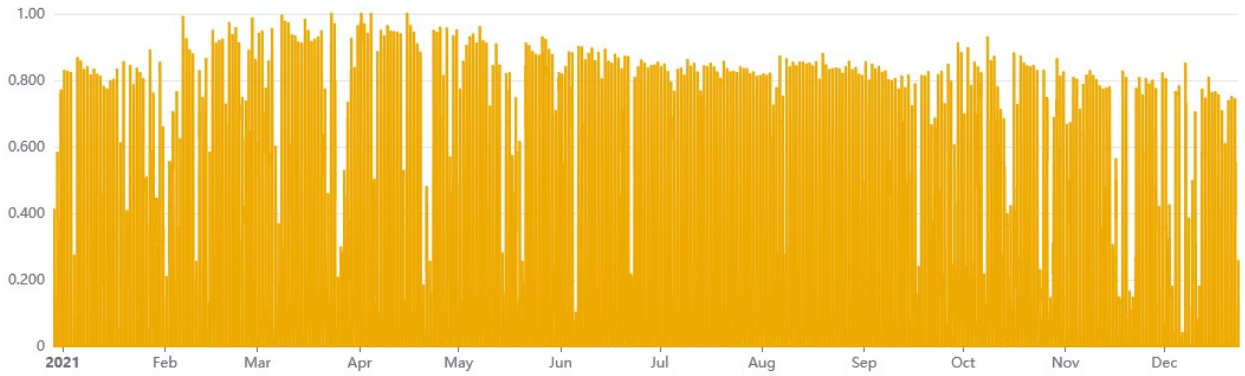

Figure 5.8: Normalized PV output power in Buccino (Italy) in 2021, from PVGIS 5.2

Table 5.14 summarizes the usage-dependent components costs and other time-series data used in the optimizations.

Component	Quantity	Years	Source	Ref	Notes
Grid	OPEX	2010-2024	GME	[83]	Italian market MGP
Gas boiler	OPEX	2016-2024	GME	[84]	Italian market MGP-GAS
PV	Output	2021-2021	PVGIS 5.2	[85]	Location: Buccino (SA, Italy)

Table 5.14: Summary of OPEX (usage-dependent) costs and other timeseries data used in this study

According to P2H usage scenarios described previously in Section 2.4, a "peak-load almost-shifted" profile has been chosen for the thermal energy demand of the process, and the electric energy adsorbed by the load. Figure 5.9 shows the profile used (power demand for 10h, from 12:00 to 22:00), comparing it with the PV available power in a sunny day. The maximum power demand has been set to 15 MW for the process, and 500 kW for the load.

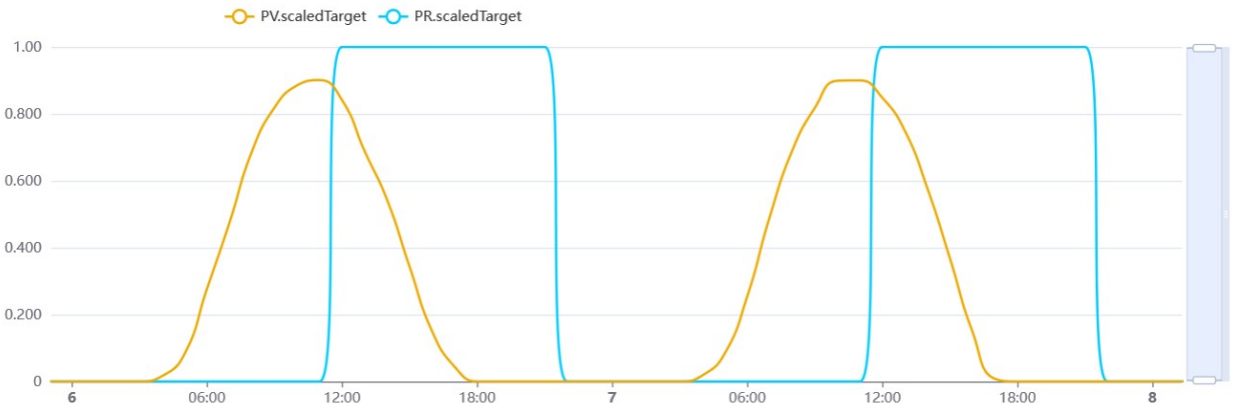

Figure 5.9: Power demand profiles for the thermal process (and the electrical load) used in ESTESO, compared to the expected PV output power in good weather conditions

Table 5.15 reports MGTES technology parameters used for the optimizations, referring to a module charging and discharging in 4 hours, producing superheated steam at 300 °C. It should be noted that these values may change depending on working temperatures and other factors. For instance, for energy-intensive applications requiring longer charge and/or discharge times, MGTES modules can be equipped with fewer resistors or steam tubes units, keeping the same energy capacity with a reduced input and/or output power, according to user's needs.

Parameter	Symbol	Value
Storage capacity	$K^{MG.SA}$	0.1 MWh/t
Resistors power	$K^{MG.RE}$	25 kW/t
Steam tubes power	$K^{MG.ST}$	25 kW/t
Resistors efficiency	$\eta^{MG.RE}$	98%
Steam tubes efficiency	$\eta^{MG.ST}$	98%
Wall losses	τ^{MG}	2 %/d

Table 5.15: MGTES technology parameters used for the optimizations

5.7 Model performance and LP approximation

The introduction of binary activation variables s^{MG}, $s^{MG.RE}$, $s^{MG.ST}$ made the optimization problem mixed-integer, requiring the use of a MILP solver, instead of a standard LP one, with a considerable increase in computation times.

For this reason, a LP approximation has been introduced in the model, to reduce computation times to a reasonable scale. In fact the MILP solver could not find a solution for any of the sizing optimization tests considering more than 4 days of operation. The binary activation variables (0 or 1) have been transformed into continuous ones (real values between 0 and 1), and Equations 5.3 have been modified, using = instead of $\leq$, yielding Equations 5.14.

$$p_{in}^{MG.RE} = P_{in}^{MG.RE}\, s^{MG.RE} \qquad p_{in}^{MG.ST} = P_{in}^{MG.ST}\, s^{MG.ST} \tag{5.14}$$

Finally, Equation 5.4 has been replaced by 5.15, introducing the term $1/2$ to ensure that $s^{MG} \leq 1$, even when simultaneously charging and discharging MGTES at maximum power.

$$s^{MG} = \frac{1}{2}\left(\frac{p_{in}^{MG.RE}}{P_{in}^{MG.RE}} + \frac{p_{out}^{MG.ST}}{P_{out}^{MG.ST}}\right) \tag{5.15}$$

To assess the impact of the approximation on model accuracy and computation performance, preliminary optimizations have been performed, considering four operation durations (from 1 to 4 days), testing both sizing and management optimization with and without the LP approximation. A dedicated `MILP` flag (`MILP` = 1: binary activation variable, `MILP` = 0: continuous activation variable) has been introduced, in order to easily compare the optimization results of the same system, with different values for the flag.

Table 5.16 and Figures 5.10 summarize the computation times of the optimizations, showing in red the (longer) times of the MILP solver, and in green those of the optimizations with LP approximation. Table 5.17 reports values of total system costs with and without the approximation, along with the associated errors, and Table 5.18 reports values (and errors) of optimal PV and grid power capacities, obtained from sizing optimizations.

For management optimizations, the following components sizes have been adopted: 10 MW for the PV plant, 5 MW for the grid connection, and 1 MW for the battery storage, with 1 MWh energy capacity. For all tests, ESTESO has been configured to minimize total costs, and constrained to achieve a decarbonization level of 0.5.

Duration	Sizing optimization				Management optimization			
	MILP	LP	Saved time		MILP	LP	Saved time	
days	s	s	s	%	s	s	s	%
1	0.30	0.17	0.12	41%	0.31	0.20	0.11	36%
2	0.83	0.24	0.59	71%	0.58	0.47	0.11	19%
3	12.80	0.70	12.10	95%	2.78	0.56	2.22	80%
4	30.00	0.54	29.46	98%	5.20	0.81	4.39	84%

Table 5.16: Computation performance comparison with and without LP approximation

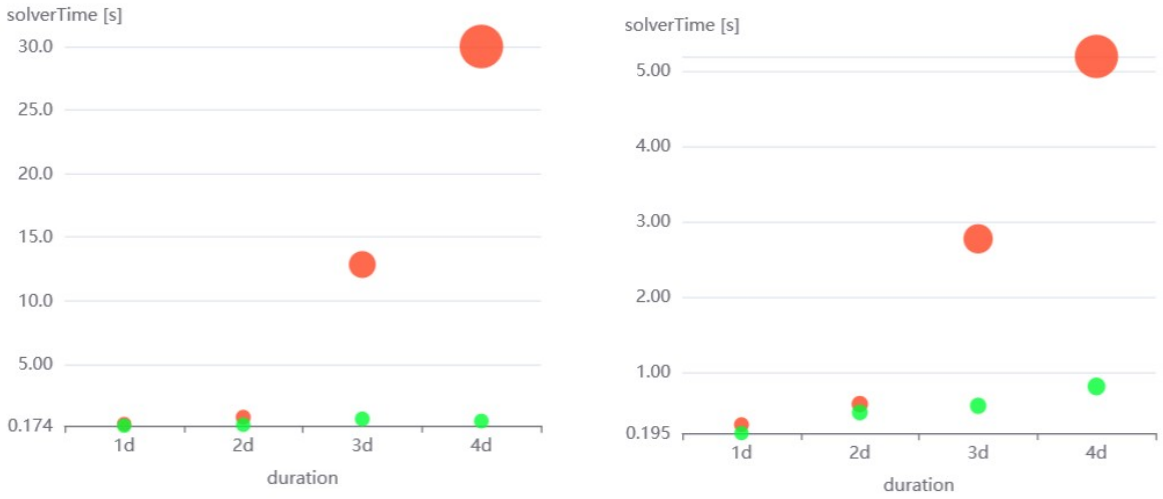

(a) Sizing optimization **(b)** Management optimization

Figure 5.10: Computation performance comparison with and without LP approximation

Duration	Sizing optimization				Management optimization			
	MILP	LP	Error		MILP	LP	Error	
days	k€	k€	k€	%	k€	k€	k€	%
1	6.90	6.78	-0.12	-1.7%	7.2	7.0	-0.2	-2.8%
2	13.90	13.70	-0.20	-1.4%	14.6	14.2	-0.4	-2.7%
3	21.40	20.90	-0.50	-2.3%	23.4	22.5	-0.9	-3.8%
4	28.90	28.30	-0.60	-2.1%	32.3	30.9	-1.4	-4.3%

Table 5.17: Total system costs comparison with and without LP approximation

Duration	Optimal PV size				OPtimal grid size			
	MILP	LP	Error		MILP	LP	Error	
days	MW	MW	MW	%	MW	MW	MW	%
1	0.75	0.63	-0.12	-16.0%	11.7	11.3	-0.4	-3.4%
2	0.75	0.63	-0.12	-16.0%	11.9	11.5	-0.4	-3.4%
3	0.75	0.70	-0.05	-6.7%	12.1	11.7	-0.4	-3.3%
4	0.69	0.63	-0.06	-8.7%	12.2	11.7	-0.5	-4.1%

Table 5.18: PV and grid optimal size comparison with and without LP approximation

In all the analyzed cases, the approximation caused an underestimation of about 5% in optimal values, except for grid capacity (errors up to 16%, but limited below 1 MW). Such errors are acceptable, given the remarkable performance gain obtained through the approximation, and the significant uncertainty of scenario data.

In the following, additional comparisons (with and without the approximation) for the management optimizations lasting 2 days are presented, in order investigate further the error found in total values, looking at individual components costs and power profiles.

Figures 5.11 and 5.12 show the cost breakdown of the system, optimized with and without the LP approximation; in the diagrams, more intense red color corresponds to more money spent for a component. The only difference between the two figures lies in grid OPEX costs, underestimated by the LP approximation of about 500 € (around 3% of total costs).

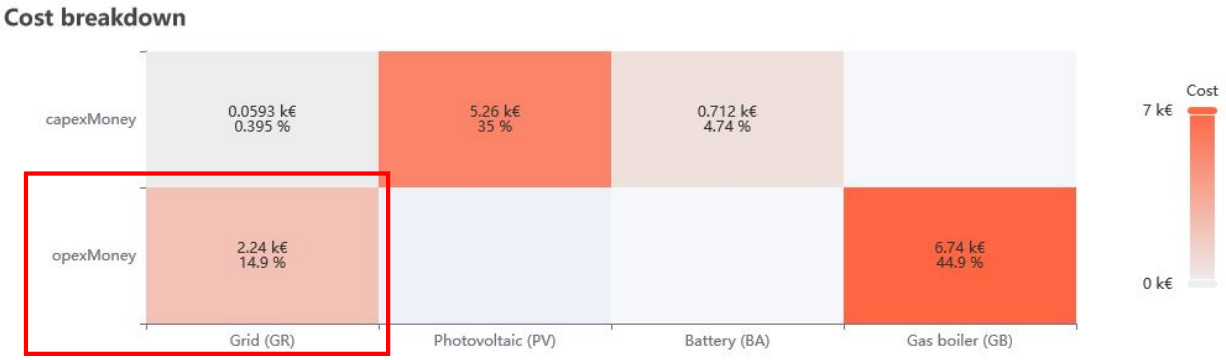

Figure 5.11: Cost breakdown of the system optimized without LP approximation (`MILP` = 0)

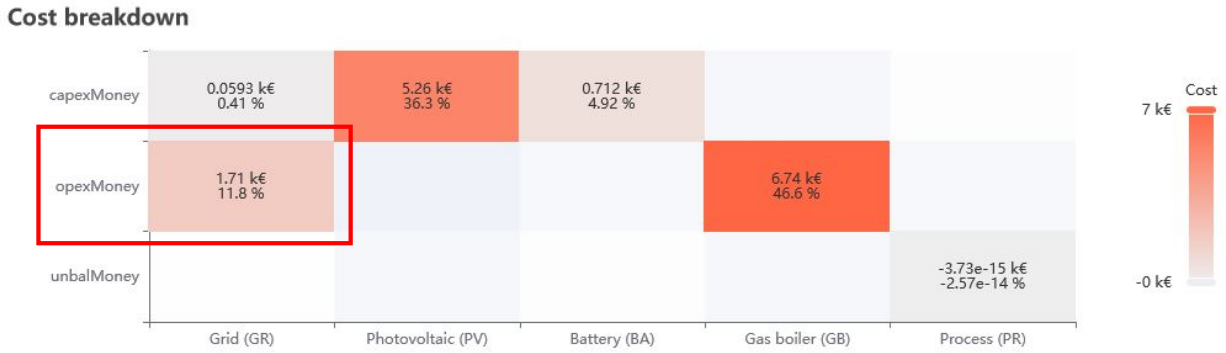

Figure 5.12: Cost breakdown of the system optimized with LP approximation (`MILP` = 1)

The same difference can be found also comparing Figures 5.13 and 5.14, showing the energy breakdown of the system, optimized with and without the LP approximation; more intense blue color corresponds to more energy adsorbed, provided or dissipated by a component.

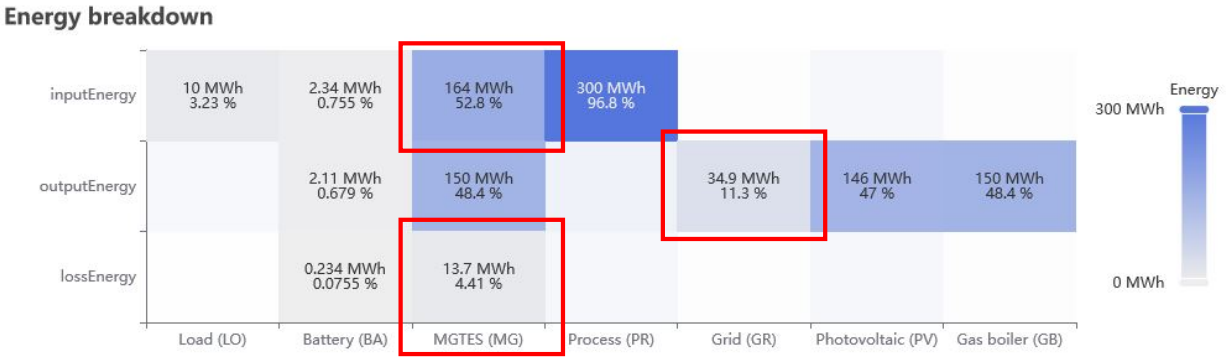

Figure 5.13: Energy breakdown of the system optimized without LP approximation (`MILP` = 0)

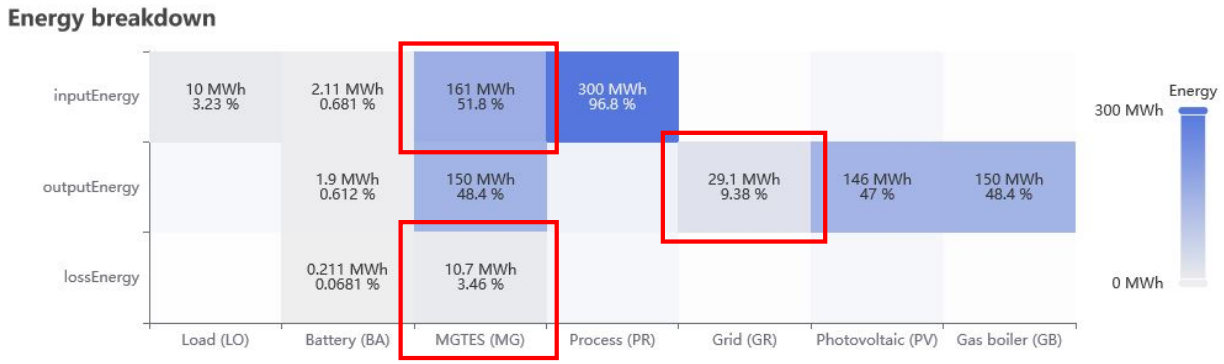

Figure 5.14: Energy breakdown of the system optimized with LP approximation (`MILP` = 1)

The comparison between the two diagrams reveals that the approximation caused the underestimation of grid output energy for about 6 MWh, corresponding to around 2% of the total energy served to the thermal process and the electrical load. This underestimation reflect into MGTES input energy, underestimated of 3 MWh, and the same for its lost energy, thus overestimating MGTES efficiency to 93% instead of 91%.

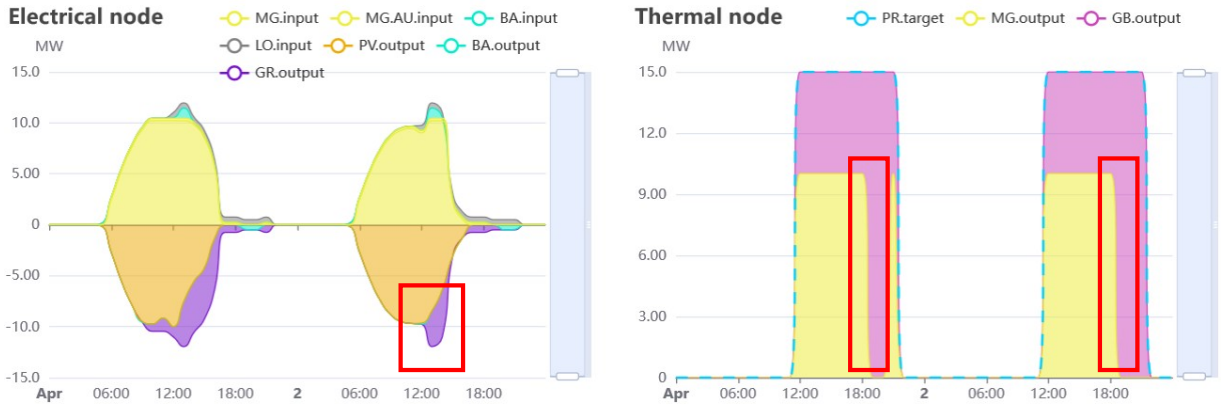

Figure 5.15: Electric (left) and thermal (right) power flows in the system optimized without LP approximation (`MILP` = 1)

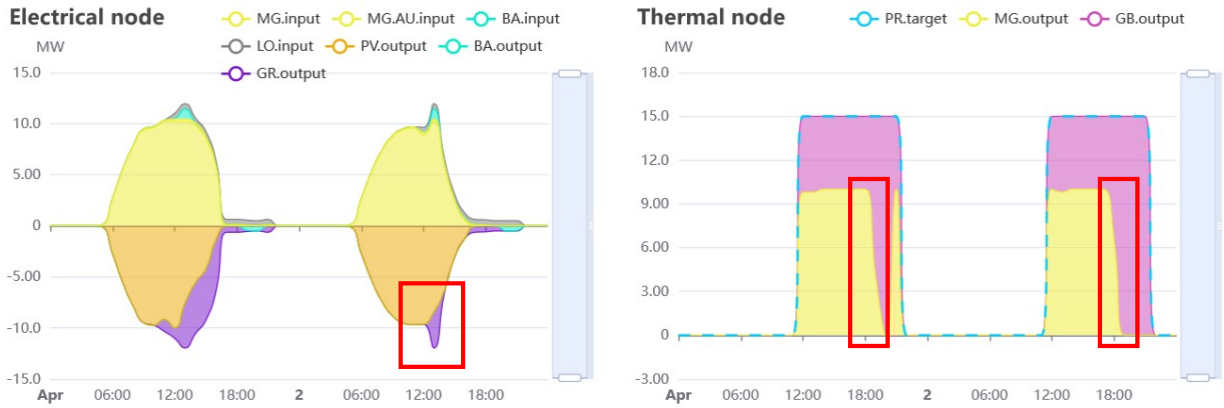

Figure 5.16: Electric (left) and thermal (right) power flows in the system optimized with LP approximation (`MILP` = 0)

Figures 5.15 and 5.16 show the electric and thermal power flows in the system, before and after the LP approximation, highlighting three main differences. The leftmost figure shows the underestimation of grid input energy (purple area) due to the approximation, recognized also in the previous charts, whereas the rightmost figure evidences a different profile of MGTES output power (yellow area). Regarding the latter, the MILP model preferred turning off MGTES rapidly after 18:00 of both days; for sure, this behaviour can be attributed to the presence of boolean activation variables in the model. On the contrary, the LP approximation chosed to turn off MGTES steam tubes more gradually, for both days.

This behaviour is found also in the rightmost part of Figures 5.17 and, 5.18, depicting the evolution of stored energy of MGTES, together with its input and output power profiles. The difference in the discharge profile of the first day brings a different value for the energy stored into sand between the first and the second day, as evidenced in the leftmost MGTES charts.

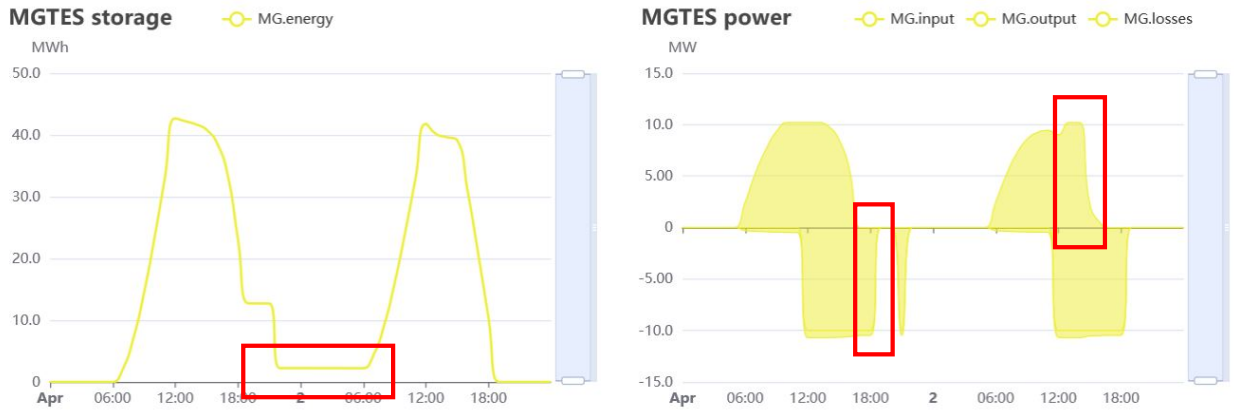

Figure 5.17: Stored energy (left) and power (right) profiles of MGTES in the system optimized without LP approximation (`MILP` = 1)

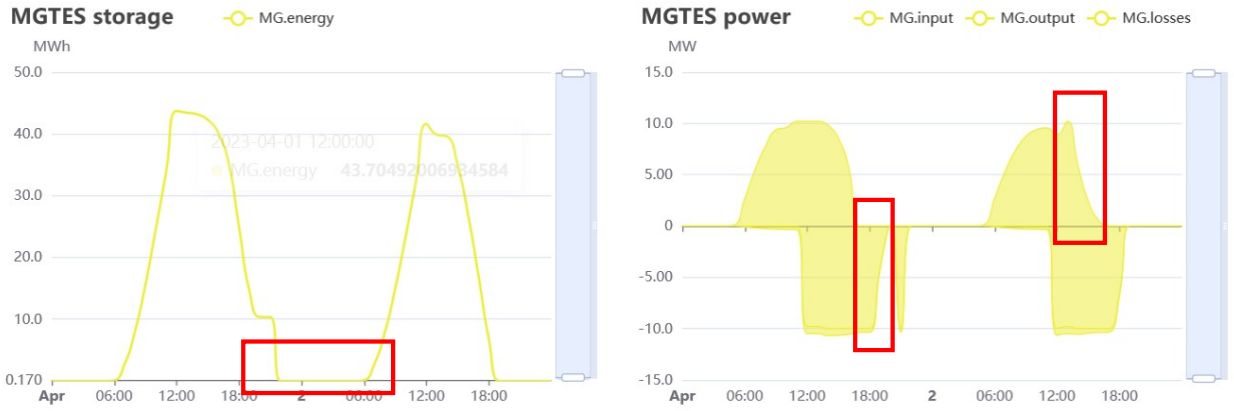

Figure 5.18: Stored energy (left) and power (right) profiles of MGTES in the system optimized with LP approximation (`MILP` = 0)

5.8 Sizing optimization results

Sizing optimization has been performed considering 3 MGTES sizes (125t, 250t, and 500t of sand), setting the decarbonization level as objective to maximize, for different fixed amounts of total costs, from 160 to 400 k€/month. Figures 5.19 illustrates ESTESO results for the optimization, showing one point for every solver run, highlighting different MGTES sizes in distinct colors (red for smaller sizes, green for larger ones), and higher decarbonization levels with bigger points.

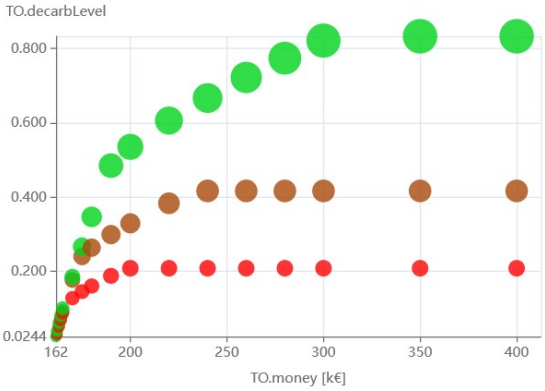

(a) Evolution of decarbonization level

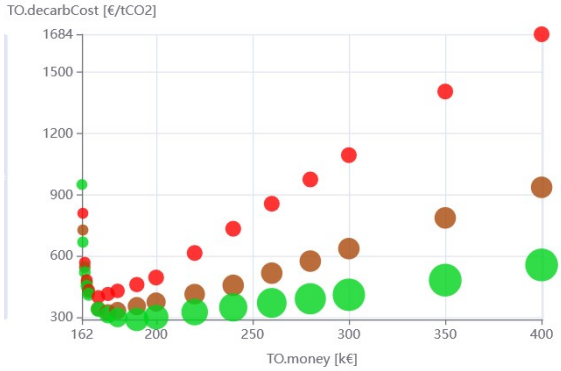

(b) Evolution of decarbonization cost

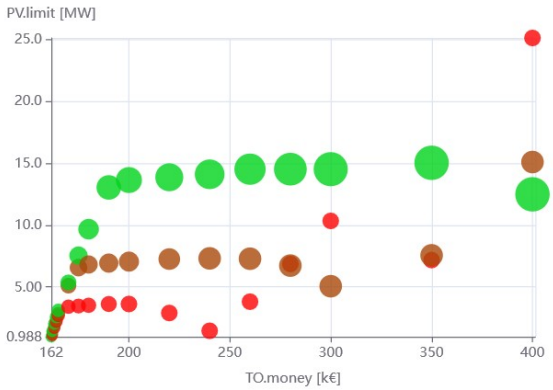

(c) Evolution of optimal PV power

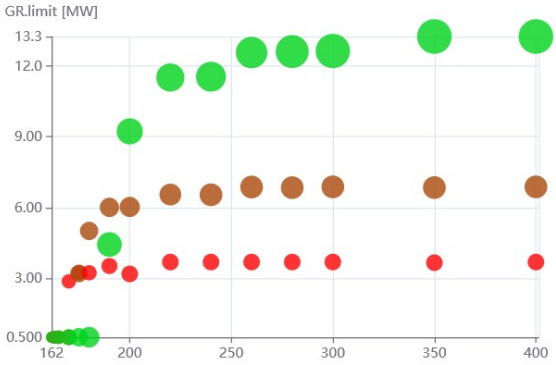

(d) Evolution of optimal grid connection power

Figure 5.19: Results of sizing optimization, considering different MGTES sizes and total system costs

Figure 5.19a displays the decarbonization level achieved by different values for total costs, evidencing an upper limit of saved emissions, depending on MGTES size (the maximum decarbonization level is proportional to sand mass). The steep rise of points in the leftmost part of the chart indicate a considerable decarbonization impact on the system for the first 200 k€. This is manifested also by Figure 5.19b, showing a minimum in decarbonization cost around that value, evidencing again that expenses above 200 k€ lead to a limited additional effect on system decarbonization.

Figure 5.19c and 5.19d exhibit the optimal sizes for the PV plant and the grid connection, for every MGTES size and total costs value. PV sizes raise rapidly around lower system costs (below 200 k€), then stabilize around a fixed value, close to resistors power capacity of every MGTES size. For higher values of total costs, optimal PV capacity start decreasing, thereafter increasing again. On the contrary, grid sizes remain around 500 kW (load power) for lower total costs, then increase quickly at a certain point, and consolidating around resistors power capacity.

As described below, Figure 5.20 evidences three distinct trends in the decarbonization cost achieved by each MGTES size. In contrast with the previous Figures, point sizes are proportional to total system costs.

1. **Descending trend**: decarbonization cost reduces with the rise of decarbonization level. During this trend, the optimal PV power capacity increases gradually, whereas the optimal power capacity for the grid connection remains fixed to a low value.
2. **Ascending trend**: decarbonization cost rises with decarbonization level. During this trend, the optimal grid connection capacity increases gradually, with a slight increase in PV capacity.
3. **Vertical trend**: decarbonization cost keeps increasing, with constant (maximum) decarbonization level, thus with no improvement in terms of emissions. During this trend, PV capacity starts increasing considerably again, with fixed grid connection power.

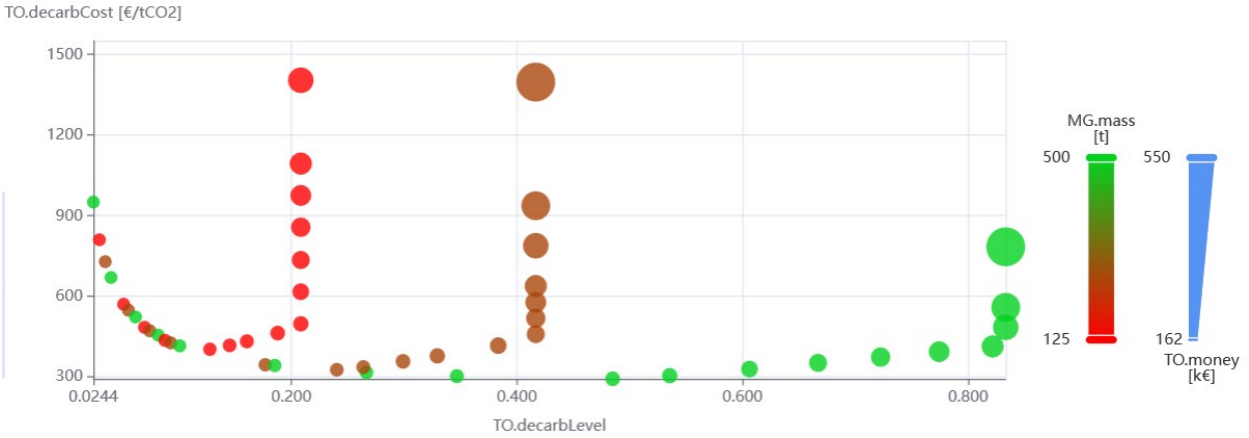

Figure 5.20: Decarbonization cost vs decarbonization level for different MGTES sizes

The point between descending and ascending decarbonization cost trends represents the minimum of the curve (γ_{min}), corresponding to the highest decarbonization effect per unit cost, for a given MGTES size. On the other hand, the point between ascending and vertical decarbonization cost trends identifies the maximum decarbonization level D_{max} attainable thanks to an MGTES module of defined size. Taking into account total costs beyond this point is not convenient, as the extra money spent for the system cannot save additional emissions.

Table 5.19 summarizes the results of the optimization, reporting the values of PV and grid power capacity, for the two key optimal points identified above, and for every MGTES size considered. The selection of the final system configuration is done based on the total available budget, to be spent both for MGTES and the rest of the system.

Due to their high CAPEX, batteries are never included in the system by the solver performing sizing optimizations. Given the limited electrical power adsorbed by the load and MGTES auxiliaries, in the scenario considered in this study a small grid connection is always more convenient than using a battery storage.

It should be noted that optimization results depend on various factors, including thermal process demand profile, components size-dependent costs, energy and gas prices, and geographical location. Therefore, these results must not be considered as general values for MGTES technology, since they may change according to specific use-case and applications.

Sand	Resistors	Minimum decarbonization cost					Maximum decarbonization level				
Λ^{MG}	$P_{in}^{MG.RE}$	P_{out}^{PV}	P_{out}^{GR}	D	$\mathbb{M}$	γ_{min}	P_{out}^{PV}	P_{out}^{GR}	D_{max}	$\mathbb{M}_{max}$	γ
t	MW	MWp	MW	-	k€	€/tCO$_2$	MW	MW	-	k€	€/tCO$_2$
125	3.1	3.4	0.5	0.12	170	400	3.6	3.4	0.21	200	495
250	6.3	6.5	0.5	0.23	175	320	7.3	6.9	0.42	240	460
500	12.5	12.9	0.5	0.42	185	285	14.5	13.3	0.83	310	415

Table 5.19: Results summary of sizing optimization of the modeled system, for different MGTES sizes

Chapter 6

Conclusions

The thesis deals with MGTES technology, focusing on the design of its electrical distribution system and resistor power supply, and describing the optimization carried out to maximize its performance and costs, thus fostering its widespread adoption in the industrial sector as a sustainable replacement for natural gas boilers.

6.1 Key results on hardware

For the connection of MGTES electric heaters to a renewable power plant and the power grid, the MVAC solution (centralized architecture with AC heaters) has been identified as the most adequate to MGTES technology; such solution minimizes the adoption of costly power electronic converters for the electrical distribution system.

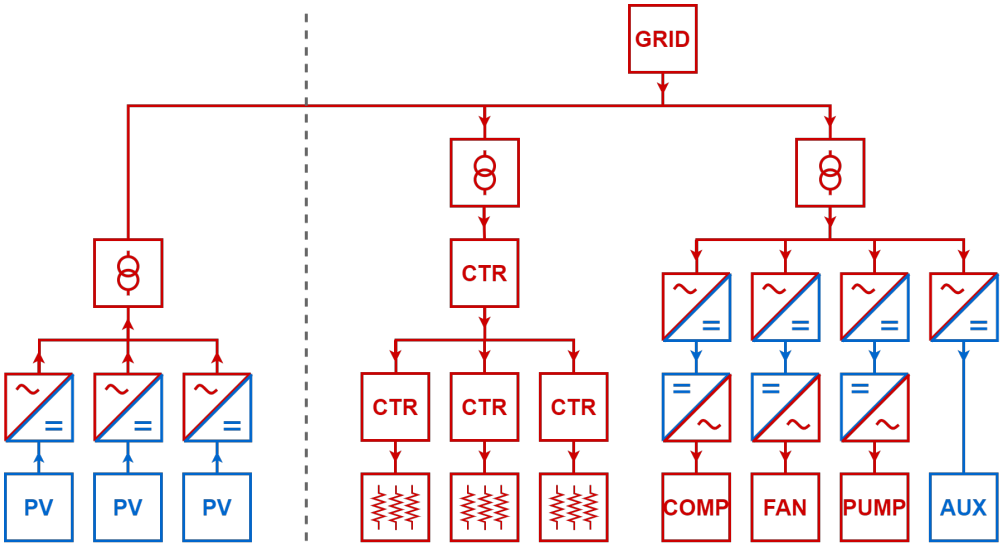

Figure 6.1: MVAC configuration schematic, chosen as the standard one for MGTES

For the adjustment of MGTES input power, three solutions have been identified and examined: power electronic devices (continuous control), OLTCs (step-wise control) and contactors (on/off control).

Technology	Power electronics	OLTC	Contactors
Control mode	Continuous	Discrete	Discrete / ON-OFF
Resolution	High	Medium	Medium / Low
Response time	Fast (∼ms)	Slow (∼s)	Fast (∼ms)
Technical life	5-10 years	15-20 years	25-30 years
EMC problems	Yes	Transient	No

Table 6.1: Comparison of different devices for MGTES heaters power control

OLTCs and contactors represent interesting alternatives to power electronic devices for applications that do not require a precise control, achieving proper resolution at limited cost, high reliability and recyclability. In fact, star-delta reconfiguration strategies can be effectively employed for a 100%-33.3%-0% power adjustment, leveraging readily available industrial hardware, thus benefiting from low costs and a streamlined supply chain. To achieve finer control resolution, two Contactors as Secondary Tap Selector (CSTS) solutions (simple and advanced) have been proposed. The advanced solution integrates star-delta contactors into the simple CSTS setup, ensuring comparable control characteristics at reduced costs and minimized losses.

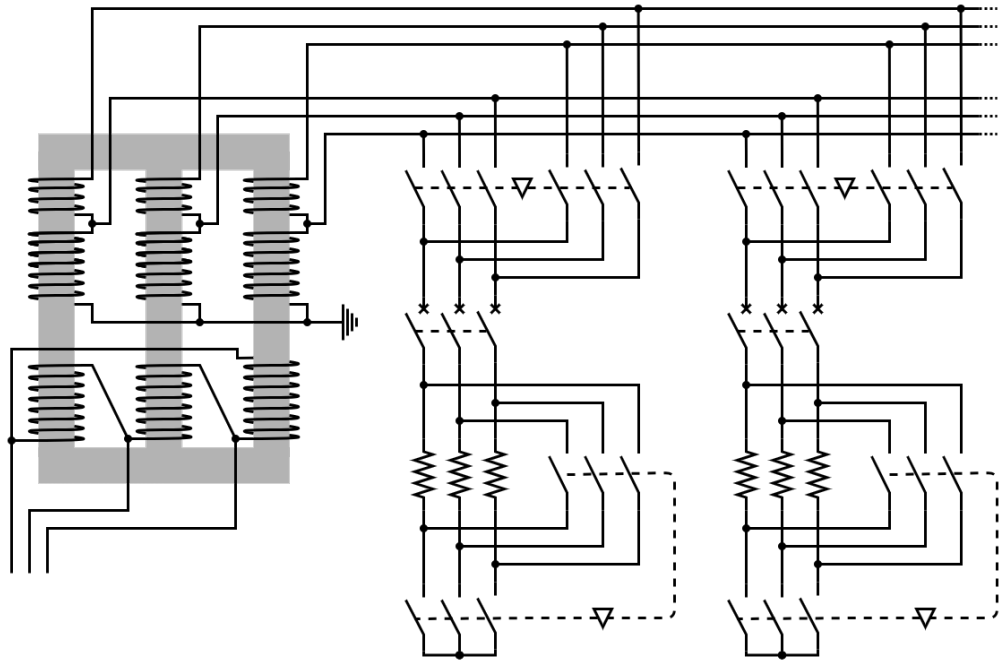

Figure 6.2: Basic schematic of the advanced CSTS configuration with two taps, for two resistors banks

It has been proven analytically that, in the case of discrete power control, the minimum charging time is achieved by choosing the power steps to follow a geometric progression, enabling finer power adjustment during the final part of the charging phase. This allowed to define an optimized setup, which employs a transformer with two taps on the same secondary winding: one at full voltage and the other at 76% of the maximum voltage ($1/\sqrt[4]{3}$), enabling discrete four-step control with power levels following a geometric progression with ratio $1/\sqrt{3} \approx 0.577$: 100%, 57.7%, 33.3%, 19.2%.

6.2 Key results on software and models

Models and algorithms have been developed to simulate and optimize MGTES across diverse scenarios, culminating in the realization of a powerful optimization software, named Elastic Software for Thermal Energy Storage Optimization (ESTESO). ESTESO adheres to a "one-tool approach", offering a versatile and unified solution to optimize both design and operation of MGTES systems; this approach enables the collection of all models and data into a unique place, to manage them consistently, streamlining the workflow to boost the continuous improvement of MGTES technology. Beyond its research applications, ESTESO has been designed for practical engineering usage, facilitating the sizing of MGTES systems.

A P2H system has been modeled in ESTESO to optimize the impact of MGTES in terms of decarbonization and system costs. The system comprises a thermal process, supplied by a gas boiler and MGTES, whose resistors are connected to the power grid, a PV plant, and a battery storage. The rich set of ESTESO standard properties allowed to model easily almost every part of the system, except for MGTES, whose peculiarities have been included adding custom properties and equations. For almost all components, online datasets have been exploited to extract size-dependent usage-independent costs (CAPEX), usage-dependent costs (OPEX), the output power profile for the PV plant, and other data used in the model for the optimization.

An LP approximation has been adopted to improve computational performances of the optimization, replacing binary (0/1) variables with continuous ones, enabling the use of a LP solver in place of a MILP one, undoubtedly slower than the other. Different optimization tests have been carried out to evaluate the effect of the approximation, obtaining encouraging results. In fact, the approximation exhibited a remarkable performance improvement, allowing to shrink computation times considerably, from 20% to even up to a 98% reduction. Figure 6.3 shows in red the long computation times required to perform the optimization without the approximation (MILP model), whereas in green the shorter times obtained exploiting the LP approximation.

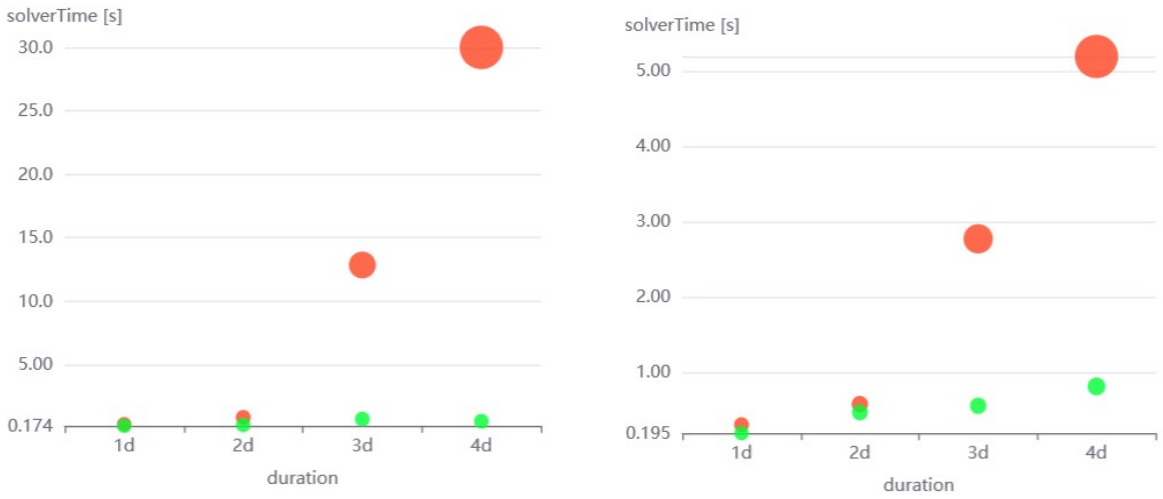

(a) Sizing optimization **(b)** Management optimization

Figure 6.3: Computation performance comparison with and without LP approximation

Regarding accuracy, the approximation revealed errors between 1.5 and 3% in most tests. Such values are surely acceptable and satisfactory, since these optimizations rely on uncertain scenario data, with typical errors above 5%. Therefore, the additional error introduced by the approximation remains marginal, with no significant negative impact on results quality.

However, additional comparisons were conducted, looking at individual components costs and power profiles. Figure 6.4 shows the thermal power adsorbed by the process, highlighting in yellow the power provided by MGTES. The red rectangles highlight a small but meaningful difference in MGTES output power: the results of MILP model (leftmost chart) evidences a sudden thermal energy supply interruption around 18:00 of both days, whereas the LP approximation (rightmost chart) shows a progressive output power descent.

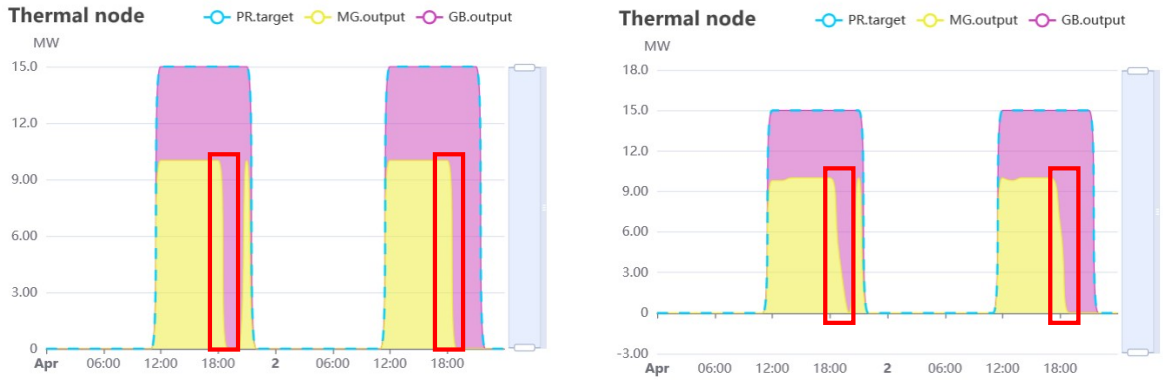

(a) Management optimization without approximation **(b)** Management optimization with LP approximation

Figure 6.4: Thermal power flows in the system optimized for 2 days

Besides total system costs, two indicators have been defined to assess MGTES impact in terms of emission reduction: decarbonization level D, indicating the fraction of thermal energy supplied by MGTES to the process, and decarbonization cost γ, measuring the emissions reduction against the sustained costs, thus quantifying the decarbonization effectiveness of the expenses.

Sizing optimizations were performed considering different MGTES sizes (125t, 250t, and 500t of sand), discovering for each one three distinct correlation trends between the decarbonization cost and the decarbonization level. As shown in Figure 6.5, for low decarbonization levels the decarbonization cost decreases until its minimum value (descending trend), then it increases again (ascending trend) until reaching maximum decarbonization level, thereafter increasing without any additional decarbonization impact (vertical trend). Minimum decarbonization cost (between descending and ascending trends) and maximum decarbonization level (between ascending and vertical trends) represent key indicators for MGTES sizing, together with the associated optimal values of PV and grid power capacity. All these values depend on MGTES sand mass, as summarized in Table 6.2.

The optimal power capacity for the grid connection stays fixed to a constant value in the descending trend of decarbonization cost, then raises during the ascending trend, reaching MGTES resistors power capacity upon maximum decarbonization level. On the contrary, the optimal PV capacity increases in the descending trend, then keeps approximately constant during ascending trend. Due to their high CAPEX, batteries are never included in the system by the solver.

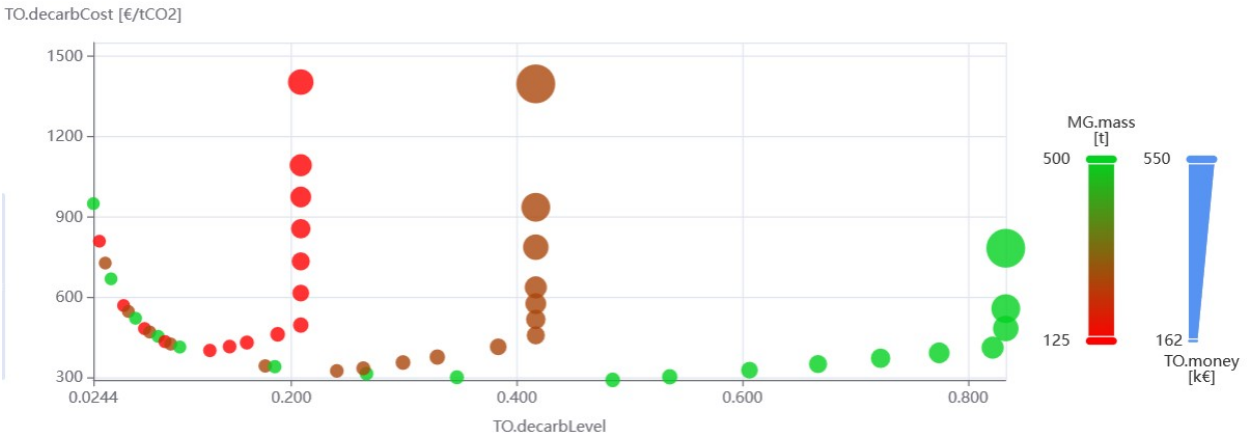

Figure 6.5: Decarbonization cost vs decarbonization level for different MGTES sizes

Sand mass	Resistors power	Minimum decarbonization cost			Maximum decarbonization level		
Λ^{MG}	$P_{in}^{MG.RE}$	P_{out}^{PV}	P_{out}^{GR}	D	P_{out}^{PV}	P_{out}^{GR}	D_{max}
t	MW	MWp	MW	-	MW	MW	-
125	3.1	3.4	0.5	0.12	3.6	3.4	0.21
250	6.3	6.5	0.5	0.23	7.3	6.9	0.42
500	12.5	12.9	0.5	0.42	14.5	13.3	0.83

Table 6.2: Results summary of sizing optimization of the modeled system, for different MGTES sizes

6.3 Future developments for ESTESO

MGTES models will be enriched to reflect the internal thermal behavior of the module. This enhancement will be useful to perform the design optimization of the heating elements. In accordance to the one-tool approach, the framework will be expanded to allow selecting among various models (with different complexity) for the same component. This will ensure the correct balance between model accuracy and computation burden, based on the scope of the simulation or optimization.

A dedicated forecaster for energy prices, PV output and electrical load will be developed and integrated into ESTESO, to generate predictions for MGTES operation optimization. After completing the required features for the purpose, ESTESO will be used to control working MGTES systems in real-time, to optimize its operation. The models will be fitted to experimental data, with improved automatic estimation of technology parameters: losses, auxiliary consumption, and efficiency.

In addition, the modeling of multiple modules will allow taking into account bigger plants, consisting of many modules, connected in series or in parallel, depending on the application. This will require the extension of the framework to take into account variables defined over multiple dimensions, other than time.

Bibliography

[1] Global Carbon Project. Supplemental data of global carbon project, 2022. URL https://www.icos-cp.eu/GCP/2022.

[2] Council of European Union. 'fit for 55': delivering the eu's 2030 climate target on the way to climate neutrality, 2023. URL https://eur-lex.europa.eu/legal-content/EN/TXT/?uri=CELEX:52021DC0550.

[3] TERNA (Italian Transmission System Operator). National transmission grid development plan, 2023. URL https://www.terna.it/it/sistema-elettrico/rete/piano-sviluppo-rete.

[4] Bloomberg New Energy Finance (BNEF). Global low carbon energy technology investment surges past $1 trillion for the first time, 2023. URL https://about.bnef.com/blog/global-low-carbon-energy-technology-investment-surges-past-1-trillion-for-the-first-time

[5] Marialaura Di Somma, Maria Carmen Falvo, Giorgio Graditi, Matteo Manganelli, Matteo Scanzano, and Maria Valenti. Integration of renewable energy source in transmission grids: issues and perspectives. In *2021 IEEE International Conference on Environment and Electrical Engineering and 2021 IEEE Industrial and Commercial Power Systems Europe (EEEIC / I&CPS Europe)*, pages 1–8, 2021. doi: 10.1109/EEEIC/ICPSEurope51590.2021.9584553.

[6] Tarun Kataray, B. Nitesh, Bharath Yarram, Sanyukta Sinha, Erdem Cuce, Saboor Shaik, Pethurajan Vigneshwaran, and Abin Roy. Integration of smart grid with renewable energy sources: Opportunities and challenges – a comprehensive review. *Sustainable Energy Technologies and Assessments*, 58, 2023. ISSN 2213-1388. doi: https://doi.org/10.1016/j.seta.2023.103363. URL https://www.sciencedirect.com/science/article/pii/S2213138823003569.

[7] Osama Majeed Butt, Muhammad Zulqarnain, and Tallal Majeed Butt. Recent advancement in smart grid technology: Future prospects in the electrical power network. *Ain Shams Engineering Journal*, 12(1):687–695, 2021. ISSN 2090-4479. doi: https://doi.org/10.1016/j.asej.2020.05.004. URL https://www.sciencedirect.com/science/article/pii/S2090447920301064.

[8] Jeff D. Colgan, Alexander S. Gard-Murray, and Miriam Hinthorn. Quantifying the value of energy security: How russia's invasion of ukraine exploded europe's fossil fuel costs. *Energy Research & Social Science*, 103:103201, 2023. ISSN 2214-6296. doi: https://doi.org/10.1016/j.erss.2023.103201. URL https://www.sciencedirect.com/science/article/pii/S221462962300261X.

[9] Qi Zhang, Kun Yang, Yi Hu, Jianbin Jiao, and Shouyang Wang. Unveiling the impact of geopolitical conflict on oil prices: A case study of the russia-ukraine war and its channels. *Energy Economics*, 126:106956, 2023. ISSN 0140-9883. doi: https://doi.org/10.1016/j.eneco.2023.106956. URL https://www.sciencedirect.com/science/article/pii/S0140988323004541.

[10] Trading Economics. Eu natural gas ttf daily prices, 2024. URL https://tradingeconomics.com/commodity/eu-natural-gas.

[11] International Energy Agency. Real-time electricity tracker, 2022. URL https://www.iea.org/data-and-statistics/data-tools/real-time-electricity-tracker.

[12] Bloomberg New Energy Finance (BNEF). Electric vehicle outlook. Annual report, Bloomberg New Energy Finance (BNEF), 2023. URL https://about.bnef.com/electric-vehicle-outlook/.

[13] Pope Francis. *Laudato Si': On Care for Our Common Home*. Vatican Press, 2015. URL https://www.vatican.va/content/francesco/en/encyclicals/documents/papa-francesco_20150524_enciclica-laudato-si.html.

[14] Magaldi group. Official website, 2024. URL https://www.magaldi.com/en.

[15] Magaldi group. Certificates and world-class patents, 2024. URL https://www.magaldi.com/en/certificates-patents.

[16] Magaldi group. Magaldi's commitment on research and development, 2024. URL https://www.magaldi.com/en/research-development.

[17] Yoash Levron and Doron Shmilovitz. Power systems' optimal peak-shaving applying secondary storage. *Electric Power Systems Research*, 89:80–84, 2012. ISSN 0378-7796. doi: https://doi.org/10.1016/j.epsr.2012.02.007. URL https://www.sciencedirect.com/science/article/pii/S037877961200048X.

[18] Zhuoqun Liu and Yang Du. Evolution towards dispatchable pv using forecasting, storage, and curtailment: A review. *Electric Power Systems Research*, 223:109554, 2023. ISSN 0378-7796. doi: https://doi.org/10.1016/j.epsr.2023.109554. URL https://www.sciencedirect.com/science/article/pii/S0378779623004431.

[19] Michael Emmanuel and Ramesh Rayudu. Evolution of dispatchable photovoltaic system integration with the electric power network for smart grid applications: A review. *Renewable and Sustainable Energy Reviews*, 67:207–224, 2017. ISSN 1364-0321. doi: https://doi.org/10.1016/j.rser.2016.09.010. URL https://www.sciencedirect.com/science/article/pii/S1364032116304981.

[20] Erphan A. Bhuiyan, Md. Zahid Hossain, S.M. Muyeen, Shahriar Rahman Fahim, Subrata K. Sarker, and Sajal K. Das. Towards next generation virtual power plant: Technology review and frameworks. *Renewable and Sustainable Energy Reviews*, 150:111358, 2021. ISSN 1364-0321. doi: https://doi.org/10.1016/j.rser.2021.111358. URL https://www.sciencedirect.com/science/article/pii/S1364032121006444.

[21] Rona George Allwyn, Amer Al-Hinai, and Vijaya Margaret. A comprehensive review on energy management strategy of microgrids. *Energy Reports*, 9:5565–5591, 2023. ISSN 2352-4847. doi: https://doi.org/10.1016/j.egyr.2023.04.360. URL `https://www.sciencedirect.com/science/article/pii/S2352484723007230`.

[22] Noshirwan K. Medora and Alexander Kusko. Battery management for hybrid electric vehicles using supercapacitors as a supplementary energy storage system. In *Intelec 2012*, pages 1–8, 2012. doi: 10.1109/INTLEC.2012.6374473.

[23] Muhammad Aamir, Kafeel Ahmed Kalwar, and Saad Mekhilef. Review: Uninterruptible power supply (ups) system. *Renewable and Sustainable Energy Reviews*, 58:1395–1410, 2016. ISSN 1364-0321. doi: https://doi.org/10.1016/j.rser.2015.12.335. URL `https://www.sciencedirect.com/science/article/pii/S1364032115017189`.

[24] Sarah M. Jordaan, Jiyun Park, and Shreya Rangarajan. Innovation in intermittent electricity and stationary energy storage in the united states and canada: A review. *Renewable and Sustainable Energy Reviews*, 158:112149, 2022. ISSN 1364-0321. doi: https://doi.org/10.1016/j.rser.2022.112149. URL `https://www.sciencedirect.com/science/article/pii/S1364032122000776`.

[25] Mohammed Yekini Suberu, Mohd Wazir Mustafa, and Nouruddeen Bashir. Energy storage systems for renewable energy power sector integration and mitigation of intermittency. *Renewable and Sustainable Energy Reviews*, 35:499–514, 2014. ISSN 1364-0321. doi: https://doi.org/10.1016/j.rser.2014.04.009. URL `https://www.sciencedirect.com/science/article/pii/S1364032114002366`.

[26] Dhivya Sampath Kumar, Salish Maharjan, Albert, and Dipti Srinivasan. Ramp-rate limiting strategies to alleviate the impact of pv power ramping on voltage fluctuations using energy storage systems. *Solar Energy*, 234:377–386, 2022. ISSN 0038-092X. doi: https://doi.org/10.1016/j.solener.2022.01.059. URL `https://www.sciencedirect.com/science/article/pii/S0038092X22000706`.

[27] Ali Shahmohammadi, Ramteen Sioshansi, Antonio J. Conejo, and Saeed Afsharnia. The role of energy storage in mitigating ramping inefficiencies caused by variable renewable generation. *Energy Conversion and Management*, 162:307–320, 2018. ISSN 0196-8904. doi: https://doi.org/10.1016/j.enconman.2017.12.054. URL `https://www.sciencedirect.com/science/article/pii/S0196890417312062`.

[28] J.D. Nixon, K. Bhargava, A. Halford, and E. Gaura. Analysis of standalone solar streetlights for improved energy access in displaced settlements. *Renewable Energy*, 177:895–914, 2021. ISSN 0960-1481. doi: https://doi.org/10.1016/j.renene.2021.05.105. URL `https://www.sciencedirect.com/science/article/pii/S0960148121007886`.

[29] Ahmed Zayed AL Shaqsi, Kamaruzzaman Sopian, and Amer Al-Hinai. Review of energy storage services, applications, limitations, and benefits. *Energy Reports*, 6:288–306, 2020. ISSN 2352-4847. doi: https://doi.org/10.1016/j.egyr.2020.07.028. URL `https://www.sciencedirect.`

com/science/article/pii/S2352484720312464. SI:Energy Storage - driving towards a clean energy future.

[30] Gulin Yurter, Emre Nadar, and Ayse Selin Kocaman. The impact of pumped hydro energy storage configurations on investment planning of hybrid systems with renewables. *Renewable Energy*, 222:119906, 2024. ISSN 0960-1481. doi: https://doi.org/10.1016/j.renene.2023.119906. URL https://www.sciencedirect.com/science/article/pii/S0960148123018219.

[31] Shahid Ali, Rodney A. Stewart, and Oz Sahin. Drivers and barriers to the deployment of pumped hydro energy storage applications: Systematic literature review. *Cleaner Engineering and Technology*, 5:100281, 2021. ISSN 2666-7908. doi: https://doi.org/10.1016/j.clet.2021.100281. URL https://www.sciencedirect.com/science/article/pii/S266679082100241X.

[32] Anuoluwapo Aluko and Andy Knight. A review on vanadium redox flow battery storage systems for large-scale power systems application. *IEEE Access*, 11:13773–13793, 2023. doi: 10.1109/ACCESS.2023.3243800.

[33] Mohammad Ali Abdelkareem, Mohamad Ayoub, Siren Khuri, Abdul Hai Alami, Enas Taha Sayed, T D Deepa, and A.G. Olabi. Environmental aspects of batteries. *Sustainable Horizons*, 8:100074, 2023. ISSN 2772-7378. doi: https://doi.org/10.1016/j.horiz.2023.100074. URL https://www.sciencedirect.com/science/article/pii/S2772737823000287.

[34] Zhijun Ren, Huajie Li, Wenyi Yan, Weiguang Lv, Guangming Zhang, Longyi Lv, Li Sun, Zhi Sun, and Wenfang Gao. Comprehensive evaluation on production and recycling of lithium-ion batteries: A critical review. *Renewable and Sustainable Energy Reviews*, 185:113585, 2023. ISSN 1364-0321. doi: https://doi.org/10.1016/j.rser.2023.113585. URL https://www.sciencedirect.com/science/article/pii/S1364032123004422.

[35] Alberto Berrueta, Alfredo Ursúa, Idoia San Martín, Ali Eftekhari, and Pablo Sanchis. Supercapacitors: Electrical characteristics, modeling, applications, and future trends. *IEEE Access*, 7:50869–50896, 2019. doi: 10.1109/ACCESS.2019.2908558.

[36] Weiming Ji, Feng Hong, Yuzheng Zhao, Lu Liang, Hao Du, Junhong Hao, Fang Fang, and Jizhen Liu. Applications of flywheel energy storage system on load frequency regulation combined with various power generations: A review. *Renewable Energy*, 223:119975, 2024. ISSN 0960-1481. doi: https://doi.org/10.1016/j.renene.2024.119975. URL https://www.sciencedirect.com/science/article/pii/S0960148124000405.

[37] A.G. Olabi, Tabbi Wilberforce, Mohamad Ramadan, Mohammad Ali Abdelkareem, and Abdul Hai Alami. Compressed air energy storage systems: Components and operating parameters – a review. *Journal of Energy Storage*, 34:102000, 2021. ISSN 2352-152X. doi: https://doi.org/10.1016/j.est.2020.102000. URL https://www.sciencedirect.com/science/article/pii/S2352152X20318351.

[38] Elaheh Bazdar, Mohammad Sameti, Fuzhan Nasiri, and Fariborz Haghighat. Compressed air energy storage in integrated energy systems: A review. *Renewable and Sustainable Energy Reviews*, 167:112701, 2022. ISSN 1364-0321. doi: https://doi.org/10.1016/j.rser.2022.112701. URL https://www.sciencedirect.com/science/article/pii/S1364032122005901.

[39] Ziyu Zhang, Tao Ding, Quan Zhou, Yuge Sun, Ming Qu, Ziyu Zeng, Yuntao Ju, Li Li, Kang Wang, and Fangde Chi. A review of technologies and applications on versatile energy storage systems. *Renewable and Sustainable Energy Reviews*, 148:111263, 2021. ISSN 1364-0321. doi: https://doi.org/10.1016/j.rser.2021.111263. URL https://www.sciencedirect.com/science/article/pii/S1364032121005505.

[40] Pavlos G. Papageorgiou, Konstantinos O. Oureilidis, and Georgios C. Christoforidis. A systematic review of hybrid superconducting magnetic/battery energy storage systems: Applications, control strategies, benefits, limitations and future prospects. *Renewable and Sustainable Energy Reviews*, 183:113436, 2023. ISSN 1364-0321. doi: https://doi.org/10.1016/j.rser.2023.113436. URL https://www.sciencedirect.com/science/article/pii/S1364032123002939.

[41] Bukola Babatunde Adetokun, Oghenewvogaga Oghorada, and Sufyan Ja'afar Abubakar. Superconducting magnetic energy storage systems: Prospects and challenges for renewable energy applications. *Journal of Energy Storage*, 55:105663, 2022. ISSN 2352-152X. doi: https://doi.org/10.1016/j.est.2022.105663. URL https://www.sciencedirect.com/science/article/pii/S2352152X22016516.

[42] Laura Pompei, Fabio Nardecchia, and Adio Miliozzi. Current, projected performance and costs of thermal energy storage. *Processes*, 11(3), 2023. ISSN 2227-9717. doi: 10.3390/pr11030729. URL https://www.mdpi.com/2227-9717/11/3/729.

[43] Hafiz Muhammad Ali, Tauseef ur Rehman, Müslüm Arıcı, Zafar Said, Benjamin Duraković, Hayder I. Mohammed, Rajan Kumar, Manish K. Rathod, Ozge Buyukdagli, and Mohamed Teggar. Advances in thermal energy storage: Fundamentals and applications. *Progress in Energy and Combustion Science*, 100:101109, 2024. ISSN 0360-1285. doi: https://doi.org/10.1016/j.pecs.2023.101109. URL https://www.sciencedirect.com/science/article/pii/S0360128523000394.

[44] T. Hegbom. *Integrating Electrical Heating Elements in Product Design*. Electrical and Computer Engineering. Taylor & Francis, 1997. ISBN 9780824798406. URL https://books.google.it/books?id=JKpfn0OpXEsC.

[45] Md. Nasimul Islam Maruf, Germán Morales-España, Jos Sijm, Niina Helistö, and Juha Kiviluoma. Classification, potential role, and modeling of power-to-heat and thermal energy storage in energy systems: A review. *Sustainable Energy Technologies and Assessments*, 53:102553, 2022. ISSN 2213-1388. doi: https://doi.org/10.1016/j.seta.2022.102553. URL https://www.sciencedirect.com/science/article/pii/S2213138822006038.

[46] I. Erro, P. Aranguren, F.J. Sorbet, I. Bonilla-Campos, and D. Astrain. Enhancement of the power-to-heat energy conversion process of a thermal energy storage cycle through the use of a thermoelectric heat pump. *Applied Thermal Engineering*, page 122923, 2024. ISSN 1359-4311. doi: https://doi.org/10.1016/j.applthermaleng.2024.122923. URL https://www.sciencedirect.com/science/article/pii/S135943112400591X.

[47] Meiling Yue, Hugo Lambert, Elodie Pahon, Robin Roche, Samir Jemei, and Daniel Hissel. Hydrogen energy systems: A critical review of technologies, applications, trends and challenges. *Renewable and Sustainable Energy Reviews*, 146:111180, 2021. ISSN 1364-0321.

doi: https://doi.org/10.1016/j.rser.2021.111180. URL https://www.sciencedirect.com/science/article/pii/S1364032121004688.

[48] Hong Zhang and Dan Jiang. Risk analysis of fire in hydrogen storage system of ship hydrogen fuel cell based on fsa. In *2023 7th International Conference on Transportation Information and Safety (ICTIS)*, pages 2480–2490, 2023. doi: 10.1109/ICTIS60134.2023.10243733.

[49] Saad Ahmad, Md Shafiullah, Chokri Belhaj Ahmed, and Maad Alowaifeer. A review of microgrid energy management and control strategies. *IEEE Access*, 11:21729–21757, 2023. doi: 10.1109/ACCESS.2023.3248511.

[50] Xiong Liu, Tianyang Zhao, Hui Deng, Peng Wang, Jizhen Liu, and Frede Blaabjerg. Microgrid energy management with energy storage systems: A review. *CSEE Journal of Power and Energy Systems*, 9(2):483–504, 2023. doi: 10.17775/CSEEJPES.2022.04290.

[51] Babangida Modu, Md Pauzi Abdullah, Abba Lawan Bukar, and Mukhtar Fatihu Hamza. A systematic review of hybrid renewable energy systems with hydrogen storage: Sizing, optimization, and energy management strategy. *International Journal of Hydrogen Energy*, 48 (97):38354–38373, 2023. ISSN 0360-3199. doi: https://doi.org/10.1016/j.ijhydene.2023.06.126. URL https://www.sciencedirect.com/science/article/pii/S0360319923029853.

[52] Tao Ding, Wenhao Jia, Mohammad Shahidehpour, Ouzhu Han, Yuge Sun, and Ziyu Zhang. Review of optimization methods for energy hub planning, operation, trading, and control. *IEEE Transactions on Sustainable Energy*, 13(3):1802–1818, 2022. doi: 10.1109/TSTE.2022.3172004.

[53] Germánico López and Pablo Arboleya. Short-term wind speed forecasting over complex terrain using linear regression models and multivariable lstm and narx networks in the andes mountains, ecuador. *Renewable Energy*, 183:351–368, 2022. ISSN 0960-1481. doi: https://doi.org/10.1016/j.renene.2021.10.070. URL https://www.sciencedirect.com/science/article/pii/S0960148121015299.

[54] Jesus Lago, Grzegorz Marcjasz, Bart De Schutter, and Rafał Weron. Forecasting day-ahead electricity prices: A review of state-of-the-art algorithms, best practices and an open-access benchmark. *Applied Energy*, 293:116983, 2021. ISSN 0306-2619. doi: https://doi.org/10.1016/j.apenergy.2021.116983. URL https://www.sciencedirect.com/science/article/pii/S0306261921004529.

[55] Blessing Olatunde Abisoye, Yanxia Sun, and Wang Zenghui. A survey of artificial intelligence methods for renewable energy forecasting: Methodologies and insights. *Renewable Energy Focus*, 48:100529, 2024. ISSN 1755-0084. doi: https://doi.org/10.1016/j.ref.2023.100529. URL https://www.sciencedirect.com/science/article/pii/S1755008423001254.

[56] Romano Acri, Fulvio Bassetti, Maria Carmen Falvo, Letizia Magaldi, Matteo Manganelli, Lorenzo Romagnoli, Federico Santi, and Antonio Scafuri. A new thermal energy storage technology for power system services. In *2021 IEEE International Conference on Environment and Electrical Engineering and 2021 IEEE Industrial and Commercial Power Systems Europe (EEEIC / I&CPS Europe)*, pages 1–6, 2021. doi: 10.1109/EEEIC/ICPSEurope51590.2021.9584535.

[57] Magaldi group. Solar thermoelectric magaldi (stem), 2024. URL https://www.magaldi.com/en/applications/stemr-concentrated-solar-power-and-thermal.

[58] Antonio Scafuri, Matteo Scanzano, Antonio De Caro, Lorenzo Romagnoli, Fulvio Bassetti, Letizia Magaldi, and Maria Carmen Falvo. Control algorithms and hardware for a concentrating solar plant based on fluidized bed with improved heliostat calibration system. *International Journal of Energy Research*. Pending publication approval, 2024.

[59] K. Vignarooban, Xinhai Xu, A. Arvay, K. Hsu, and A.M. Kannan. Heat transfer fluids for concentrating solar power systems: a review. *Applied Energy*, 146:383–396, 2015. ISSN 0306-2619. doi: https://doi.org/10.1016/j.apenergy.2015.01.125. URL https://www.sciencedirect.com/science/article/pii/S0306261915001634.

[60] Thomas Bauer, Nicole Pfleger, Nils Breidenbach, Markus Eck, Doerte Laing, and Stefanie Kaesche. Material aspects of solar salt for sensible heat storage. *Applied Energy*, 111:1114–1119, 2013. ISSN 0306-2619. doi: https://doi.org/10.1016/j.apenergy.2013.04.072. URL https://www.sciencedirect.com/science/article/pii/S0306261913003681.

[61] Lina Ma, Cancan Zhang, Yuting Wu, and Yuanwei Lu. Comparative review of different influence factors on molten salt corrosion characteristics for thermal energy storage. *Solar Energy Materials and Solar Cells*, 235:111485, 2022. ISSN 0927-0248. doi: https://doi.org/10.1016/j.solmat.2021.111485. URL https://www.sciencedirect.com/science/article/pii/S0927024821005249.

[62] V.M.B. Nunes, C.S. Queirós, M.J.V. Lourenço, F.J.V. Santos, and C.A. Nieto de Castro. Molten salts as engineering fluids: A review. *Applied Energy*, 183:603–611, 2016. ISSN 0306-2619. doi: https://doi.org/10.1016/j.apenergy.2016.09.003. URL https://www.sciencedirect.com/science/article/pii/S0306261916313058.

[63] Lorenzo Romagnoli, Antonio Scafuri, Matteo Scanzano, Maria Carmen Falvo, Fulvio Bassetti, and Letizia Magaldi. Evaluation of the integration of thermal energy storage technologies in power to heat configuration within the electrical power system. *IEEE Transaction on Sustainable Energy*. Under review, 2024.

[64] TERNA (Italian Transmission System Operator). Progetto pilota per la partecipazione delle unità virtuali miste (uvam) al msd - approvazione con delibera 70/2021/r/eel delle modifiche proposte da terna, 2021. URL https://www.terna.it/it/sistema-elettrico/pubblicazioni/news-operatori/dettaglio/uvam-del-70-2021.

[65] Kristof De Vos, Simon De Rijcke, and Johan Driesen. Asymmetric reserve power delivered by large wind power plants. In *2010 Innovative Smart Grid Technologies (ISGT)*, pages 1–8, 2010. doi: 10.1109/ISGT.2010.5434732.

[66] Matteo Scanzano, Maria Carmen Falvo, Antonio Scafuri, Fulvio Bassetti, and Letizia Magaldi. Integration of a new thermal energy storage in electrical grids: power supply and control options. In *2021 IEEE International Conference on Environment and Electrical Engineering and 2021 IEEE Industrial and Commercial Power Systems Europe (EEEIC / I&CPS Europe)*, pages 1–6, 2021. doi: 10.1109/EEEIC/ICPSEurope51590.2021.9584803.

[67] Matteo Scanzano, Antonio Scafuri, Rocco Sorrenti, Lorenzo Romagnoli, Maria Carmen Falvo, Fulvio Bassetti, and Letizia Magaldi. A thermal energy storage based on fluidized sand bed: a proposal for an optimized discrete power control. *Journal of Energy Storage*. Under review, 2024.

[68] ABB. High power rectifiers. dc or ac power from abb – reliable, efficient and robust, 2023. URL `https://new.abb.com/power-electronics/high-power-rectifiers`.

[69] Joonas Koponen, Anton Poluektov, Vesa Ruuskanen, Antti Kosonen, Markku Niemelä, and Jero Ahola. Comparison of thyristor and insulated-gate bipolar transistor -based power supply topologies in industrial water electrolysis applications. *Journal of Power Sources*, 491:229443, 2021. ISSN 0378-7753. doi: https://doi.org/10.1016/j.jpowsour.2020.229443. URL `https://www.sciencedirect.com/science/article/pii/S0378775320317262`.

[70] Mohamed Keddar, Zhifeng Zhang, Chendhil Periasamy, and Mamadou Lamine Doumbia. Power quality improvement for 20 MW pem water electrolysis system. *International Journal of Hydrogen Energy*, 47(95):40184–40195, 2022. ISSN 0360-3199. doi: https://doi.org/10.1016/j.ijhydene.2022.08.073. URL `https://www.sciencedirect.com/science/article/pii/S0360319922035777`. The TUBA World Conference on Energy Science and Technology (TUBA WCEST-2021).

[71] Jawad Faiz and Behzad Siahkolah. Solid-state tap-changer of transformers: Design, control and implementation. *International Journal of Electrical Power & Energy Systems*, 33(2):210–218, 2011. ISSN 0142-0615. doi: https://doi.org/10.1016/j.ijepes.2010.08.016. URL `https://www.sciencedirect.com/science/article/pii/S0142061510001523`.

[72] Abolfazl Babaei, Waldemar Ziomek, and Aniruddha M. Gole. Transient characteristics of on-load tap changers during change-over operation. *Electric Power Systems Research*, 197:107296, 2021. ISSN 0378-7796. doi: https://doi.org/10.1016/j.epsr.2021.107296. URL `https://www.sciencedirect.com/science/article/pii/S0378779621002777`.

[73] Yuhang Pan, Song Han, Chao Zhou, and Xi Guo. On switching transient modeling and analysis of electronic on-load tap-changers based sen transformer. *International Journal of Electrical Power & Energy Systems*, 130:107024, 2021. ISSN 0142-0615. doi: https://doi.org/10.1016/j.ijepes.2021.107024. URL `https://www.sciencedirect.com/science/article/pii/S0142061521002647`.

[74] US EPA (United States Environmental Protection Agency. Greenhouse gases equivalencies calculator, 2023. URL `https://www.epa.gov/energy/greenhouse-gases-equivalencies-calculator-calculations-and-references#therms`.

[75] NREL (US National Renewable Energy Laboratory). Annual technology baseline: Commercial pv, 2024. URL `https://atb.nrel.gov/electricity/2024/commercial_pv`.

[76] NREL (US National Renewable Energy Laboratory). Annual technology baseline: Utility-scale pv, 2024. URL `https://atb.nrel.gov/electricity/2024/utility-scale_pv`.

[77] e distribuzione. Costi di connessione alla rete, 2024. URL https://www.e-distribuzione.it/connessione-alla-rete/importi-per-le-connessioni.html.

[78] Terna. Documento metodologico per l'applicazione dell'analisi costi-benefici al piano di sviluppo 2023, 2023. URL https://download.terna.it/terna/Terna_Piano_Sviluppo_2023_Documento_Metodologico_applicazione_analisi_costi_benefici_8db254c3b3edff1.pdf.

[79] Terna. Manuali, tutorial e tutte le risposte alle domande più frequenti sulle richieste di connessione, 2024. URL https://www.terna.it/it/sistema-elettrico/programmazione-territoriale-efficiente/connessione-rete/info-documenti-faq.

[80] NREL (US National Renewable Energy Laboratory). Annual technology baseline: Commercial battery storage, 2022. URL https://atb.nrel.gov/electricity/2022/commercial_battery_storage.

[81] NREL (US National Renewable Energy Laboratory). Annual technology baseline: Utility-scale battery storage, 2022. URL https://atb.nrel.gov/electricity/2022/utility-scale_battery_storage.

[82] Zihui Lin, Dagang Li, and Yuntao Zou. Energy efficiency of lithium-ion batteries: Influential factors and long-term degradation. *Journal of Energy Storage*, 74:109386, 2023. ISSN 2352-152X. doi: https://doi.org/10.1016/j.est.2023.109386. URL https://www.sciencedirect.com/science/article/pii/S2352152X23027846.

[83] Gestore Mercati Energetici. Dati storici MGP (Mercato del Giorno Prima), 2024. URL https://mercatoelettrico.org/It/Download/DatiStorici.aspx.

[84] Gestore Mercati Energetici. Dati storici MGP-GAS (Mercato del Giorno Prima del gas), 2024. URL https://mercatoelettrico.org/It/Download/DatiStoriciGas.aspx.

[85] EU Science Hub. Photovoltaic Geographical Information System (PVGIS), 2022. URL https://joint-research-centre.ec.europa.eu/photovoltaic-geographical-information-system-pvgis/pvgis-releases/pvgis-52_en.

Appendix A

Publications related to the thesis

The following publications, part of the bibliography of the thesis, were produced within the PhD focusing on different aspects of MGTES technology. The publications report concisely the core information regarding the research carried out, whereas the thesis discusses the same topics in more detail, including additional considerations and further clarifications. The last publication of the list reports a general overview about the integration of renewable energy sources.

[58] Antonio Scafuri, Matteo Scanzano, Antonio De Caro, Lorenzo Romagnoli, Fulvio Bassetti, Letizia Magaldi, Maria Carmen Falvo. Control algorithms and hardware for a concentrating solar plant based on fluidized bed with improved heliostat calibration system. *International Journal of Energy Research*, Wiley, 2023. Pending publication approval.

[63] Lorenzo Romagnoli, Antonio Scafuri, Matteo Scanzano, Maria Carmen Falvo, Fulvio Bassetti, Letizia Magaldi. Evaluation of the integration of Thermal Energy Storage technologies in Power to Heat configuration within the electrical power system. *IEEE Transactions on Sustainable Energy*, 2024. Under review.

[66] Matteo Scanzano, Maria Carmen Falvo, Antonio Scafuri, Fulvio Bassetti, Letizia Magaldi. Integration of a new thermal energy storage in electrical grids: power supply and control options. *2021 EEEIC International Conference on Environment and Electrical Engineering and 2021 IEEE Industrial and Commercial Power Systems Europe (EEEIC/I&CPS Europe)*, pages 1–6, 2021. doi: 10.1109/EEEIC/ICPSEurope51590.2021.9584803.

[67] Matteo Scanzano, Antonio Scafuri, Rocco Sorrenti, Lorenzo Romagnoli, Maria Carmen Falvo, Fulvio Bassetti, Letizia Magaldi. A Thermal Energy Storage based on fluidized sand bed: a proposal for an optimized discrete power control. *Journal of Energy Storage*, 2024. Under review.

[5] Marialaura Di Somma, Maria Carmen Falvo, Giorgio Graditi, Matteo Manganelli, Matteo Scanzano, Maria Valenti. Integration of renewable energy sources in transmission grids: issues and perspectives. *2021 EEEIC International Conference on Environment and Electrical Engineering and 2021 IEEE Industrial and Commercial Power Systems Europe (EEEIC/I&CPS Europe)*, pages 1–8, 2021. doi: 10.1109/EEEIC/ICPSEurope51590.2021.9584553.

The following publications, produced within the PhD as side projects, are not directly related to MGTES. However, they regarded the optimization of transmission networks and railway power systems, involving the realization of dedicated optimization tools. The structure of ESTESO and a lot of its features were inspired to them, as a result of the experience acquired during their development.

- Temistocle Baffa Scirocco, Enrico Maria Carlini, Fabio Ciasca, Alessio Sallati, Maria Carmen Falvo, Cristina Moscatiello, Matteo Scanzano. International benchmarking and new proposals on CBA methodology for the Italian transmission grid. *2022 AEIT International Annual Conference*, pp. 1-5, 2022, doi: 10.23919/AEIT56783.2022.9951784.
- Alessandro Ruvio, Maria Carmen Falvo, Regina Lamedica, Jacopo Dell'Olmo, Matteo Scanzano. A novel railway power systems design methodology using genetic algorithms: models and application. *IEEE Access*, 2024, ISSN 2169-3536, doi: 10.1109/ACCESS.2024.3455945.

Appendix B

Open source libraries used by ESTESO

I want to express my gratitude to the open-source community. They provide free access to their software, tools and knowledge, sharing their work and actively collaborating with commitment to transparency and fairness. Without their efforts, this research would not have been possible.

Here the list of open source libraries and projects used by ESTESO:

- **streamlit** for web-based user interface
- **pint** for units handling
- **pandas** for timeseries management
- **pyomo** + **glpk** for MILP optimization
- **echarts** for charts visualization
- **pyvis** for graph visualization
- **selenium** for online market data scraping
- **pvgis** for historic PV data collection

Appendix C

ESTESO interface pages

C.1 System inspection

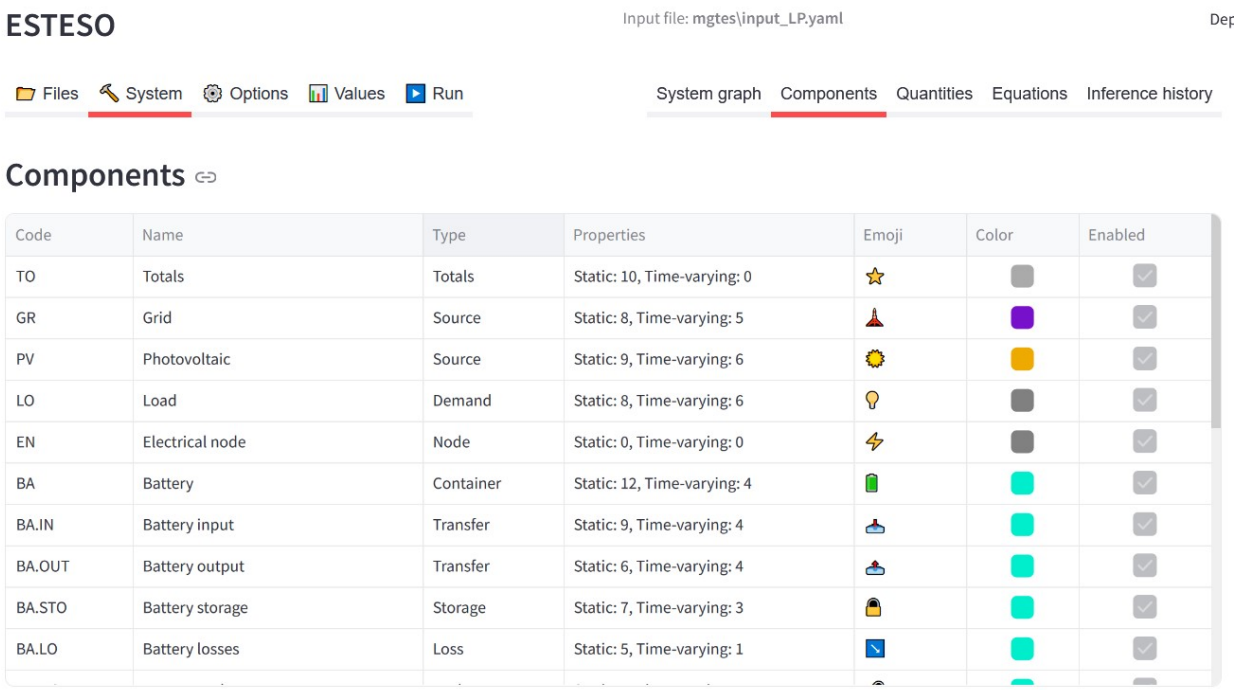

Code	Name	Type	Properties	Emoji	Color	Enabled
TO	Totals	Totals	Static: 10, Time-varying: 0			
GR	Grid	Source	Static: 8, Time-varying: 5			
PV	Photovoltaic	Source	Static: 9, Time-varying: 6			
LO	Load	Demand	Static: 8, Time-varying: 6			
EN	Electrical node	Node	Static: 0, Time-varying: 0			
BA	Battery	Container	Static: 12, Time-varying: 4			
BA.IN	Battery input	Transfer	Static: 9, Time-varying: 4			
BA.OUT	Battery output	Transfer	Static: 6, Time-varying: 4			
BA.STO	Battery storage	Storage	Static: 7, Time-varying: 3			
BA.LO	Battery losses	Loss	Static: 5, Time-varying: 1			

Figure C.1: ESTESO system components inspection page

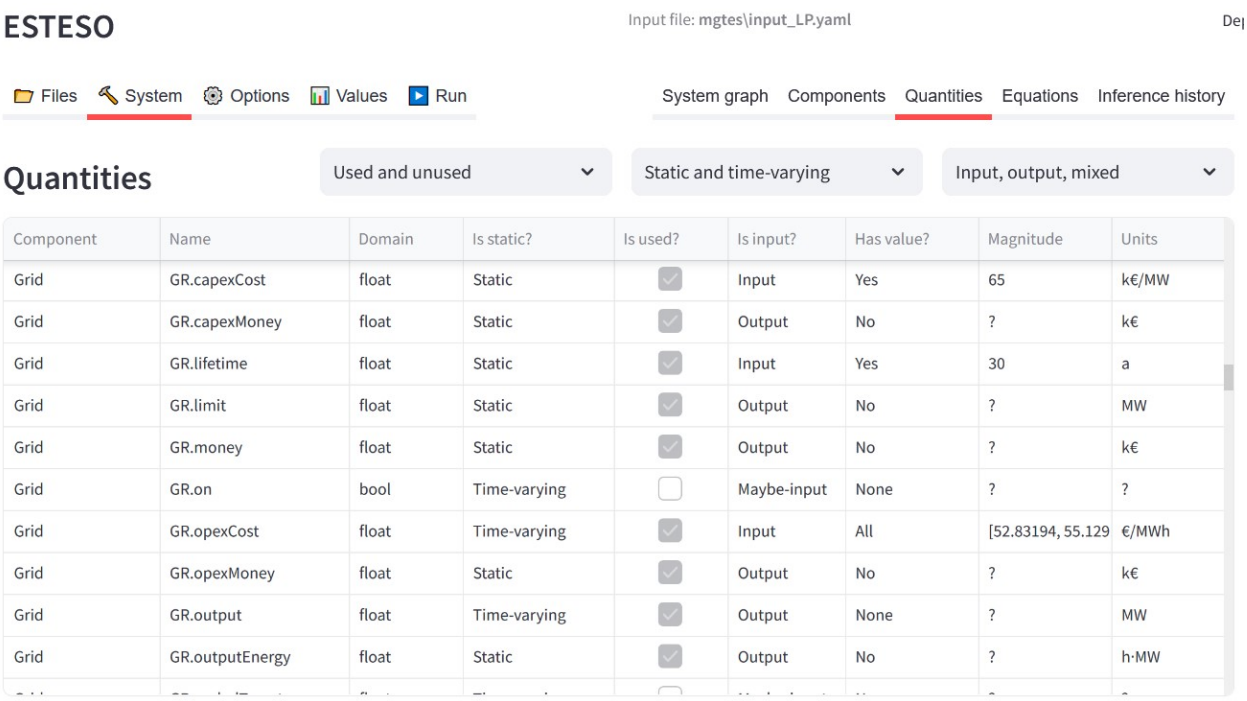

Component	Name	Domain	Is static?	Is used?	Is input?	Has value?	Magnitude	Units
Grid	GR.capexCost	float	Static	☑	Input	Yes	65	k€/MW
Grid	GR.capexMoney	float	Static	☑	Output	No	?	k€
Grid	GR.lifetime	float	Static	☑	Input	Yes	30	a
Grid	GR.limit	float	Static	☑	Output	No	?	MW
Grid	GR.money	float	Static	☑	Output	No	?	k€
Grid	GR.on	bool	Time-varying	☐	Maybe-input	None	?	?
Grid	GR.opexCost	float	Time-varying	☑	Input	All	[52.83194, 55.129	€/MWh
Grid	GR.opexMoney	float	Static	☑	Output	No	?	k€
Grid	GR.output	float	Time-varying	☑	Output	None	?	MW
Grid	GR.outputEnergy	float	Static	☑	Output	No	?	h·MW

Figure C.2: ESTESO system quantities inspection page

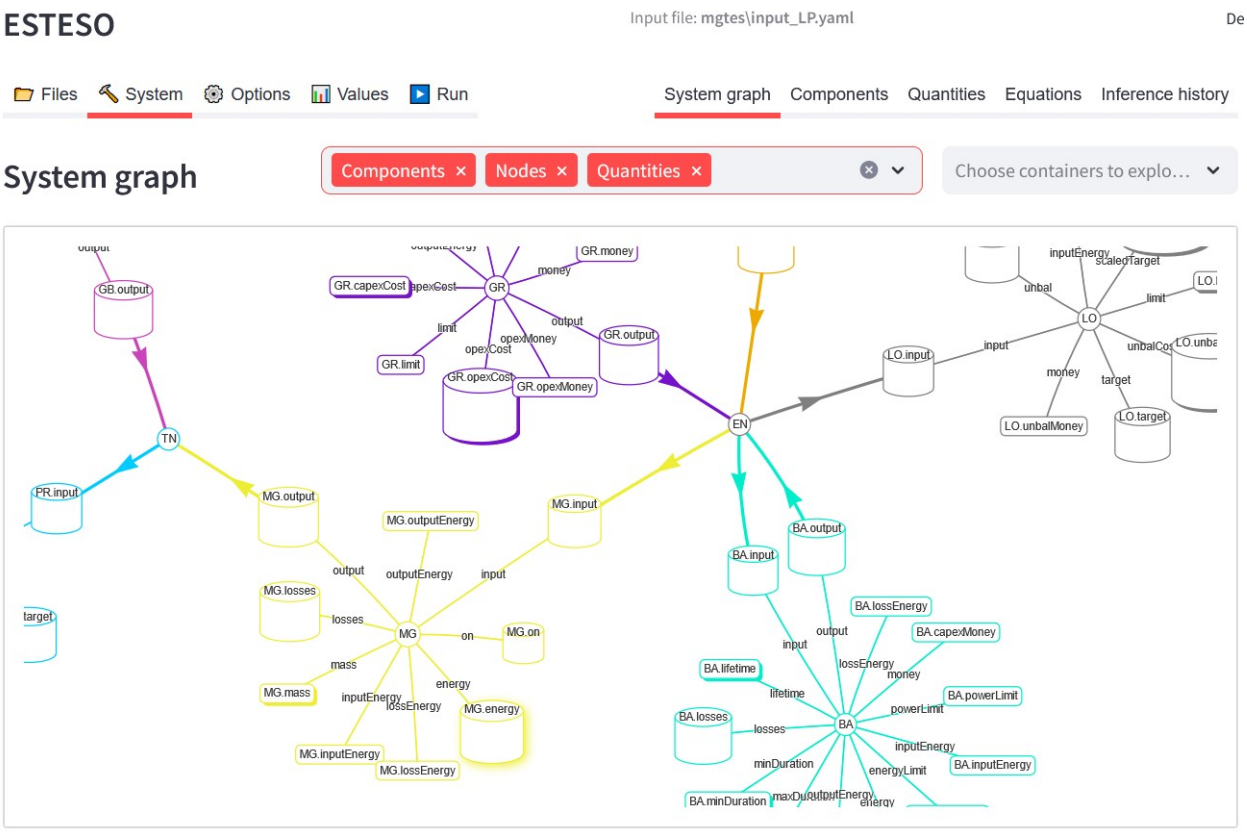

Figure C.3: ESTESO system graph exploration page

C.2 Model and computation

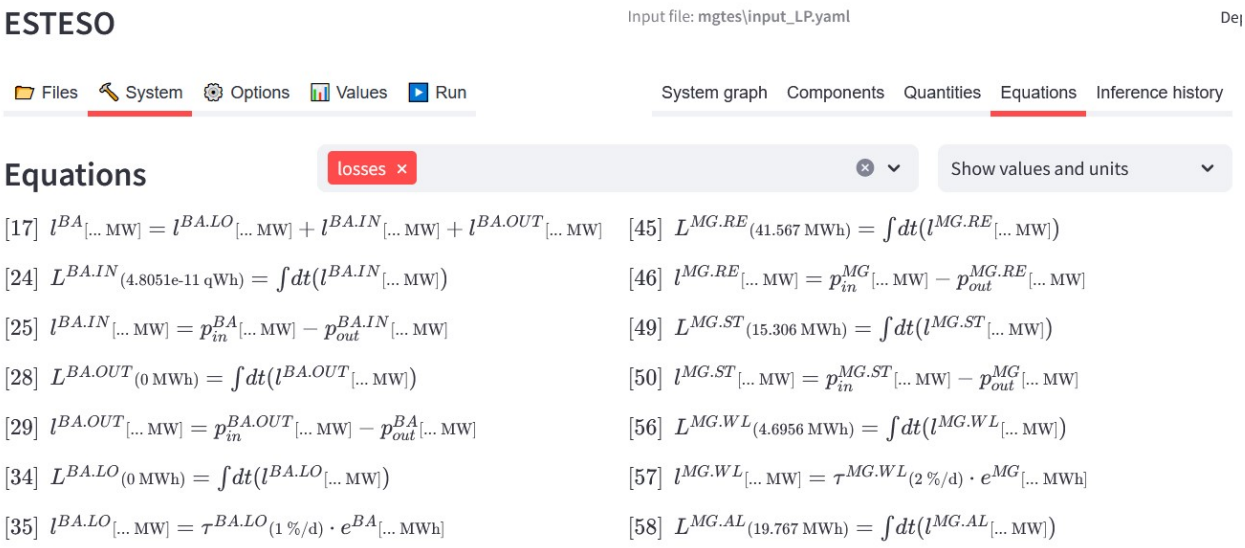

Figure C.4: ESTESO system equations visualization page

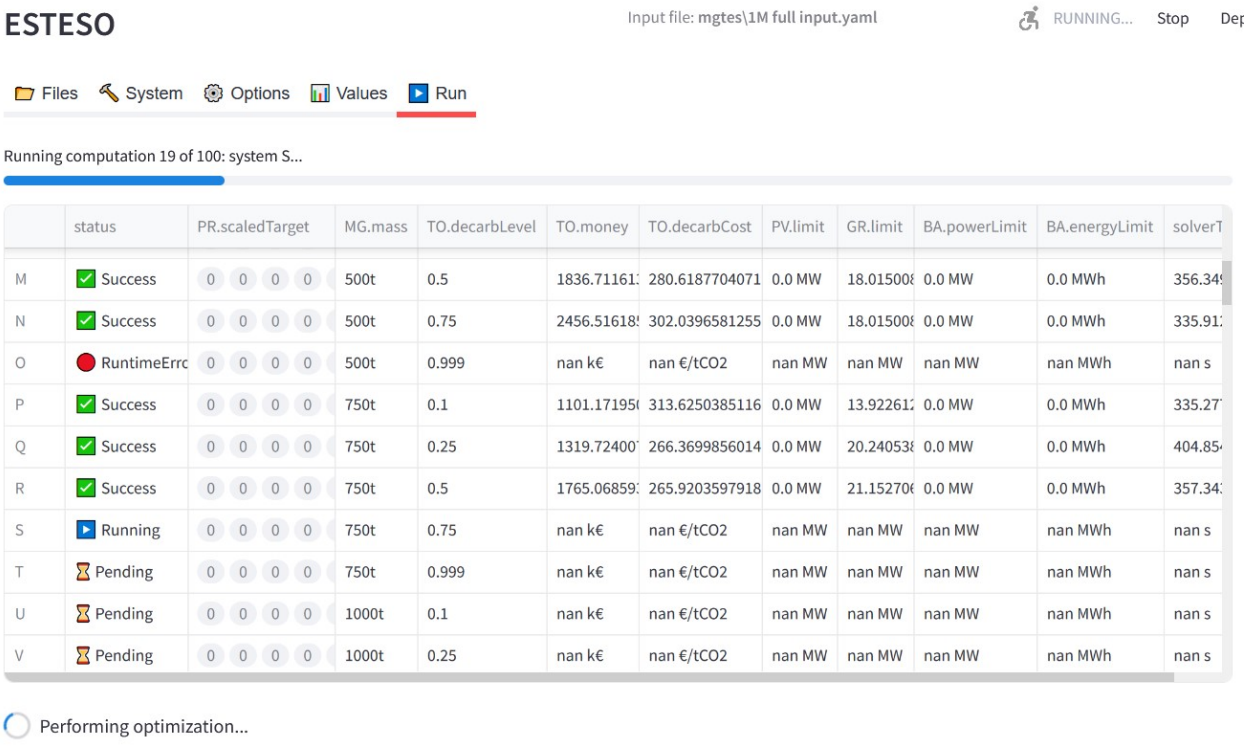

Figure C.5: ESTESO running computations monitoring page

C.3 Results analysis

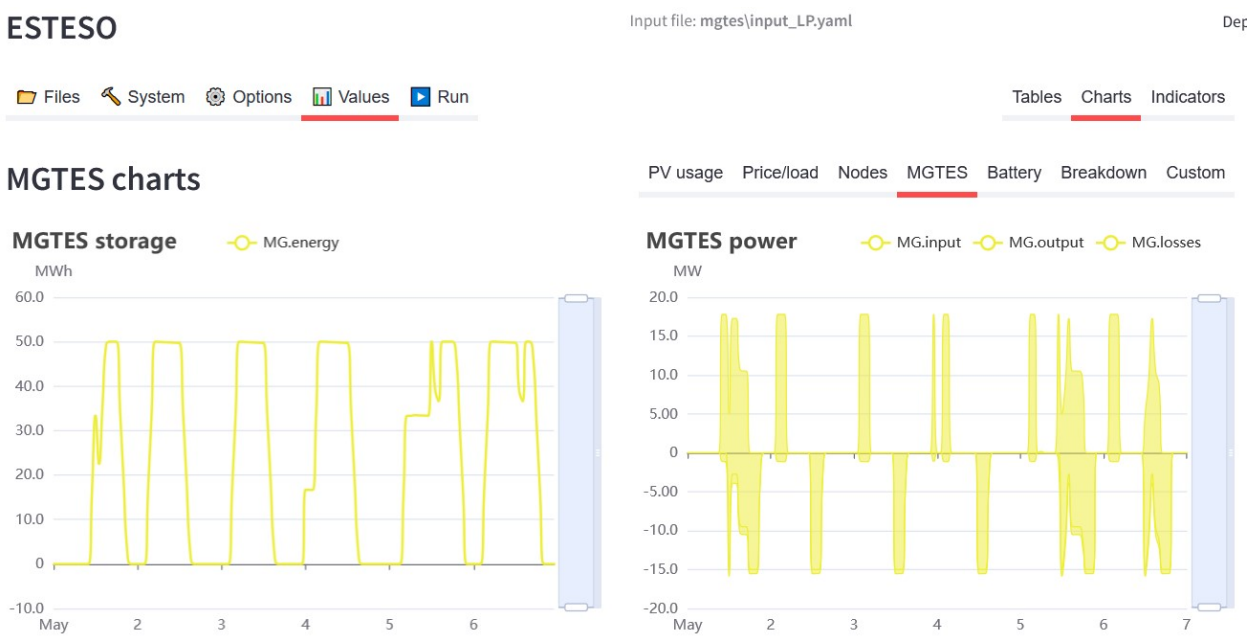

Figure C.6: MGTES charts page in ESTESO

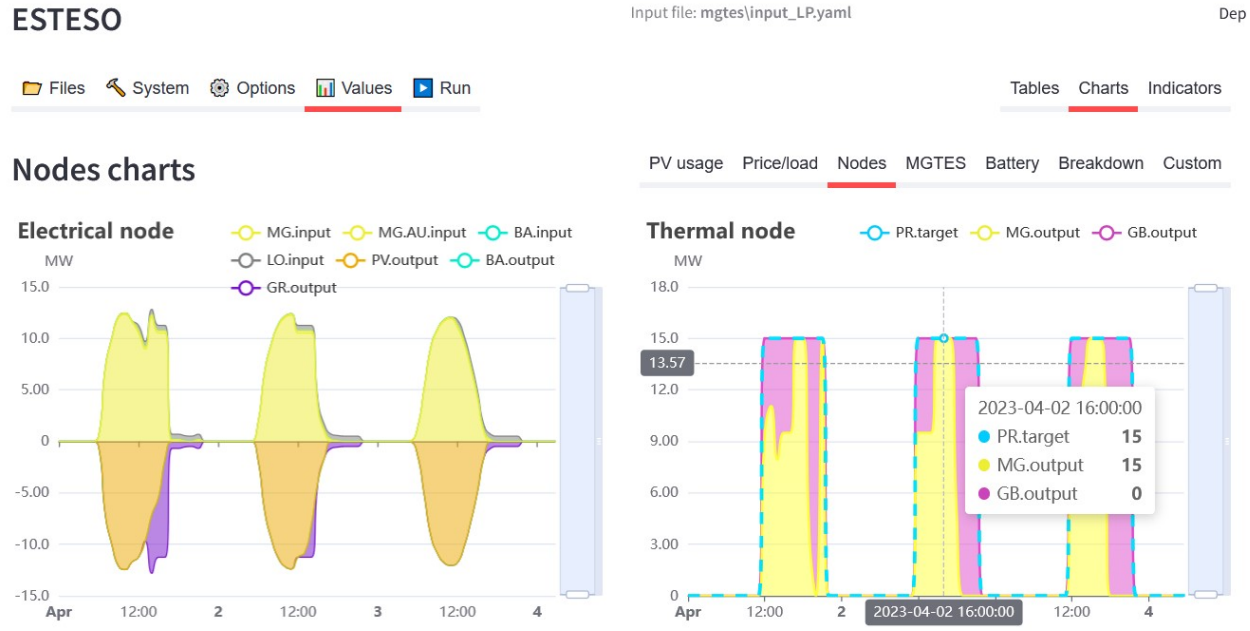

Figure C.7: ESTESO energy nodes charts exploration page

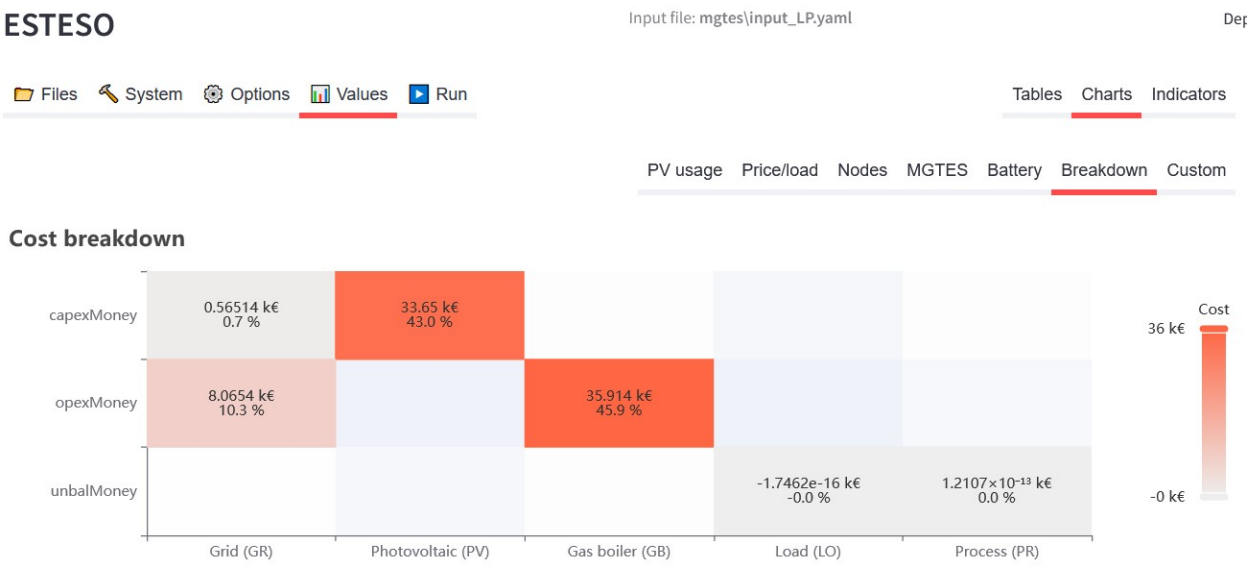

Figure C.8: ESTESO system cost breakdown visualization page

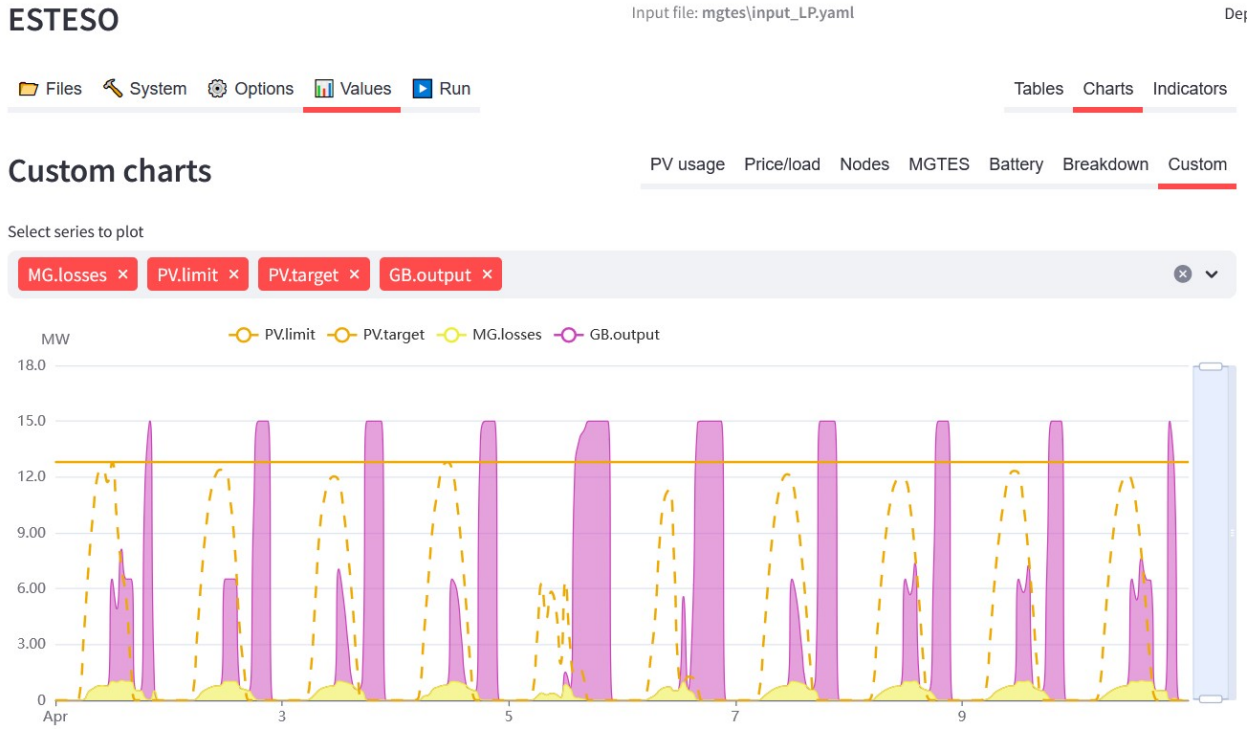

Figure C.9: ESTESO custom charts exploration page

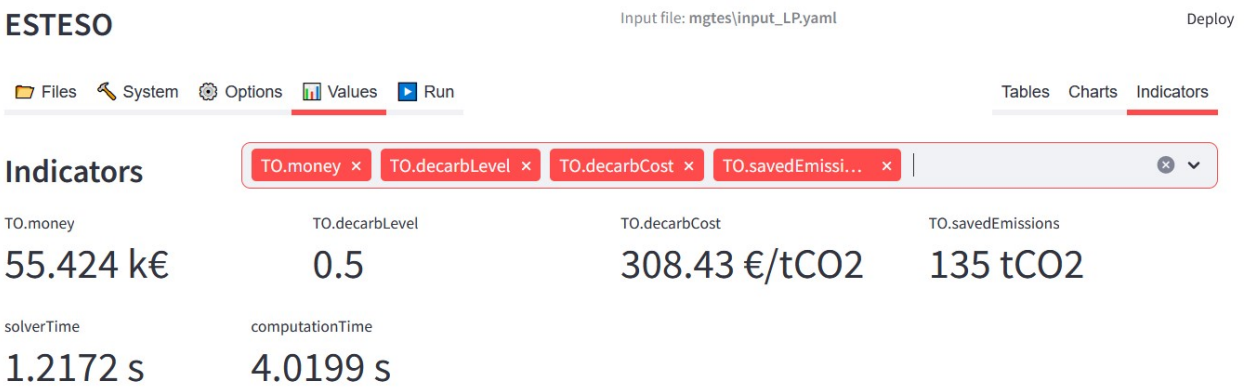

Figure C.10: ESTESO system indicators page

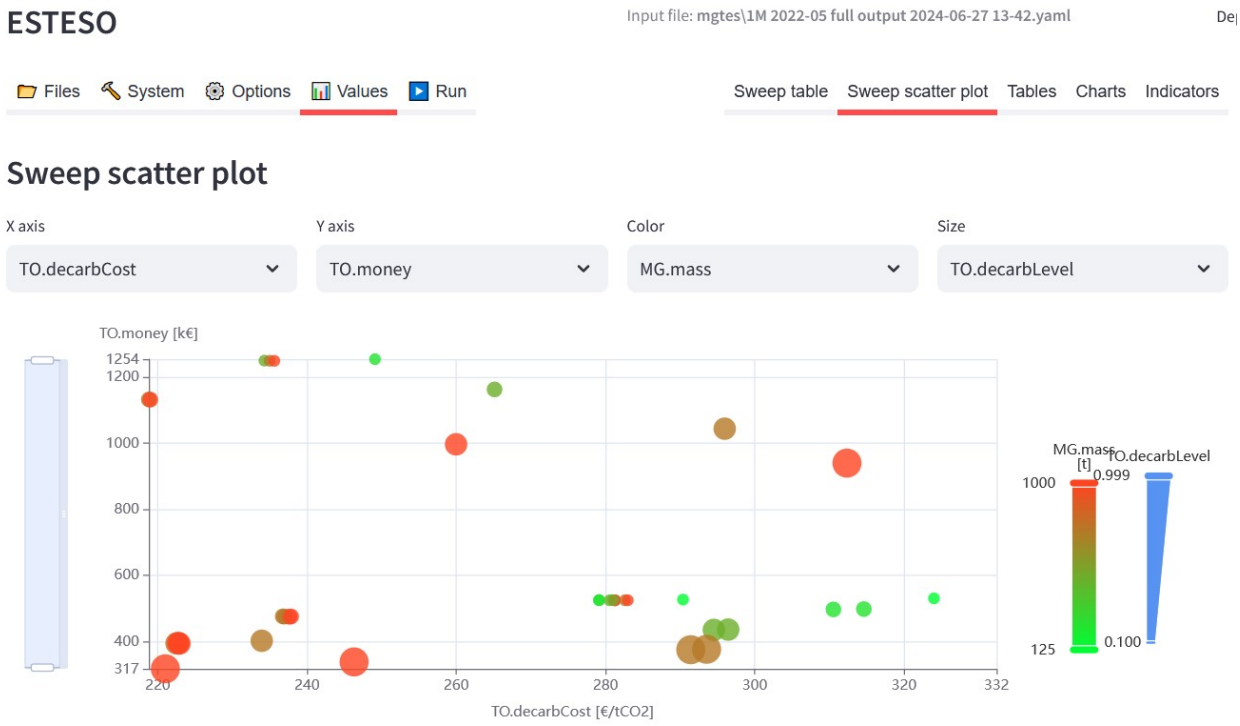

Figure C.11: ESTESO parametric sweep scatter plot page

C.4 Other

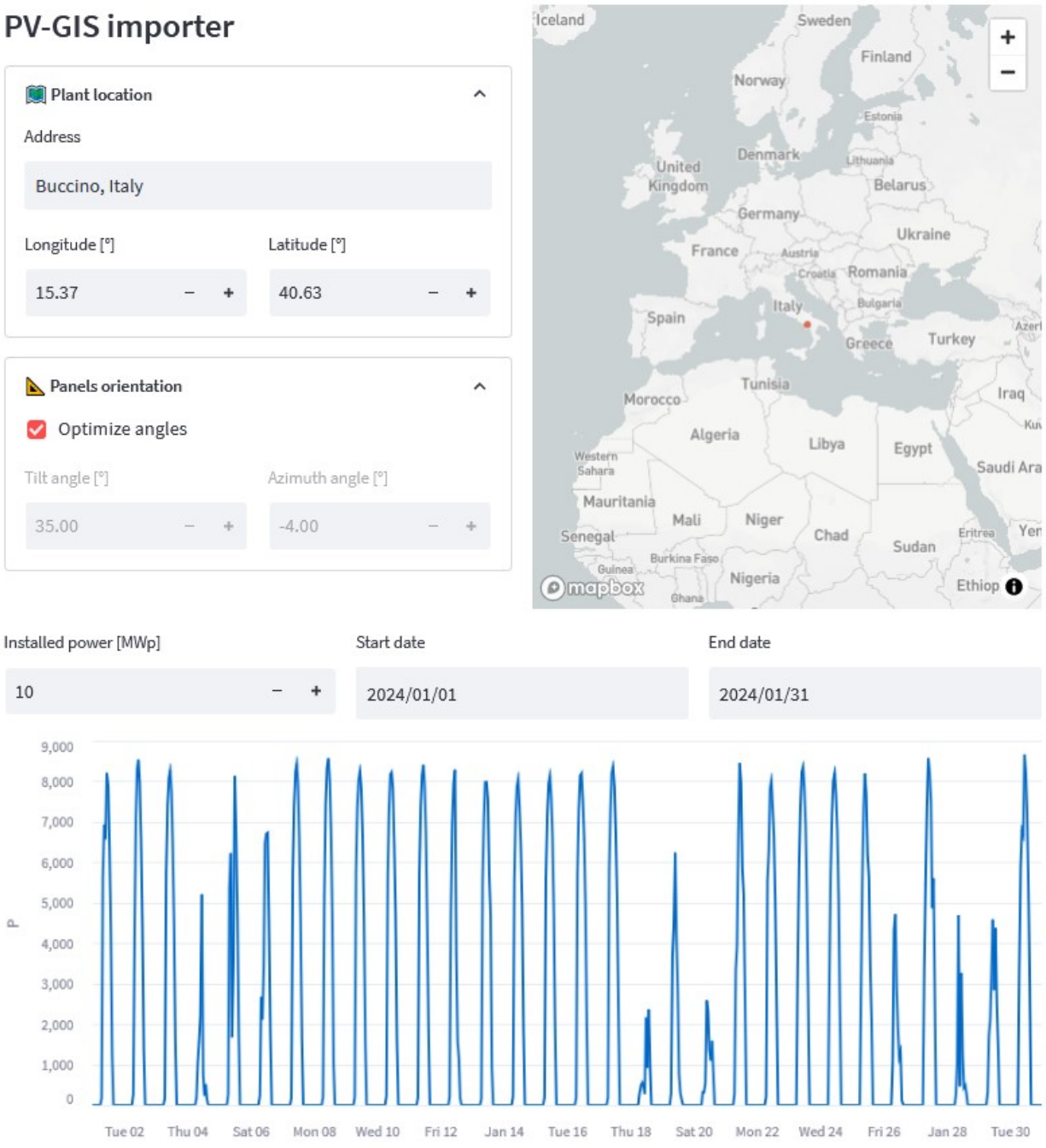

Figure C.12: ESTESO dedicated PVGIS data importer page

Appendix D

Model equations, generated by ESTESO

[1] $p_{out}^{GR} \leq P_{out}^{GR}$

[2] $M^{GR} = P_{out}^{GR} \cdot C^{GR} \cdot (T/T_{life}^{GR})$

[3] $m^{GR} = \int dt(p_{out}^{GR} \cdot c^{GR})$

[4] $\mathbb{M}^{GR} = M^{GR} + m^{GR}$

[5] $E_{out}^{GR} = \int dt(p_{out}^{GR})$

[6] $\bar{p}_{out}^{PV} = P_{out}^{PV} \cdot \hat{p}_{out}^{PV}$

[7] $\tilde{p}_{out}^{PV} = \bar{p}_{out}^{PV} - p_{out}^{PV}$

[8] $p_{out}^{PV} \leq P_{out}^{PV}$

[9] $M^{PV} = P_{out}^{PV} \cdot C^{PV} \cdot (T/T_{life}^{PV})$

[10] $E_{out}^{PV} = \int dt(p_{out}^{PV})$

[11] $\bar{p}_{in}^{LO} = P_{in}^{LO} \cdot \hat{p}_{in}^{LO}$

[12] $\tilde{p}_{in}^{LO} = \bar{p}_{in}^{LO} - p_{in}^{LO}$

[13] $\tilde{M}^{LO} = \int dt(\tilde{p}_{in}^{LO} \cdot \tilde{c}^{LO})$

[14] $p_{in}^{LO} \leq P_{in}^{LO}$

[15] $E_{in}^{LO} = \int dt(p_{in}^{LO})$

[16] $p_{out}^{PV} + p_{out}^{GR} + p_{out}^{BA} = p_{in}^{MG} + p_{in}^{MG.AU} + p_{in}^{LO} + p_{in}^{BA}$

[17] $l^{BA} = l^{BA.LO} + l^{BA.IN} + l^{BA.OUT}$

[18] $E_{in}^{BA} = \int dt(p_{in}^{BA})$

[19] $E_{out}^{BA} = \int dt(p_{out}^{BA})$

[20] $E^{BA} \leq P^{BA} \cdot T_{store,max}^{BA}$

[21] $E^{BA} \geq P^{BA} \cdot T_{store,min}^{BA}$

[22] $p_{in}^{BA} \leq P^{BA}$

[23] $M^{BA.IN} = P^{BA} \cdot C^{BA.IN} \cdot (T/T_{life}^{BA})$

[24] $L^{BA.IN} = \int dt(l^{BA.IN})$

[25] $l^{BA.IN} = p_{in}^{BA} - p_{out}^{BA.IN}$

[26] $p_{out}^{BA.IN} = p_{in}^{BA} \cdot \eta^{BA.IN}$

[27] $p_{out}^{BA} \leq P^{BA}$

[28] $L^{BA.OUT} = \int dt(l^{BA.OUT})$

[29] $l^{BA.OUT} = p_{in}^{BA.OUT} - p_{out}^{BA}$

[30] $p_{out}^{BA} = p_{in}^{BA.OUT} \cdot \eta^{BA.IN}$

[31] $e^{BA} \leq E^{BA}$

[32] $M^{BA.STO} = E^{BA} \cdot C^{BA.STO} \cdot (T/T_{life}^{BA})$

[33] $p_{out}^{BA.STO} = -\partial_t(e^{BA})$

[34] $L^{BA.LO} = \int dt(l^{BA.LO})$

[35] $l^{BA.LO} = \tau^{BA.LO} \cdot e^{BA}$

[36] $p_{out}^{BA.STO} + p_{out}^{BA.IN} = p_{in}^{BA.OUT} + l^{BA.LO}$

[37] $L^{BA} = L^{BA.IN} + L^{BA.OUT} + L^{BA.LO}$

[38] $M^{BA} = M^{BA.IN} + M^{BA.STO}$

[39] $l^{MG} = l^{MG.WL} + l^{MG.AL} + l^{MG.RE} + l^{MG.ST}$

[40] $E_{in}^{MG} = \int dt(p_{in}^{MG})$

[41] $E_{out}^{MG} = \int dt(p_{out}^{MG})$

[42] $s^{MG} = ((p_{in}^{MG}/P_{in}^{MG.RE}) + (p_{out}^{MG}/P_{out}^{MG.ST}))/2$

[43] $l^{MG.AL} = \Lambda^{MG} \cdot K^{MG.AL} \cdot s^{MG}$

[44] $p_{in}^{MG.AU} = P_{in}^{MG.AU} \cdot s^{MG}$

[45] $L^{MG.RE} = \int dt(l^{MG.RE})$

[46] $l^{MG.RE} = p_{in}^{MG} - p_{out}^{MG.RE}$

[47] $p_{out}^{MG.RE} = p_{in}^{MG} \cdot \eta^{MG.RE}$

[48] $P_{in}^{MG.RE} = \Lambda^{MG} \cdot K^{MG.RE}$

[49] $L^{MG.ST} = \int dt(l^{MG.ST})$

[50] $l^{MG.ST} = p_{in}^{MG.ST} - p_{out}^{MG}$

[51] $p_{out}^{MG} = p_{in}^{MG.ST} \cdot \eta^{MG.ST}$

[52] $P_{out}^{MG.ST} = \Lambda^{MG} \cdot K^{MG.ST}$

[53] $e^{MG} \leq E^{MG.SA}$

[54] $p_{out}^{MG.SA} = -\partial_t(e^{MG})$

[55] $E^{MG.SA} = \Lambda^{MG} \cdot K^{MG.SA}$

[56] $L^{MG.WL} = \int dt(l^{MG.WL})$

[57] $l^{MG.WL} = \tau^{MG.WL} \cdot e^{MG}$

[58] $L^{MG.AL} = \int dt(l^{MG.AL})$

[59] $p_{in}^{MG.AU} \leq P_{in}^{MG.AU}$

[60] $E_{in}^{MG.AU} = \int dt(p_{in}^{MG.AU})$

[61] $P_{in}^{MG.AU} = \Lambda^{MG} \cdot K^{MG.AU}$

[62] $p_{out}^{MG.RE} + p_{out}^{MG.SA} = p_{in}^{MG.ST} + l^{MG.WL} + l^{MG.AL}$

[63] $L^{MG} = L^{MG.RE} + L^{MG.ST} + L^{MG.WL} + L^{MG.AL}$

[64] $p_{out}^{GB} \leq P_{out}^{GB}$

[65] $m^{GB} = \int dt(p_{out}^{GB} \cdot c^{GB})$

[66] $E_{out}^{GB} = \int dt(p_{out}^{GB})$

[67] $\bar{p}_{in}^{PR} = P_{in}^{PR} \cdot \hat{p}_{in}^{PR}$

[68] $\tilde{p}_{in}^{PR} = \bar{p}_{in}^{PR} - p_{in}^{PR}$

[69] $\tilde{M}^{PR} = \int dt(\tilde{p}_{in}^{PR} \cdot \tilde{c}^{PR})$

[70] $p_{in}^{PR} \leq P_{in}^{PR}$

[71] $E_{in}^{PR} = \int dt(p_{in}^{PR})$

[72] $p_{out}^{GB} + p_{out}^{MG} = p_{in}^{PR}$

[73] $\gamma = E_{out}^{MG} \cdot K_{\gamma}$

[74] $E_{PR} = \int dt(\bar{p}_{in}^{PR})$

[75] $D = E_{out}^{MG} / E_{PR}$

[76] $E_{served} = E_{in}^{PR} + E_{in}^{LO}$

[77] $L = L^{BA} + L^{MG}$

[78] $M = M^{GR} + M^{PV} + M^{BA}$

[79] $m = m^{GR} + m^{GB}$

[80] $\tilde{M} = \tilde{M}^{LO} + \tilde{M}^{PR}$

[81] $\mathbb{M} = M + m + \tilde{M}$